T.C.
USKUDAR UNIVERSITY
INSTITUTE OF SCIENCE

DEPARTMENT OF COMPUTER ENGINEERING

MASTER'S DEGREE PROGRAM OF COMPUTER ENGINEERING

MASTER'S DEGREE THESIS

Reconstructed Tissues for Drug Delivery System Using MRA Images

Khaled Alsayad

Thesis Advisor

Dr, Ihab ELAFF

ISTANBUL-2024

T.C.
USKUDAR UNIVERSITY
INSTITUTE OF SCIENCE

DEPARTMENT OF COMPUTER ENGINEERING

MASTER'S DEGREE PROGRAM OF COMPUTER ENGINEERING

MASTER'S DEGREE THESIS

Reconstructed Tissues for Drug Delivery System Using MRA Images

Khaled Alsayad

Thesis Advisor

Dr, Ihab ELAFF

ISTANBUL-2024

ABSTRACT

RECONSTRUCTED TISSUES FOR DRUG DELIVERY SYSTEM USING MRA IMAGES

In recent years, the increase in diseases and the spread of epidemics have put human life in the face of various and serious challenges, while struggling with crises on the health, economic and social levels. Some of these crises stemmed from the COVID-19 pandemic and its repercussions. The pandemic claimed millions of lives, while taking a toll on people's social relations and finances. Lockdowns imposed on workplaces and vital service facilities, along with social distancing measures have all highlighted the importance of good healthcare infrastructure, strong communication and cooperation between governments, and careful risk assessment for the management of future epidemics. The effects of the pandemic, many of which are long-term, have changed people's daily lives and perspectives on physical presence, whether at work or in terms of personal contact. Both our bodies and health were revaluated and today are prioritized. Getting rid of diseases and stopping epidemics required different measures; however, medicine and pharmaceutical methods were the most important. Under these circumstances, drug delivery systems have been getting a lot of attention lately, especially from new research and projects that focus on reducing the negative effects of drugs and delivering it to the target organs without influencing the rest of the body.

In this study, we demonstrate the best means to use magnetic resonance angiography images of a human organ to locate arteries and veins. Next, we exhibit the methods utilized to figure out where the organ is in the body and isolate it from the rest of the details in the images by using advanced algorithms in the field of artificial intelligence and computer vision related to the medical field. Using the output from the previous steps, we show how a three-dimensional map of the organ is created for better examination and view of boundaries. This is done to define the easiest was for the drug to travel from the injection point to the target point, considering factors like the direction of blood flow, the distance between the injection point and the body's boundary, and the size of the artery. With this information, researchers can determine the best path for the drug to take to reach its destination.

Keywords: Drug delivery system, Fuzzy c-means, K-means, Otsu

ÖZET

MRA GÖRÜNTÜLERİ KULLANILARAK İLAÇ TAŞIMA SİSTEMİ İÇİN YENİDEN YAPILANDIRILMIŞ DOKULAR

Son yıllarda hastalıkların artması ve salgınların yayılması, insan hayatını sağlık, ekonomik ve sosyal düzeylerde krizlerle mücadele ederken çeşitli ve ciddi zorluklarla karşı karşıya bırakmaktadır. Bu krizlerden bazıları COVID-19 pandemisinin ve onun yansımalarından kaynaklanmıştır. Pandemi, milyonlarca insanın hayatını kaybetmesine neden olurken, insanların sosyal ilişkilerini ve mali durumlarını da olumsuz etkilemiştir. İşyerleri ve hayati hizmet tesislerine uygulanan kapanmalar, sosyal mesafe önlemleriyle birlikte, iyi bir sağlık altyapısının, hükümetler arası güçlü iletişim ve işbirliğinin, gelecekteki salgınların yönetimi için dikkatli bir risk değerlendirmesinin önemini vurgulamıştır. Birçoğu uzun vadeli olan salgının etkileri, insanların günlük yaşamlarını ve hem işte hem de kişisel temas açısından fiziksel varlığa ilişken görüşlerini değiştirmiştir. Bugün, bedenimiz ve sağlığımız yeniden değerlendirilip önceliklendirilmiştir. Hastalıklardan kurtulmak ve salgınları durdurmak, farklı önlemler gerektirirdi; ancak tıp ve farmasötik yöntemler en önemlileriydi. Bu koşullar altında ilaç dağıtım sistemleri son zamanlarda özellikle ilaçların olumsuz etkilerini azaltmaya ve vücudun geri kalanını etkilemeden hedef organlara ulaştırmaya odaklanan yeni araştırma ve projelerle büyük ilgi görmektedir.

Bu çalışmada, atardamarların ve damarların yerini tespit etmek için insan organlarının manyetik rezonans anjiyografisini kullanmanın en iyi yollarını göstermektedir. Buna ek olarak, tıbbi yapay zekâ ve bilgisayarlı görme alanındaki gelişmiş algoritmaları kullanarak organın vücuttaki konumunu tespit etmek ve onu görüntülerdeki diğer ayrıntılardan izole etmek için kullanılan yöntemleri sunmaktayız. Önceki adımların çıktısını kullanarak, daha iyi inceleme ve sınırların görülebilmesi için organın üç boyutlu haritasının nasıl oluşturulduğunu göstermekteyiz. Bu, kan akışının yönü, enjeksiyon noktası ile vücut sınırı arasındaki mesafe ve arterin boyutu gibi faktörler dikkate alınarak, ilacın enjeksiyon noktasından hedef noktaya gitmesinin en kolay yolu olduğunu tanımlamak için yapılır. Bu bilgilerle araştırmacılar, ilacın hedefine ulaşması için izleyeceği en iyi yolu belirleyebilirler.

Anahtar Kelimeler: İlaç dağıtım sistemi, Bulanık c-ortalamalar, K-ortalamalar, Otsu

THANKS TO

I would like to express my sincere gratitude to all those who contributed to the completion of this thesis. First and foremost, I extend my heartfelt thanks to my dedicated thesis advisor, whose guidance and expertise were invaluable throughout the entire research process. Their mentorship provided clarity and direction, enabling me to navigate the complexities of academic inquiry. Their collective efforts underscore the collaborative spirit that fuels meaningful research. Lastly, I appreciate the encouragement and understanding from my family and friends, who stood by me during the challenging moments of this academic endeavor. This thesis would not have been possible without the unwavering support of these individuals, and for that, I am truly thankful.

FORM OF DECLARATION

Herewith I declare, that I obtained all the information and documents in this study within the framework of academic rules, presented all visual, auditory, and written information and results in accordance with scientific ethics, did not falsify the data I used, referred to the sources I used in accordance with scientific norms, that my thesis was original except in the cases cited, produced by me and written in accordance with the Thesis Writing Guide of Uskudar University Institute of Health Sciences.

Date: 09/02/2024

Student's Name and Surname: Khaled Alsayad

Signature:

CONTENTS

ABSTRACT ..... **i**

ÖZET ..... **ii**

THANKS TO ..... **iii**

FORM OF DECLARATION ..... **iv**

CONTENTS ..... **v**

INDEX OF TABLES ..... **vii**

INDEX OF FIGURES ..... **viii**

INDEX OF IMAGERY AND ABBREVIATIONS ..... **x**

1. INTRODUCTION **1**

2. Diseases and Therapy: **2**

2.1. Classifications and Types of Diseases 3

2.2. Medication Therapies 5

2.3. Drugs 7

3. LITERATURE REVIEW **18**

3.1. Types of Targeted Drug Delivery Systems 19

3.2. Medical Image Segmentation: 28

4. SYSTEM DESIGN **36**

4.1. The Dataset 36

4.2. Veins Extraction 37

4.3. Brain Extraction 41

4.4. 3D Map Construction 42

4.5. Best Route 42

5. RESULTS **44**

5.1. Veins Extraction Results: 45

5.2. Brain Extraction Results: 85

5.3. 3D Map Results:.....85
5.4. Shortest Path Results:.....87
6. CONCLUSION AND FUTURE WORKS 90
RESOURCES.....92
APPENDIX 98
Appx. 1. Curriculum Vitae 98

INDEX OF TABLES

Page

TABLE 1 THE ROOTS FROM THE SECOND DERIVATIVE OF POLYNOMIAL CURVE FOR FCM. 54
TABLE 2 THE VALUES FROM THE SECOND DERIVATIVE OF CUMULATIVE CHANGE PLOT FOR OTSU. 67
TABLE 3 THE VALUES FROM THE SECOND DERIVATIVE OF CUMULATIVE CHANGE PLOT FOR K-MEANS. 80

INDEX OF FIGURES

Page

FIGURE 1 ANGLES OF INSERTION OF PARENTERAL DRUG ADMINISTRATION. 10
FIGURE 2 THE HUMAN CARDIOVASCULAR SYSTEM. 14
FIGURE 3 A MULTIPHYSICS MODEL OF MAGNETIC HYDROGEL UNDER A MOVING MAGNET FOR TARGETED DRUG DELIVERY. 24
FIGURE 4 SYSTEM DESIGN OF A ROBOTIZED MAGNETIC PLATFORM FOR TARGETED DDS IN THE COCHLEA. 25
FIGURE 5 FOUR PERMANENT MAGNETS BASED ACTUATOR. 26
FIGURE 6 MAGNETIC FORCES VECTORS GENERATED BY FOUR-MAGNETS ACTUATOR. 26
FIGURE 7 3D PRINTED PROTOTYPE FOR THE SYSTEM. 28
FIGURE 8 IMAGE SEGMENTED BY FUZZY CLUSTERING. [50] 30
FIGURE 9 EM CLUSTERING OF OLD FAITHFUL ERUPTION DATA. [51] 32
FIGURE 10 AN IMAGE THRESHOLDED USING OTSU'S ALGORITHM [52] 33
FIGURE 11 AN OVERVIEW OF RESEARCH PROCEDURES. 43
FIGURE 12 IMPLEMENTATION METHODOLOGY. 44
FIGURE 13 MRA SLICES OF THE BRAIN. 44
FIGURE 14 FCM WITH 3 - 6 CLUSTERS. 45
FIGURE 15 FCM WITH 7- 10 CLUSTERS. 46
FIGURE 16 FCM'S PIXELS COUNT BY CLUSTER. 47
FIGURE 17 CUMULATIVE CHANGE PLOT FOR FCM WITH 3 CLUSTERS. 48
FIGURE 18 CUMULATIVE CHANGE PLOT FOR FCM WITH 4 CLUSTERS. 48
FIGURE 19 CUMULATIVE CHANGE PLOT FOR FCM WITH 5 CLUSTERS. 49
FIGURE 20 CUMULATIVE CHANGE PLOT FOR FCM WITH 6 CLUSTERS. 49
FIGURE 21 CUMULATIVE CHANGE PLOT FOR FCM WITH 7 CLUSTERS. 50
FIGURE 22 CUMULATIVE CHANGE PLOT FOR FCM WITH 8 CLUSTERS. 50
FIGURE 23 CUMULATIVE CHANGE PLOT FOR FCM WITH 9 CLUSTERS. 51
FIGURE 24 CUMULATIVE CHANGE PLOT FOR FCM WITH 10 CLUSTERS. 51
FIGURE 25 FIRST DERIVATIVE OF POLYNOMIAL CURVE OF CUMULATIVE CHANGE OF DEGREE 8 AND 3 CLUSTERS. 52
FIGURE 26 SECOND DERIVATIVE OF POLYNOMIAL CURVE OF CUMULATIVE CHANGE OF DEGREE 8 AND 3 CLUSTERS. 53
FIGURE 27 COMPARISON OF FCM'S PIXELS' VALUES BEFORE AND AFTER SMALL AREA FILTERING. 55
FIGURE 28 FCM WITH 3 - 6 CLUSTERS AND SMALL AREA FILTER. 56
FIGURE 29 FCM WITH 7 - 10 CLUSTERS AND SMALL AREA FILTER. 57
FIGURE 30 OTSU WITH 3 - 6 CLUSTERS. 58
FIGURE 31 OTSU WITH 7 - 10 CLUSTERS. 59
FIGURE 32 OTSU'S PIXELS COUNT BY CLUSTER. 60
FIGURE 33 CUMULATIVE CHANGE PLOT FOR OTSU WITH 3 CLUSTERS. 61
FIGURE 34 CUMULATIVE CHANGE PLOT FOR OTSU WITH 4 CLUSTERS. 61
FIGURE 35 POLYNOMIAL CURVE FOR OTSU WITH 5 CLUSTERS. 62
FIGURE 36 CUMULATIVE CHANGE PLOT FOR OTSU WITH 6 CLUSTERS. 62

FIGURE 37 CUMULATIVE CHANGE PLOT FOR OTSU WITH 7 CLUSTERS. 63
FIGURE 38 CUMULATIVE CHANGE PLOT FOR OTSU WITH 8 CLUSTERS. 63
FIGURE 39 CUMULATIVE CHANGE PLOT FOR OTSU WITH 9 CLUSTERS. 64
FIGURE 40 CUMULATIVE CHANGE PLOT FOR OTSU WITH 10 CLUSTERS. 64
FIGURE 41 FIRST DERIVATIVE OF POLYNOMIAL CURVE OF CUMULATIVE CHANGE OF DEGREE 8 AND 9 CLUSTERS. 65
FIGURE 42 SECOND DERIVATIVE OF POLYNOMIAL CURVE OF CUMULATIVE CHANGE OF DEGREE 8 AND 9 CLUSTERS. 66
FIGURE 43 COMPARISON OF OTSU'S PIXELS' VALUES BEFORE AND AFTER SMALL AREA FILTERING. 68
FIGURE 44 OTSU WITH 3 - 6 CLUSTERS AND SMALL AREA FILTER. 69
FIGURE 45 OTSU WITH 7 – 10 CLUSTERS AND SMALL AREA FILTER. 70
FIGURE 46 K-MEANS WITH 3 – 6 CLUSTERS. 71
FIGURE 47 K-MEANS WITH 7 - 10 CLUSTERS. 72
FIGURE 48 K-MEANS PIXELS COUNT BY CLUSTER. 73
FIGURE 49 CUMULATIVE CHANGE PLOT FOR K-MEANS WITH 3 CLUSTERS. 74
FIGURE 50 CUMULATIVE CHANGE PLOT FOR K-MEANS WITH 4 CLUSTERS. 74
FIGURE 51 CUMULATIVE CHANGE PLOT FOR K-MEANS WITH 5 CLUSTERS. 75
FIGURE 52 CUMULATIVE CHANGE PLOT FOR K-MEANS WITH 6 CLUSTERS. 75
FIGURE 53 CUMULATIVE CHANGE PLOT FOR K-MEANS WITH 7 CLUSTERS. 76
FIGURE 54 CUMULATIVE CHANGE PLOT FOR K-MEANS WITH 8 CLUSTERS. 76
FIGURE 55 CUMULATIVE CHANGE PLOT FOR K-MEANS WITH 9 CLUSTERS. 77
FIGURE 56 CUMULATIVE CHANGE PLOT FOR K-MEANS WITH 10 CLUSTERS. 77
FIGURE 57 FIRST DERIVATIVE OF POLYNOMIAL CURVE OF CUMULATIVE CHANGE OF DEGREE 4 AND 4 CLUSTERS. 78
FIGURE 58 SECOND DERIVATIVE OF POLYNOMIAL CURVE OF CUMULATIVE CHANGE OF DEGREE 4 AND 4 CLUSTERS. 79
FIGURE 59 COMPARISON OF K-MEANS PIXELS' VALUES BEFORE AND AFTER SMALL AREA FILTERING. 81
FIGURE 60 K-MEANS WITH 3 - 6 CLUSTERS AND SMALL AREA FILTER. 82
FIGURE 61 K-MEANS WITH 7 - 10 CLUSTERS AND SMALL AREA FILTER. 83
FIGURE 62 OUTPUT SLICES OF BRAIN EXTRACTION. 85
FIGURE 63 BRAIN'S SKULL AND ARTERIES 3D MAP. 86
FIGURE 64 BRAIN'S ARTERIES 3D MAP. 87
FIGURE 65 3D MAP OF BRAIN'S SKULL, ARTERIES, AND DRUG DELIVERY BEST PATH. 88
FIGURE 66 3D MAP OF BRAIN'S ARTERIES, AND DRUG DELIVERY BEST PATH. 89

INDEX OF IMAGERY AND ABBREVIATIONS

DDS: Drug Delivery System

FCM: Fuzzy C-Means

1. INTRODUCTION

While this thesis is mainly preoccupied with drug delivery systems (DDSs) for its subject matter, it is imperative to mention that the DDSs intervene at a developed stage in the complex therapeutic process, which starts with a malfunctioning body. Therefore, it is necessary to provide an overview of the remaining and interconnected elements of the curative equation, namely diseases, drugs, therapy, the circulatory system, and DDSs. To this end, this thesis provides simple definitions of the elements and locates each of them within the context of healing.

2. Diseases and Therapy:

To put the concept of disease in perspective, it is effective to define what the concept of health generally means. In their 2017-article, Svalastog, A. L., Donev, D., Kristoffersen, N. J., and Gajović, S. define health as a correlative status, under which individuals can properly function on the physical, social, mental, and spiritual levels, in a manner that allows them to display the entirety of their distinctive capabilities within their surrounding environment [1]. This status is one side to a "spectrum" to professor of biostatistics Mirjana Kujundžić Tiljak, who places illness at the opposite side, demonstrating that individuals throughout their lives tend to shift between states of "wellness and optimal functioning" to "illness culminating in death" [2]. Therefore, illness is the opposite of health, and a deeper level, is unwellness and hamper functionality or altogether dysfunctionality.

In their 2019 article, Anna-Henrikje Seidlein and Sabine Salloch list several concepts and terms that, though distinctive in nature, are used interchangeably to refer to the state of disrupted health. These include the "concept of illness" and relevant ideas such as disease and sickness, in addition to terms "such as injury, malady and disability" [3], in addition to impairments and syndromes. As a linguistic expression of this disruption, this set of concepts and terms describes an abnormal condition, which affects the body or the mind of a person. Under this condition, the affected person might experience one or several symptoms, including pain, fatigue, or a reduced ability to perform a wide range of activities, usually done with ease, as well as aberrant behaviors, or unusual changes in structure and function.

It is worth noting that, while all these terms are routinely used describe physical alterations and mental symptoms, diseases remain the most established at the level of definitions, branching out into a wide variety of classifications and types.

2.1. Classifications and Types of Diseases

Classification helps diagnosticians and physicians to obtain statistics on the underlying causes of an illness, as well as consequent rates of mortality among affected persons. While it is a key statistical tool, various factors play into the process of classification of diseases, among which are the course of alteration the disease imposes on an organ, and the targeted organ itself. Classification approaches resulted in five major paradigms [4]:

- **Anatomic Classification:** This category derives its properties from the organ or tissue impacted by the illness, often having the name of the organ, which operations are disrupted, and includes heart diseases. Such single-organ diseases are addressed by specialized medical professionals, a cardiologist in the case of heart issues [5].

- **Topographic Classification:** Rather than an organ, it is the whole area affected that gives this category its name and properties. Under this classification, categorized are cardiovascular diseases, chest diseases, gastrointestinal illnesses, and abdominal diseases. Treatment in these cases is the domain of medical subspecialties with expertise on the affected areas [6].

- **Physiological Classification:** This category derives its name from the manner in which the diseases interfere with a process or a function, affecting metabolism, digestion, or respiration for instance [7].

- **Pathological Classification:** For this category, the fundamental characteristics of the illness are at heart of the process of classification, in addition to the causes and the effects of the diseases. One such disease is cancer, which is mainly characterized by the uncontrolled proliferation of cells [8].

- **Epidemiological classification**: This category is built on the rate at which a disease occurs, the way it spreads and is distributed within a population, and the manner in which it is controlled [9].

Like classification, the process of typification is contingent on several factors, including the manner with which certain diseases manifest and the properties they have in common. There are four major types:

- **Infectious diseases:** Diseases typified as infectious are those caused by the entry of foreign germs into the body. Relating to the scale of risk, significant variations in severity have been registered under infectious illnesses, which in some are acute and can even be deadly. Microorganisms, including viruses, bacteria, fungus, and parasites, are the most prevalent causes of such diseases. Additionally, infectious diseases are contagious, often spreading from one person to another by bug bites, consumption of tainted food or drink, or sexual interaction [10].

- **Deficiency diseases:** These diseases are triggered by a lack of essential nutrients or elements, such as vitamins and minerals. These conditions may be prevented through commitment to balanced diet that must also be comprehensive of all nutrient elements the body needs [11].

- **Hereditary illnesses:** These diseases are disorders caused by mutations in specific genes or chromosomes, transferred from parent to child, while some tend to be non-dependent to genes [12]. When the case is genetic, the condition, inherited from one or both parents, might affect several members of a patient's immediate family. Achondroplasia and Marfan syndrome are both examples of hereditary illnesses.

  On the other hand, there are hereditary conditions that do not involve a specific gene mutation or genetic defect. These conditions are referred to as non-genetic hereditary disorders. These disorders emerge when the body is affected by a shift in the surrounding environment, or an infection caused by a particular virus.

- **Physiological illnesses:** These are conditions that patients develop due to dysfunction in one or more organs. These illnesses include diabetes, cancer, asthma, and heart conditions. Two scenarios govern the occurrence of physiological disorders. Some disorders occur when the body's normal or

proper functioning is disrupted due to a malfunction or inoperability of organs. Others happen when the actual cellular structures change over time, eventually causing the disease [13].

2.2. Medication Therapies

As diseases vary, courses of treatment also do. Medical professionals opt for either surgery, radiation, movement or pharmaceuticals, with the latter often being referred to as medication therapy, pharmacotherapy, or pharmaceutical care. In their 1990 article [14], Charles Heplhr and Linda Strand define the term, and explain the purposes it aims to achieve and how it is applied. They posit that it is "the responsible provision of drug therapy" to realize results that boost the quality of a patient's life. They add that drugs, thus, are delivered to achieve either of the following results: treat a disease; mitigate or eradicate symptoms, inhibit or curb the progress of a disease, or ward off a symptom or a disease. They highlight that decisions as to the pharmaceutical care are made jointly by a pharmacist, other health professionals, and patients themselves, who cooperate to come up with a therapeutic plan, implement it, and keep tabs on its progress.

Additionally, as a mode of therapy pharmaceutical care essentially revolves around determining which medications to apply. Central to making that decision are several related processes, which include analyzing the patient's current pharmaceutical regimen. This analysis provides doctors with indicators that demonstrate whether the chosen drug meets the recipient's needs or not. Later processes include prescribing and/or administering the medicine and monitoring the effects and side effects of the drug being used on the patient's mental and physical health [15].

Notably, medication-based therapies are of two types:

2.2.1. Invasive therapies:

An invasive treatment is a medical procedure in which the doctors' channel the medications into the body directly, by either cutting or puncturing the skin or inserting various types of medical equipment to target areas.

This course of action is widely used. A 2019 study by Sian Cousins, Natalie S Blencowe, and Jane M Blazeby documents that at least 230 million invasive procedures are carried out every year all over the world. However, the authors anticipate an acute increase in the deployment of the measure, with a growing

number of medical professionals prioritizing minimally invasive, image-guided procedures [16].

Notably, minimal invasive therapy has both benefits and downsides. On the one hand, this mode of therapy provides many benefits to patients and doctors. Through this measure, doctors improved surgical site visibility, thus smaller incision size and a quicker closure, which, in turn, leaves patients less scarring. In addition to the practical sides, the much-improved visualization minimally invasive surgery provides is a vital educational tool. On the other, even though endoscopic surgery has often resulted in significant cost savings for human medical practices, acquiring equipment alone has been registered as an extremely costly measure. Equipment procurement costs are not the only expenditures involved, for there also the costs of extra supplies necessary for each case, and operational costs. These downsides, the higher learning curve and the difficulties that come along have been discouraging surgeons from using the minimally invasive surgery technique on a large scale [17].

2.2.2. Non-invasive therapies:

Contrary to the invasive measure, "non-invasive therapy" refers to a conservative treatment that does not involve skin incisions or tissue removals. Medical professionals recommend this course of treatment for a wide range of conditions, including the treatment of backaches. To ease the patient's pain, the overseeing doctor applies a combination of non-surgical therapies, such as chiropractic care, physical therapy, and heat therapy. These treatments are often performed on patients over the course of several weeks. This course of treatment is used when pain management is the main goal. Therefore, it has been gaining more popularity and replacing several invasive surgeries [18].

In addition to safety, or lesser risks for patients, non- invasive therapies offer several advantages, including higher rates of acceptability and adherence to the designed regiment [19]. Away from patients, this therapeutic course of action has been registering a reduction in healthcare costs.

2.3. Drugs

While non-invasive drug delivery therapies promise to optimize medical and healthcare services, and of course patient wellbeing, these therapies function in nexus with drugs and the human circulatory systems. For their part, drugs, also referred to as medications, are chemical substances which, after being ingested by the body, can perform, or restore the normal activities of the affected organ.

Defined rather elaborately, according to Dictionary.com [20], a drug is "a chemical substance used in the treatment, cure, prevention, or diagnosis of illness or used to promote physical or mental well-being." Among the other various and vital uses of drugs there is also the improvement of physical or mental health. Physicians prescribe medications for long-term and consistent periods or for a predetermined interval, based on the type of the disease, including whether it is chronic or not, as well as the independent case of each patient. Drugs are channeled into the body in many ways:

- **Oral Route:** due to its unassailability, inexpensiveness, and suitability, the oral route remains the most used path compared to other administration methods. Tablets, drinks, and pills are examples of many drugs that can be given by mouth through the digestive tract. There are two ways the body absorbs the medication: The stomach and the mouth absorb a few drugs, whereas the small intestine absorbs most drugs.

  When administrated orally, the drug spreads across the body when absorbed by the mouth and stomach, which absorb only a few types of drugs, while the small intestine absorbs most of the types.

  The drug first passes through the intestinal wall, then travels to the liver, and finally is transported through the blood to its targets. The intestinal wall and liver chemically alter many drugs to reduce the amount that reaches the blood.

  Considering the factors that affect drug absorption, when delivered orally, it is recommended that patients take drugs on an empty stomach, with no food or other medications. Such factors include the food in the gastrointestinal tract, gastrointestinal emptying time, interaction with other substances, the potential of hydrogen, and membrane permeability.

Most oral dosages are used to produce systemic effects that result from drug absorption across the mucous membrane of the gastrointestinal tract. Occasionally, oral medications are used to give local effects on the intestinal gastrointestinal tract [21].

- **Parenteral Route:** A syringe injects the drug directly into the body. Administrating drugs to patients through injections is used in many cases [22]:
    - When the drugs used are not well absorbed in the intestine.
    - When the drugs used cannot tolerate the environment of the gastrointestinal tract.
    - When treated, patients are unconscious.
    - When a rapid start of the therapeutic effect is needed.
    - When a specific concentration of the drug must be maintained inside the body.

  The parental route disadvantages are the fact that the injected drugs cannot be retrieved or undone, cause pain and fear for patients, and damage the tissues at the injection site.

  The injection is applied to the body in many ways:

    - **Intravenously:** it is the most commonly used parenteral method, especially for drugs that cannot take orally. Intravenous injection has several advantages, as it allows the drug to be delivered directly into the systemic cycle, which ensures a quick start of the pharmacological effect and tight control of the drug level in the blood plasma.

      The disadvantage of this way is the possibility of it being faulted, and the injection causes the sedimentation or decomposition of blood components.

- **Intramuscularly:** It is an injection of a substance into a muscle. This method is preferred over other methods because the muscle is more extensive and has many blood vessels, which speeds up the absorption of the drug.
  Common sites for intramuscular injection are the triangularis muscle of the shoulder and the gluteus maximus muscle in the lower extremity. For infants, the injection is usually done into the vastus lateralis.

- **Intradermal:** It is an injection into the fatty tissue just under the skin, requiring less depth than intramuscular injection. Such injections are usually used for medicines that must be administrated slowly and continuously into the bloodstream because there are fewer blood vessels in the fatty layer of subcutaneous connective tissue compared to muscle tissue.

- **Subcutaneous:** It is an injection an injection into the subcutaneous tissue to the located layer directly under the dermis and the epidermis.

As shown in **Figure 1** the insertion angles of the syringe into the body of parenteral drug administration: intramuscular, subcutaneous, intravenous, and intradermal [23].

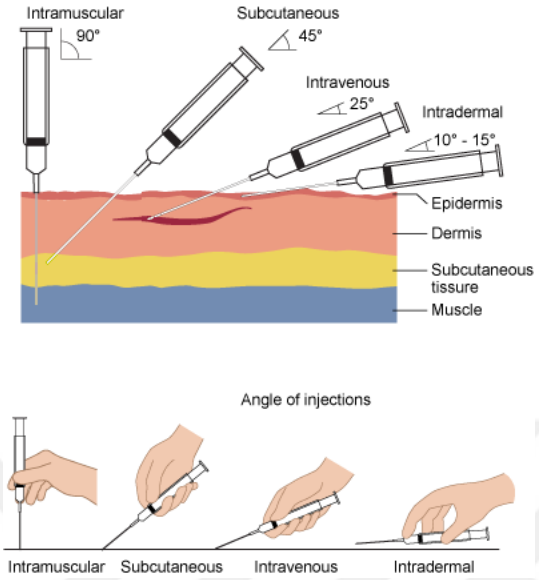

Figure 1 Angles of insertion of parenteral drug administration.

- **Buccal Route:** In some cases, the oropharyngeal can bend concave to organismic colicky and shrivel up. In this case, absorption allows the drug to dissolve within the oral cavity while avoiding ingestion (or swallowing only a tiny amount of it). This process can be carried out using suppositories that have a high solubility in water in the form of uncoated tablets [24].

- **Rectal Route:** Using the rectum to give drugs or some other fluids to provide local effects, where the drug is absorbed by the rectum's blood vessels and then carried into to the circulatory system, which transports it to the body's organs and systems.
  Compounds absorbed in the lower rectum avoid hepatic first metabolism passage compared to compounds absorbed in the upper rectum. Therefore, rectal absorption is usually slower than oral absorption. However, rectal absorption tends to be superior to oral absorption because it is capable of avoiding the first hepatic passage after rectal delivery for some drugs [25].

- **Ocular Route:** The ocular route is used to administer a drug made of liquid or gel into the eye to treat illnesses and diseases. However, gels and ointments could cause side effects, including blurry vision, when a medicine requiring an extended period of contact with the eye's surface is used. This method can be challenging when the drugs administrated into the eye must be released continuously and slowly.
  Because of their topical effects, physicians always opt for ophthalmic medications. Fake tears are among the drugs used to treat dry eyes [26].

- **Inhalation Route:** It is sprayed into the nose, absorbed through the nasal membranes, and inhaled into the lungs, usually by mouth (by inhalation) or mouth and nose (by mist).
  When the substance is inhaled, it is exposed to the membranes of the nose, mouth, pharynx, trachea, bronchi, and pulmonary alveoli. The lung has an absorption surface area of about 11 square meters, which is greater than the absorption surface of the small intestine. So, if we can deliver substances to the surface area of the lung, the absorption will be very efficient.
  The respiratory route is beneficial for treating asthma problems, such as salbutamol sulfate aerosols. Recently, interest in the respiratory route has increased, and it is used to administer therapeutic agents prepared with the help of biotechnology [27].

- **Dermal Route:** Drugs are applied topically to the skin for a systemic effect, including the drugs used on the skin to provide local effects. Among these are antiseptics, antifungals, anti-inflammatory agents, and skin emollients.
  Skin absorption is often weak. However, several skin patches are used to administer transdermal medication and obtain systemic effects, such as the nitroglycerin patch used to prevent and treat myocardial infarction. Pharmaceutical topical preparations include semisolid pharmaceutical forms, including ointments, creams, and pastes, and liquid forms, such as

solutions and lotions. Or solid in the form of a powder for medicine, such as some antifungals [28].

- **Vaginal and Urethral Route:** In some cases, drugs can be inserted through the vagina or urethra to obtain topical local effects by using suppositories (vaginal eggs), tablets, or lozenges. However, good systemic absorption in the vagina and the ability of the vagina to hold administration devices affect many types of vaginal dosage forms, especially in hormonal contraceptives.
  As for the urethral route, the administration of drugs is limited to suppositories and solutions.
  Some systemic effects may occur after vaginal or urethral administration due to drug absorption through the mucous membranes at the drug administration sites [29].

Notably, while drugs play a major role in the curative process, they continue to pose challenges and sometimes risks, depending on the course of therapy applied. For instance, common approaches to cancer treatment include “tumor surgery, chemotherapy, and hormonal treatment” [30]. However, each of these treatments has intrinsic limitations. In the case where chemotherapy is applied, researchers discovered that the anti-cancer drug often spreads across the body at a rapid rate, affecting both tumorous cells and healthy ones, while having no effect on metastatic cancer cells. To counter these effects, physicians are opting for non-invasive methods, using several DDSs that both “target tumor cells, and release active biomolecule at specific site”.

2.4. Human Circulatory System:

The other element in this nexus is the circulatory system, which is an organ network that includes the heart, lymphatic system, blood vessels, and blood. It distributes throughout the human body and includes two sections: systemic and pulmonary circulatory [31].

Running across the human body, the “circulatory system” is a web of organs that mainly either channel or pump blood. Called interchangeably as the “cardiovascular” or the “vascular” system, this intricate circuit encompasses several organs, no less complicated in their structure and purpose, notably the heart and the blood vessels, in addition to the complementary lymphatic system.

Supplying blood for the cells, this system operates through two “pathways” or “circuits”, namely the “pulmonary” and the “systemic”. Each of these circuits carries distinctive operations related to transferring oxygen-rich or –poor blood from two different sets of organs. While the former threads the lungs and the heart, the latter connects the heart and tissues.

The “systemic circuit” conveys blood, high in oxygen and nourishing substances, from the heart to the cells. Running in the opposite direction, this circuit also takes blood, full of carbon dioxide, back to the heart.

The “Pulmonary circuit”, traversing a shorter distance, first carries deoxygenated blood to the lungs, absorbing oxygen and excreting carbon dioxide, and then conveys the fresh supply to the heart.

Figure 2 shows the human circulatory system (simplified). Red indicates oxygenated blood carried in arteries. Blue indicates deoxygenated blood taken in veins. Capillaries join the arteries and veins.

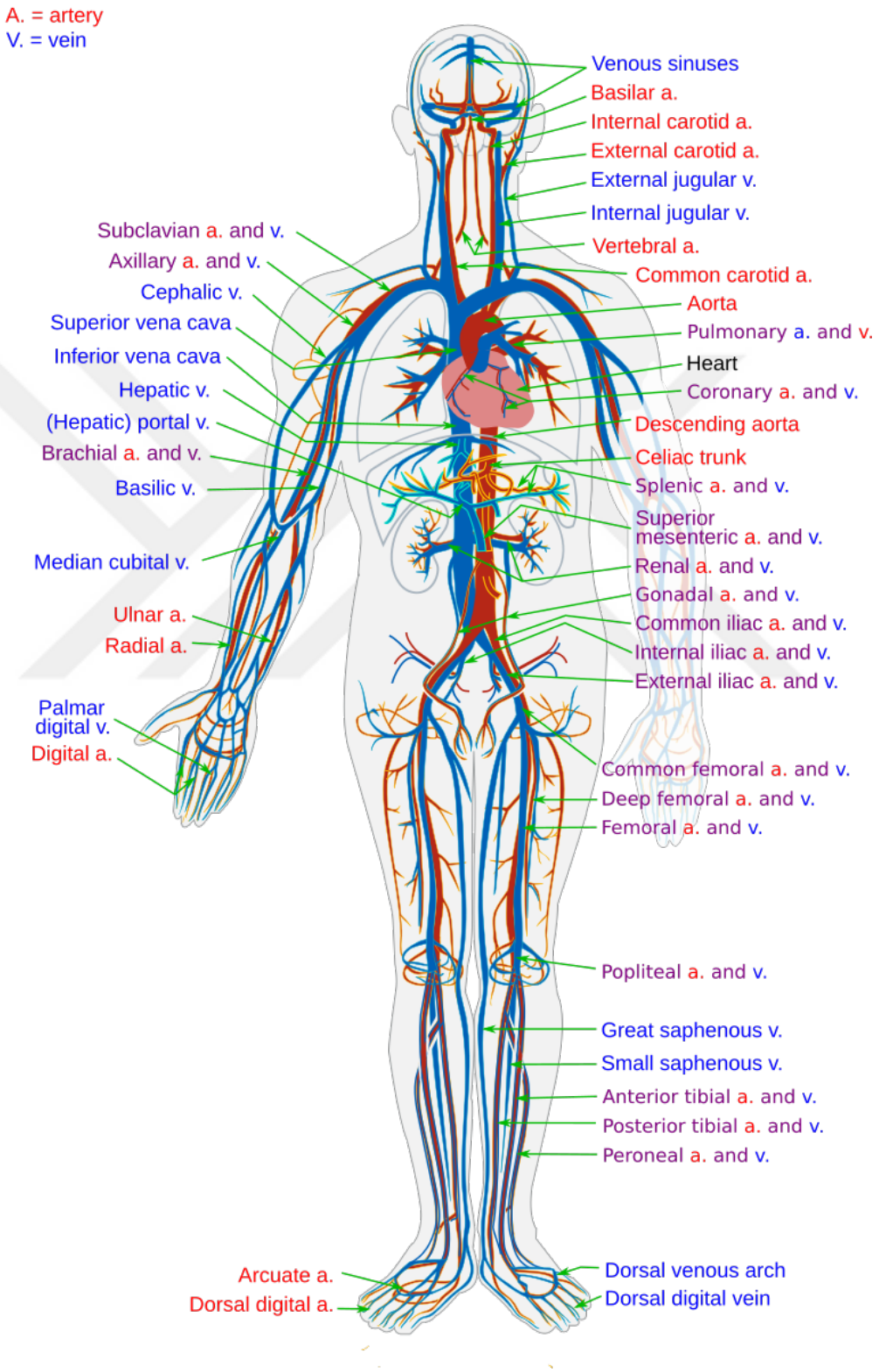

Figure 2 The human cardiovascular system.

The human “circulatory system” incorporates four key constituents:

1. **Heart:** It consists of several layers, with a multi-layered “wall” of firm muscular tissues engulfed with a thinner covering called the “pericardial membrane” that is naturally fibrous. It is located in the chest cavity, between the lungs, with a minor tilt to the left.
   In terms of structure, the heart splits into four chambers. The upper two chambers are known as “atria”, and the lower two as “ventricles”.

2. **Blood:** Blood is the liquid tissue that interfaces the body. Its primary role is transporting hormones, minerals, nutrients, and other vital elements throughout the body. Blood passes around through a mesh of conduits known as “blood vessels” and is pumped by the heart blood to different body areas. The components of the human blood are blood cells, proteins, plasma, and other mineral ingredients.
   There are three types of blood cells:

- **Red Blood Cells:** RBCs absorb oxygen in the lungs and release it into tissues as they cram through the body's veins.
- **White Blood Cells:** WBCs are immune system cells that help to protect the body from infectious illnesses and external intruders.
- **Platelets:** are the component that clumps in response to bleeding from the damaged blood vessels.

3. **Blood Vessels:** They operate as a grid of paths, bear blood within the body, and are divided into two function-based types, arteries, and veins.
   On the one hand, arteries are blood channels that transfer oxygenated blood from the heart to the rest of the body. They are thick and flexible, creating a small network known as capillaries. While all arteries’ heads from the heart are aimed at other organs full of oxygen, the pulmonary arteries are an exception, carrying deoxygenated blood to the lungs. Veins, on the other, are blood channels that transport deoxygenated blood from various regions of the body to the heart. They are thin, flexible, and near to the skin's surface.

However, only the pulmonary and umbilical veins transport oxygenated blood throughout the body.

4. **Lymphatic system:** Of a fluid nature like blood, the lymph contributes to the human circulatory system. The lymph is produced by the lymphatic system, which comprises interconnecting organs, nodes, and ducts. Lymph is a colorless fluid made up of water, proteins, and salts that carries and circulates digested food and absorbs lipids into tissue intercellular spaces. Unlike the circulatory system, lymph travels passively through a network of channels rather than being pushed out.

   Notably, the circulatory system is the initial target of drugs admitted into the body. It is pivotal to any treatment because it spreads drugs across its channels and into the different organs while also contributing to absorption.

2.5. Drug Delivery Systems:

Considering the advantages and disadvantages, both the healthcare system and the pharmaceutical business have placed a considerable emphasis on drug delivery systems (DDSs). Therefore, they continue to invest massive efforts into the production of medications, while developing new effect-tracking mechanisms, as well as improving existing DDSs or comping up with new ones.

The delivery technology has been attracting the interest of an increasing number of researchers, who have been expanding the scope of therapeutics. These researchers have dedicated studies to several issues that remain challenging, including drug delivery into sensitive tissue, such as the brain, retina, and spine.

Drugs today are administrated into the body through a variety of ways, whereby medical professionals' resort to transmucosal, topical, non-invasive peroral, and inhalation routes.

While conventional approaches still hold oral administration as the most effective technique, progress in medical research has successfully brought up alternatives, which managed to expedite the process of healing in many health conditions.

The treatments of disorders of the nervous system and cancer have particularly benefited greatly from these recent developments in drug delivery systems. The new means of administration reduced likely adverse effects of the pharmaceuticals, as well as the damage they produced to the cells and tissues.

Drug administration strategies that make use of the surrounding physical environment, such as light, electricity, ultrasonic, and magnetic fields, have been among the most explored and suggested techniques in recent years.

Notably, these intelligent drug delivery systems promise to provide targeted specificity, controlled release, and the capacity to traverse biological barriers. Due to these characteristics, these systems improved therapeutic benefits while lowering systemic adverse effects in a variety of courses of treatment, particularly in cancer treatment.

The Wenlu et al. study benefited from the development of nanosized drug delivery systems and the advances in treating tumor hypoxia, which has increased the effectiveness of anti-tumor treatment. The study summarized various strategies to mitigate tumor hypoxia to improve the efficacy of anti-tumor therapies such as chemotherapy, radiotherapy, phototherapy, and immunotherapy. The techniques include increasing oxygen supply, decreasing oxygen consumption, and inhibiting HIF-associated signaling pathways based on nanosized drug delivery systems [32].

3. LITERATURE REVIEW

The thesis focuses on targeted drug delivery systems (DDSs), particularly ones that hinge on image segmentation methods. However, as it ventures to propose a new technique of incorporating image segmentation into the meditative process, it builds on and from the various techniques available and already in use.

Therefore, this section first introduces a number of DDSs in use, the core elements they are made of, and the approaches applied though them for a targeted administration of drugs. As it does so, this section highlights the advantages and the disadvantages of the DDSs listed, marking even the places where they converge and where they diverge, while backing the discussion with recent studies that demonstrate the effects or under-effects of each. Some of the DDS exhibited are ultrasound or magnetic based.

Since image segmentation is central to the thesis, this section will also describe the most commonly used methods, delve into their operation dynamics, and the value they add to drug streaming process.

Notably, all DDS discussed in this section function in a non-conventional context, whereby the drug delivery operation aims to boost the concentration of the drugs in some body parts but not others, particularly aiming at damaged tissue while avoiding hampering the health of non-affected ones. In detail, the purpose of deploying DDSs, also known as smart delivery systems, is to lengthen, confine the effect to an exact location, target, and have a safe drug interaction with the tissue needing treatment.

The location of injection for a drug delivery system refers to the specific area of the body where the medication is administered. It is important to give the injection in the right place to make sure that the medicine is absorbed properly and gets to where it needs to go in the body. When administering cancer medications, the importance of the injection site can be clearly explained; these drugs are frequently designed to target specific areas of the body where cancer cells are present. On the one hand, if a medication is designed to target cancer cells in the liver but is injected into a muscle instead, it may not reach the liver in sufficient quantities to be effective. On the other hand, if the medication is injected into a vein, it may be more likely to reach the liver, but it may also be more likely to cause side effects throughout the rest of the body. Therefore, it is important for healthcare

providers to carefully consider the location of injection when administering cancer medications to optimize the balance between effectiveness and safety.

3.1. Types of Targeted Drug Delivery Systems

DDS differ largely from conventional means of drug administration, which depend on the absorption of the drug across cells. Unconventionally, DDs administrates drug in the form of dosage, which results in a set of advantages. The advantages include cutting down the dosage frequency, maintaining a stable effect while minimizing the side-effects of the drug use, and controlling the levels of the circulating.

3.1.1. Ultrasound

Ultrasound-based DDSs remain among the most novel and noninvasive modes, which have been proven effective in enhancing the delivery of a variety of therapeutic agents, including proteins, small chemical and chemotherapeutic agents, as well as genetic substances. In the rather traditional uses, ultrasonic waves are deployed for diagnostic ends, like imaging, and for only a few therapeutic ends, including “kidney stone disruption, liposuction, and tissue heating”. However, the recent boom in technological research had turned ultrasound into a highly efficient element with methods of targeted delivery of therapeutic agents. [33] For instance, high-intensity focused ultrasound (HIFU) has been widely studied and has proven extremely helpful in treating various malignancies through hyperthermia, while found quite adept in generating stroma in the cell membrane and increasing medication ingestion. [34]

In their 2018 research, Somoshree Senguptaab and Vamsi K. Balla examine the impact ultrasound has on cancer cells. However, before delving into some of their findings, it is important to define the nature of cancer and how it continues to be challenging at the therapeutic level. Cancer, as a term, is commonly used to refer to many illnesses affecting many body regions, with a key distinctive aspect of the rapid formation of aberrant cells that expand beyond their usual borders, being able to infiltrate neighboring body parts and migrate to other organs. This latter process is known as metastasis. It is noteworthy that cancer is a prominent cause of mortality in more and less economically developed nations, while its burden is predicted to expand globally owing to population growth and aging, particularly in less developed

countries, which have around 82% of the world's population. Smoking, poor food, physical inactivity, and reproductive changes are some of the many known reasons that raise cancer risks and have increased the cancer burden in less economically developed nations. [35] Cancer continues to be a challenge because malignancy medications are typically hampered by poor specificity and associated worries about toxicity, while other factors also threaten to jeopardize their therapeutic benefits, including low concentrations at tumor sites and drug resistance.

Several of the restrictions and the hazards of conventional therapeutic approaches are overcome by HIFU, which, according to Sengupta and Balla, has been showing remarkable potentials in lessening tissue damage and, thus, increasing the rates of “disease free survival of the patient” [33]. These advantages have been clinically assed by several researchers, including Gelet et al., who examined the effects of the approach in patients of prostate cancer, with a focus on the approaches’ efficacy and safety. The researchers reported observing no remaining tumorous cells in 56% and local control of localized prostate cancer” in 80% of the patients, while assessing a cluster of 50 patients.[36]

3.1.2. Milk exosomes

In addition to ultrasound, research has been experimenting with a new sensitive drug delivery method for cancer treatment. This method is based on milk exosomes. Exosomes have been found promising in this domain for serval reasons, especially the fact that they are generated from bovine milk, which guarantees that the supply is abundant. Additionally, exosomes have the advantages of both synthetic and cell-mediated micro-carriers. In one experiment, carried out by Zhang et al., the researchers created a pH/light-sensitive medication system based on milk exosomes for oral squamous cell carcinomas treatment. They linked milk exosomes to doxorubicin via a pH-cleavable connection that can rupture in an acidic environment, and loaded endoperoxides and chlorin e6 with the endoperoxides, undergoing thermal cycloreversion and releasing singlet oxygen, to destroy cancer cells. [37]

3.1.3. Nano-drug delivery systems

Nano-drug delivery systems (NDDSs) are promising anticancer therapy platforms with the potential for various enhancements in therapeutic agent distributions, behaviors, and performances, especially intelligent DDSs. Intelligent NDDSs are recognized as breakthrough because they have the potential to provide targeted specificity, controlled release, and the capacity to overcome biological barriers, resulting in better therapeutic benefits with fewer systemic adverse effects. The advancement of functionalized modules and materials, such as current biomaterials like peptides and nucleotides, has aided in the creation and investigation of numerous innovative delivery techniques. Stimuli-responsiveness to endogenous or exogenous variables allows for on-demand changes in vehicle structures or characteristics, allowing for spatial, temporal, or dosage-specific delivery. On the other hand, the various nano-drug delivery vehicles enable rational design based on appropriate therapeutic agents and pro-drugs, combinational treatments, and multi-responsive platforms.

The Wang et al. study concentrate on current advancements in nano-drug delivery systems. Therefore, the study emphasized the essential techniques and processes of bright drug loading and release for anticancer therapy and reviewed the existing delivery systems that enable these tactics. [38] The researchers focused on the creation of "smart" nanoparticles, which employs passive targeting tactics by integrating technical advances with protein chemistry, as well as and the physiological properties of the tumor microenvironment.

They found out that the increased permeability and retention (EPR) effect has the benefit of promoting preferred accumulation at the location of the tumor. The purpose of stimulus-responsive targeting is to cause a conformational change that releases the medication at the tumor location. Targeting and interacting precisely with molecules or receptors that are overexpressed on the surface of cancer cells is the objective of active targeting techniques. In the end, nanoparticles have shown a lot of promise for getting hydrophobic anticancer drugs to the tumor site without the immune system recognizing them, breaking them down, and storing them in the spleen, liver, and kidneys.

Therapeutic nanoparticles (NPs) have resulted in a breakthrough in cancer treatment precision medicine by combining diagnostic and therapeutic properties into a single nanoparticle to examine tumor characteristics and response to therapy in real time. Theranostic NPs need further research to be implemented in clinics. Although promising, there is yet no clinical use of NPs in the treatment of cancer. Despite the capacity of NPs to overcome various obstacles of conventional therapeutic therapies, NP formulation has problems with repeatability, mass manufacturing, and undesirable accumulation and clearance inside the body.[39]

Another investigation into NDDSs, experimented with the use of electricity, culminating in triboelectric nanogenerators (TENG). TENG have shown promise in self-powered controlled medication release and on-demand drug delivery. TENG has been widely used in biomedical research to power wearable and implantable devices due to its flexibility, lightweight, and biosafety benefits. TENG-based self-powered drug-distribution systems combine the benefits of traditional electrical-regulated drug administration with repetitive and spatiotemporally controlled release and remove the problems of frequent battery replacement or charging. Furthermore, because of TENG's flexible structural design and easy operation, this self-powered drug-delivery system is more comfortable and easier to handle for patients, which benefits the progress of customized medicine.

Zhirong Liu and Linlin Li used triboelectric nanogenerators (TENG) to study drug delivery systems through electricity. The study shows that monitoring of the signal may be wirelessly transferred, and big data can be produced to determine if various physiological indicators are typical, which is essential for diagnosing many diseases. As a result of merging real-time illness detection with on-demand drug administration, a closed-loop drug-distribution system is projected to be created. With the help of international researchers, self-powered drug-delivery devices offer significant promise for self-tuning medication administration and wearable and implantable medicine for customized healthcare.[40]

3.1.4. Magnetic-based drug delivery system

Magnetic drug targeting uses external magnetic fields to modify the body's magnetic drug carriers and enable them to reach target locations. However, an exemplary magnet system is required to guarantee successful magnetic drug targeting

through directing the drug carriers to the designated spot. A lot of studies about the magnetic-based drug delivery system have been published recently because of the benefits of reducing adverse effects, improving efficacy, and reducing drug dose.

One of the challenges to successful magnetic drug targeting has to do with how the carriers are guided and magnetic nanoparticle collections are concentrated in deep tissue in the human body using external magnetic fields from electromagnets. So far, no applied studies did test the magnet-based DDSs on human patients. However, in-vitro testing and simulations have demonstrated the possibility of dynamic control to overcome the challenge (Nacev et al. [41]; Shapiro et al. [42]). Studies by Nacev et al. and Shapiro et al addresses the targeting difficulty through constructing a dynamic model and a model-based control technique.

For their part, Qimin Liu et al. [43] focused on the issue of targeting through examining a 3D magnetic hydrogel-based drug targeting system. They explored the system using a magneto-chemo-hydro-mechanical linked model when exposed to a moving magnet. The model predicts the reactions of the hydrogel, such as fluid dispersion and flow, magnetic field distribution, magnetization, and finite deformation.

Additionally, the study evaluates the fluid-structure interaction between the magnetic hydrogel and the surrounding fluid flow through linked arbitrary Lagrangian-Eulerian method. Then, the study uses the multiphysics model to predict the movable and deformable behaviors of the magnetic hydrogel at two levels. First, the motion and deformation of the magnetic hydrogel under varying magnetic velocity, hydrogel radius, and fluid flow velocity. Second, the targeting-related performance of the drug-loaded magnetic hydrogel under different magnetic velocities. The experiment shows that a slower-moving magnet, greater hydrogel radius, and higher flow velocity can reduce the transit time of the hydrogel to the channel outlet. Moreover, by adjusting the magnet velocity and maximum magnetic field intensity, the magnetic targeting system was found as capable of achieving optimum performance for delivering the drug-loaded hydrogel to the targeted spot. The current multiphysics model is created to assist academics in designing and developing magnetic hydrogel-based drug targeting systems.

Figure 3 shows a graphical demonstration of the multiphysics model of magnetic hydrogel under a moving magnet for targeted drug delivery.

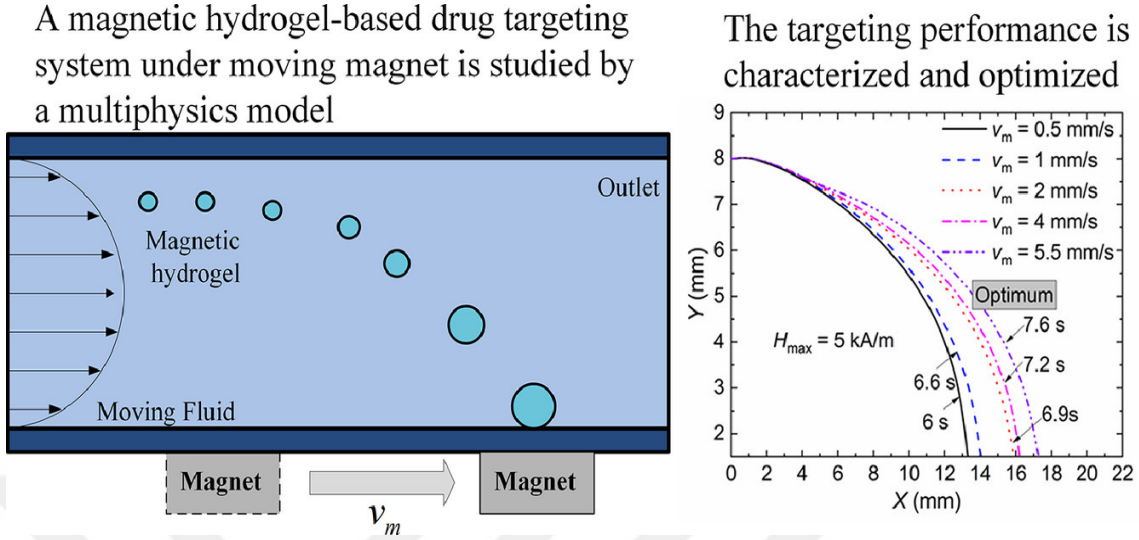

Figure 3 A multiphysics model of magnetic hydrogel under a moving magnet for targeted drug delivery.

Another study was carried out in 2022 by M. Abbes et al. [44]. The researchers proposed a system based on a robotized magnetic platform for targeted drug delivery for treating Cochlea disease. The researchers placed a magnetic actuator around the patient's head, which function is to direct magnetic particles within the Cochlea. With this, they managed to investigate the magnetic actuator's anatomical restrictions and functioning. Based on the results, they designed a tiny robotic manipulator to guide a magnetic actuator to all locations necessary for steering the magnetic particles inside the Cochlea.

Figure 4 shows a demonstration of the system's design of a robotized magnetic platform for targeted drug delivery in the cochlea.

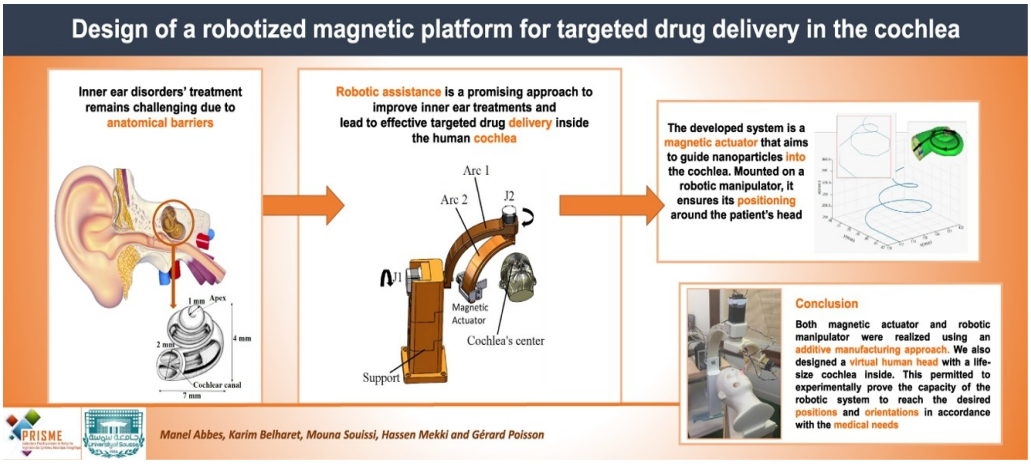

Figure 4 system design of a robotized magnetic platform for targeted DDS in the cochlea.

Notably, the position of the inner ear makes pulling the particles with an external magnet neither optimum nor applicable. Instead, the researchers' designed system uses a single permanent magnet, which consist of an actuator that combines four permanent magnets in a defined configuration.

The actuator generates five Lagrangian points, but only one is "stable" and allows the microrobot to be fixed in a particular location. When the position/orientation of the actuator alters, the magnetic fields and hence the position of the Lagrangian points shift. This magnetic actuator is unique because it has symmetrical behavior in the xz and yz planes, allowing for improved microrobot control.

Figure 5 shows the design of the actuator with four permutant magnetics.

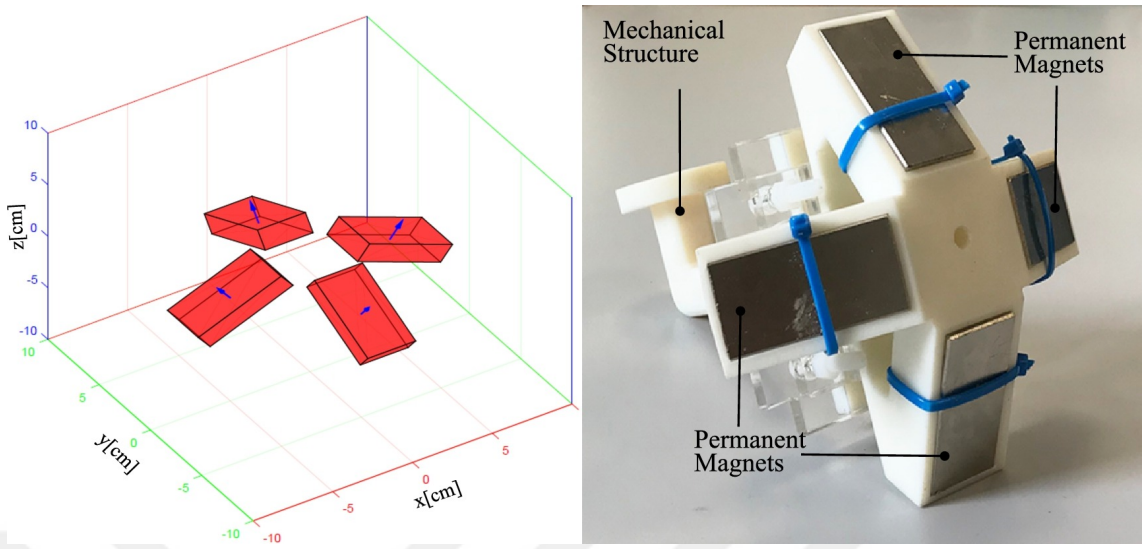

Figure 5 Four permanent magnets based actuator.

The push or pull forces are generated throughout a 2 cm region around the axis known as the actuating band. Any particle in this band converges towards the equilibrium zone, which means it can be pushed or pulled depending on its location relative to the Lagrangian point located 8 cm from the structure's center. The actuator of a magnetic microrobot must spin regarding the cochlea revolution axis to guide it along the helical route of the cochlea.

Figure 6 shows the vectors of magnetic forces created by a four-magnet actuator: (a) xz plane, (b) yz plane.

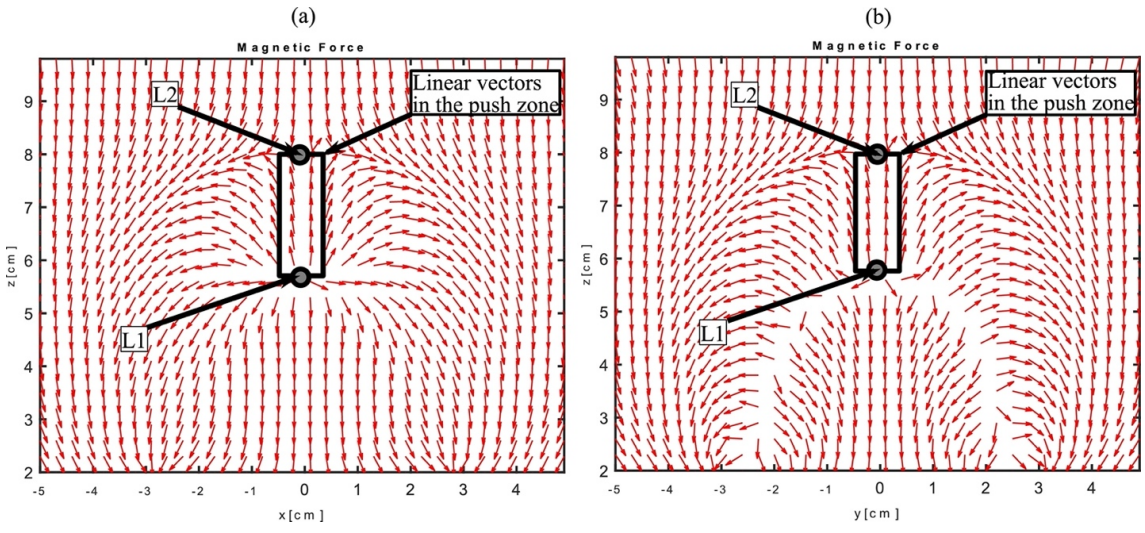

Figure 6 Magnetic forces vectors generated by four-magnets actuator.

Targeted medication administration is done through phases. First, the patient is placed on the operating table in a precise head position using a fixing appliance. Next, four markers are attached to the patient's head and used to adjust the robot's movement. The cochlea is then located, and its location and orientation in 3D space relative to the markers' frame are extracted using a Magnetic Resonance Imaging (MRI) scan.

The coordinates of the cochlea according to the four markers are provided by the 3D reconstructed picture. The patient is then moved to the operating room for the medication administration process. A tracking vision system is created and utilized to adjust to any possible head movements of the patient. It employs the marker's frame to determine the cochlea's location with the camera's frame. When the head moves with the vision system, the new location of the cochlea is detected and sent to the robot controller, allowing the trajectory to be redefined. This method will be continued until the patient's head stops moving. A magnetic actuator is also used to direct the cochlea's magnetic particles. The actuator's axis must be aligned with the particle displacement direction to push or pull particles in this direction. As a result, moving the actuator around the patient's head is required to accomplish the various directions.

Figure 7 show a prototype for the system of a robotized magnetic platform for targeted drug delivery in the cochlea.

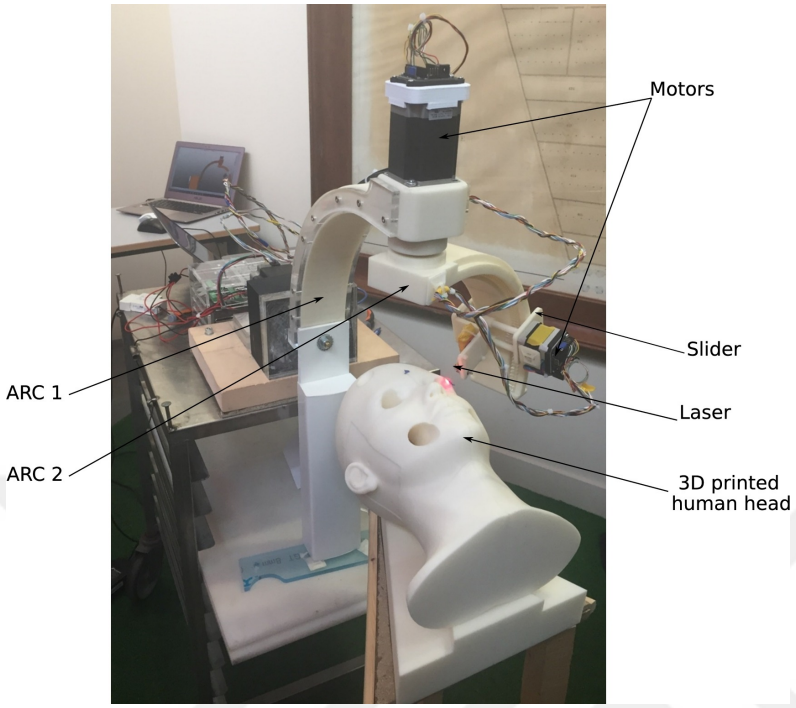

Figure 7 3D printed prototype for the system.

3.2. Medical Image Segmentation:

The clinicians' interest in examining interior anatomy in medical applications has attributed a key role onto medical images in the processes of diagnosis and therapy. Consequently, many techniques have been invented based on X-ray and cross-sectional pictures, such as Computed Tomography (CT), Magnetic Resonance Imaging (MRI), and other tomographic modalities.

For years, medical image processing has made significant contributions to medical applications, particularly in surgical domains, utilizing image segmentation, image registration, and image-guided surgery.

A variety of imaging modes deploy X-ray. While ancient X-rays were based on short wavelengths and high-energy electromagnetic radiation, a fairly recent application is computed tomography (CT). With CTs doctors use X-rays to scan inside organs and structures, transmitting X-ray pulses across the body, which creates multiple parallel slices of each organ.

Another new and highly used method is Magnetic Resonance Imaging (MRI). Using MRI, doctors utilize magnetic properties to obtain detailed information about interior organs.

All these applications function under the umbrella process of image segmentation, which remains is the most significant aspect of medical image processing.

Image segmentation is the procedure that separates the picture into multiple segments, which facilitates the examination process and converts the image's illustration into more relevant things. In other words, it is used for automatically or semi-automatically determining the area of interest (ROI) from an image. For example, it normally detects entities and edges in pictures like lines and arcs. In further detail, it tags every pixel in an image so that pixels with the same tag have specific properties. To this end, many image segmentation algorithms have been employed in medical applications to segment tissues and bodily parts.

In the last few years, algorithms presented new ways of image segmentation, with the methods differing based on the techniques they rely upon, mostly using either histogram, region, or edge.

Fuzzy c-means [45], expectation-maximization [46], and Threshold Selection Method from Gray-Level Histograms [47], Otsu [48], and K-means [49] are examples of the developed algorithm that have been widely used in image segmentation and veins extraction in recently published academic research.

3.2.1. Fuzzy c-means

A traditional FCM algorithm does not fully exploit the image's spatial information. However, the fuzzy c-means (FCM) technique for clustering adds geographical information to the membership function. The spatial function is the sum of the membership functions in the vicinity of each pixel being considered. It produces more uniform areas than other approaches, minimizes false blobs, removes noisy spots, and is less susceptible to noise than other techniques. Furthermore, the fuzzy c-means methodology effectively targets noisy picture segmentation and can handle single and multiple-feature data with spatial information.

FCM clustering is considered an unsupervised clustering that groups a set of images together with close spectral features. It uses the spectral domain distance between pixels and cluster centers to compute the membership function. The pixels in a picture are highly connected, providing spatial information that is a crucial feature for labeling. However, in FCM, the spatial link between pixels is rarely used.

In addition, adding spatial geographic information into the membership function has improved FCM segmentation outcomes. To generate cluster distribution statistics, the membership functions of the neighbors centered on a pixel in the spatial domain are counted. These statistics are converted into a weighting function and then integrated into the membership function. This adjacent impact minimizes the number of erroneous blobs and favors piecewise homogenous labeling. The proposed approach was examined using multiple cluster validity functions on MRA images. Preliminary findings revealed that the new algorithm significantly reduced the influence of noise in segmentation compared to the standard FCM. [45]

Figure 8 shows an example of segmented image by fuzzy clustering, with the original (top left), clustered (top right), and membership map (bottom).

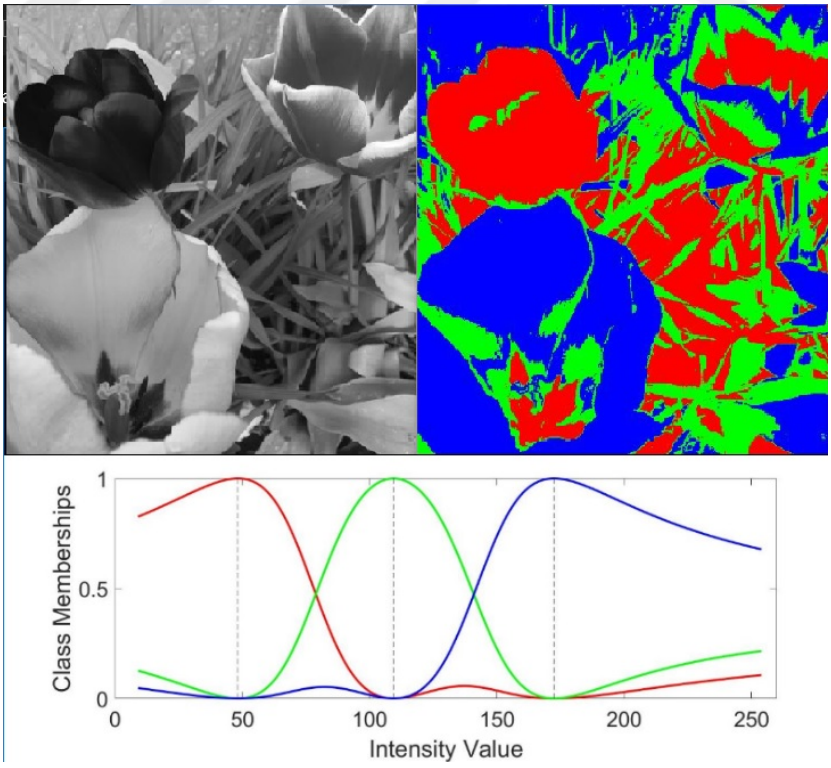

Figure 8 Image segmented by fuzzy clustering. [50]

3.2.2. The Expectation Maximization Algorithm

An expectation-maximization (EM) algorithm is an iterative approach for determining (local) maximum likelihood or maximum a posteriori (MAP) estimates of parameters in statistical models that rely on unobserved latent variables. The EM iteration alternates between an expectation (E) step, which computes parameters maximizing the expected log-likelihood discovered on the E step, and a maximization (M) step, which computes parameters maximizing the expected log-likelihood found on the E step. In the following E phase, these parameter estimates are utilized to calculate the distribution of the latent variables. [46]

The EM is used when an underlying set of known distribution function is observed via a many-to-one mapping. The E step is the most challenging and sometimes the most demanding computing step in analyzing the EM method. This is because the expectation must be computed across all unseen variable values for the generic expectation-maximization technique. Some efficient t alleviates the calculation, like the hidden Markov model, but these cannot reduce the computing strain.

In most cases, additional algorithms, such as gradient descent, are used simultaneously with EM. However, these algorithms may have issues, such as the need for derivatives or the determination of convergence-rate constants. Despite the challenges, EM continues to be a solid choice for many estimating problems due to its universality and assured convergence.

Figure 9 shows the expectation maximization clustering of old faithful eruption data. The random initial model (which, due to the different scales of the axes, appears to be two very flat and wide spheres) fits the observed data. In the first iteration, the model changes substantially.

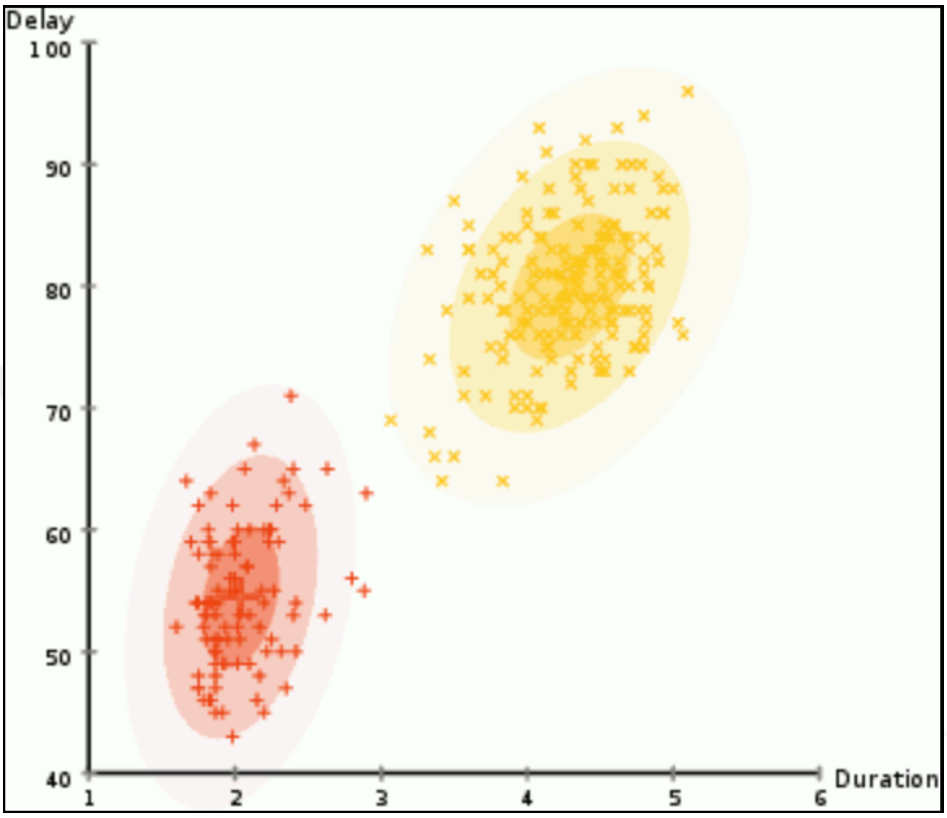

Figure 9 EM clustering of old faithful eruption data. [51]

3.2.3. Otsu

Otsu is a technique for automatically selecting a threshold from a histogram of grey levels devised using discriminant analysis. This technique directly addresses the difficulty of assessing the validity of thresholds.

The discriminant criteria determine the appropriate threshold or thresholds by maximizing the discriminant measure q. The suggested technique is characterized by its nonparametric and unsupervised threshold selection.

In the method, only the zeroth and first-order cumulative moments of the grey-level histogram are employed. Also, due to the method's underlying criteria, a straightforward extension to multithresholding issues is possible. An ideal threshold

or collection of thresholds is chosen automatically and consistently, not based on the differentiation of the histogram but on its integration.

The approach is highly generic since it encompasses many unsupervised decision-making processes. Moreover, its range of applications is more comprehensive than the thresholding of grey-level images.

It may also be used for other unsupervised classifications where a histogram of some characteristic discriminative for categorizing the objects is given. Considering these factors, this approach may be recommended as the most straightforward and standard automated threshold determination method. [48]

Figure 10 shows an example image thresholded using Otsu's algorithm.

Figure 10 An image thresholded using Otsu's algorithm [52]

3.2.4. K-means

Based on splitting, the K-Means method is a cluster algorithm introduced by J.B. MacQueen. [49] This unsupervised approach is often used in data mining and pattern identification. The square error and error criteria form the basis of this technique, which aims to minimize cluster performance index.

This method searches for K divisions that fulfill a specific condition to discover the best solution. Firstly, some dots are selected to represent the initial cluster focal points (typically, we select the first K sample dots of income to represent the initial cluster focal point). Secondly, remaining sample dots are gathered to represent their focal points based on the minimum distance criterion. Finally, the initial classification is obtained, and if the classification is illogical, it should be modified (each cluster focal point is recalculated). This is done repeatedly with iteration until a reasonable classification is obtained. The K-Means algorithm is cluster algorithm with the benefits of brevity, effectiveness, and swiftness. However, this method depends on the starting dots and the selection of beginning samples, which always results in varied outputs. In addition, this target-function-based approach always employs the gradient technique to find the extremum. In the gradient technique, the search path is always in the direction in which energy drops, which leads to the fact that if the initial cluster focal point is incorrect, the process may quickly converge to a local minimum point.

3.3. Shortest Path Algorithms

After the medical pictures have been segmented and the best algorithm for extracting the veins and arteries has been chosen, the next step would be to identify the most effective path between the injection point and the target point.

In graph theory, the challenge of finding a path between two vertices (or nodes), so that the weights of the graph's component edges are reduced, is referred to as the "shortest route issue."

Finding the shortest route between two intersections on a road map can be considered a particular illustration of the shortest path problem in graphs. In this case, the graph's vertices represent the intersections, and the edges represent the road segments, with each edge weighted by the length of the road segment it connects.

3.3.1. Dijkstra’s algorithm

The Dijkstra method works by first resolving a sub-problem called k, which computes the shortest route from the source to the vertices among the k vertices located closest to the source. For Dijkstra's method to function correctly, the graph must be directed and weighted, and the edges must not have a negative value. If the edges have a negative value, it will not be possible to determine the real shortest route. For the method to operate properly, it stores in an array called Dist the value representing the smallest distance separating vertex v from the source.

The distance from the source to itself is always zero since this is the smallest possible route. However, the other vertices' distance is set to infinity to indicate that the corresponding vertices should be processed. When the algorithm has completed the processing of the vertices, the Dist variable will include the vertex with the shortest distance from the source to each other vertex.

The algorithm's processing retains two sets, one containing all the vertices that have already been treated or included in the shortest route. The second set contains all the vertices that still need to be processed.[53]

3.3.2. A-star algorithm

The A* algorithm is a method that searches for graphs, which function to determine the path likely taken from a particular starting node to a destination node. It does this using a "heuristic estimate" h(x), which estimates the best route that goes through that node. Then, it accesses the nodes in the order the heuristic has calculated as must be accessed. It employs an approach known as "best first search." The success of Best First Search may be attributed to the fact that it combines the information used by Dijkstra's algorithm (which favors vertices close to the starting point) with the information used by Best First Search (favoring the goal). While h(n) offers a heuristic estimate of the cost from vertex n to the destination, g(n) represents the exact cost of the route from the beginning point to any vertex n in the graph, and g(n) may be used to calculate the cost of any route from the starting point to any vertex in the graph.[54]

4. SYSTEM DESIGN

For the purposes of this research, we built the medical images dataset on a collection of MRA brain scans. We used image segmentation to filter and locate the veins and arteries in the images' dataset, as well as to remove all the other pixels that were out of the study's focus. Additionally, we used three different algorithms in veins extraction of the scans, compared their results and then chose the one that performed best.

Afterwards, we used edge detection to calculate how far away the injection point is from the artery or vein that will receive the medicine. The goal of edge detection is to identify the boundaries or edges of the brain in the images.

Notably, the images from the previous steps of segmentation and brain extraction are 2D slices that were put through 3D modeling software to produce a 3D model of the brain.

The aim of this process was identifying the shortest path on a 3D map. To select the best route, we used Dijkstra's algorithm. The algorithm works by starting at the source injection node and exploring the graph one node at a time, always choosing the node closest to the source.

4.1. The Dataset

The dataset for medical images we used in this research builds on a collection of MRA scans of the brain. The dataset was compiled by a team of researchers at the radiopaedia.org website and was made public in October 2016. [55] With the dataset, we created a pool of images that we used to train and test algorithms to detect different brain conditions, including tumors and strokes.

One of the dataset's key points of strength is the condition presented by the sample images it incorporated. The dataset includes 112 scans of a man who experiences a momentary bout of weakness in his left arm after he engaged in physical activity.

Another point of strength of the dataset is the high contrast of the images. All the images in the dataset have a resolution of 512 by 512 pixels. This resolution emphasized the vibrant colors of the arteries and veins in the brain.

However, the dataset also has some limitations. One limitation is that it only includes MRA brain scans, which means that it may not be representative of other types of medical images or other parts of the body. Additionally, the images in the dataset were all collected from a single hospital, which threatens to make the patient population less representative of the general population.

With both the strengths and limitations it possesses, the dataset remains a valuable resource for researchers and clinicians working on algorithms geared towards detecting brain conditions. Despite the limitations, the large size, diversity, and detailed annotations of the dataset's images make it a useful tool for training and evaluating models. Notably, to overcome the current limitations, future research could focus on expanding the dataset to include other types of medical images and increasing the diversity of the patient population to make it more representative of the general population.

4.2. Veins Extraction

Image segmentation is the process of dividing an image into multiple segments or "regions". Each of these segments corresponds to a different object or background. It is a crucial step in image processing, as it helps to separate and analyze the different elements of an image. Image segmentation is widely and operatively used in medical imaging because it assists medical staffers to identify and classify different structures and tissues within an image. Beyond the domain of medicine, image segmentation is used in remote sensing, where it helps analyze and make sense of images from space and the air.

We used image segmentation to filter and find the veins and arteries in the images in the dataset, as well as to get rid of all the other pixels that were unnecessary or too noisy. We used three different algorithms to compare the results they yielded and then chose the one that functioned best.

Before we ran the images through segmentation algorithms, we arranged the images in the dataset in a certain order. We aligned the images horizontally and merged them into a single large image that contains all of the slices. Next, we obtained the coordinates for a single arterial segment from the pressed image by hand. Then,

we sent these coordinates to the three algorithms we intended to experiment with, seeking to gather the clusters around this point.

The first tested method was Otsu's. Under this method, the images were converted into grayscale images to separate the foreground from the background. With this measure, the method minimizes the within-class variance of the foreground and background pixels. That is, it tries to find a threshold value that gives the most space between pixels in the image's foreground and background.

Otsu's method is useful for MRA images where there is contrast between the vessels and background due to its automatic thresholding technique.

To apply the Otsu's method for veins extraction, the input image needs first to be converted to grayscale if it is not already in grayscale. Then, to figure out the best value for the threshold, we applied the following steps:

1. Calculated the histogram of the grayscale image.
2. Calculated the probability of each intensity level.
3. Calculated the cumulative probability of each intensity level.
4. Calculated the mean value for the foreground and background pixels at each threshold value.
5. Calculated within-class variance for the foreground and background pixels at each threshold value.
6. Selected the threshold value that minimizes the within-class variance.

Upon finding the best threshold value, the value can be used to divide the image into foreground and background parts by assigning the foreground value to all pixels with intensity values above the threshold and the background value to all pixels with intensity values below the threshold.

The second method we tested was the K-means clustering. The algorithm divides a set of data points into K distinct clusters based on the mean distance between the data points and the cluster centers. To use k-means for veins extraction, the input image needs to be converted to a feature space that represents the image in a more suitable format for clustering. This can be done by taking things out of the image like its intensity, color, texture, etc.

Once the feature space has been created, we applied k-means clustering to the feature space through the following steps:

1. Created K cluster centers at random or using a heuristic.
2. Assigned each data point to the cluster with the nearest cluster center.
3. Recalculated the cluster centers by taking the mean of all the data points in each cluster.
4. Repeated steps 2 and 3 until the cluster centers no longer change or a maximum number of iterations has been reached.

Then, we divided the image into different sections by giving each cluster a unique name or color.

The third method we tested was fuzzy c-means (FCM), which is a variant of the k-means algorithm. However, instead of making hard assignments of data points to clusters, the FCM allows for "fuzzy" assignments, where each data point can belong to multiple clusters with different degrees of membership. This can help with medical veins extraction because it makes it easier to move the lines between different types of tissue or structures, which may not be clear or may be different from one image to the next.

To perform veins extraction using FCM, we followed these steps:

1. Pre-processed the image. This included the removal of noise, smoothing the image, or making it stand out more, so it is easier to analyze.
2. Extracted features from the image to select relevant ones, particularly those that could be used to represent each pixel or region. These features might include intensity values, texture, or shape information.
3. Initialized clusters. To do this, we had to specify the number of clusters required for the segmentation (this is often referred to as "c" in FCM). We also had to set up the cluster centers and membership values for each data point.
4. Iterated until the algorithm convergence was achieved. For iteration, we carried out the following steps: a. Updated the membership values for each data point based on the distance to the cluster centers and the shape

parameter. b. Updated the cluster centers based on the membership values of the data points.

5. Once we obtained the results, we had to take a few more steps to improve the segmentation, such as getting rid of small areas or making the edges between clusters smoothers.

Because of the unique characteristics of MRA images, like the high contrast between blood vessels and surrounding tissues, the mentioned methods offer a balance between sensitivity to these features and computational efficiency.

Based on the results from the veins extraction, we made the decision as to which method to deploy ahead. Our next step involved cleaning the pictures of any "noisy pixels," which are defined as tiny regions that do not belong to any particular cluster.

The values of these removed pixels were ranged from 1 to 500 pixels to determine the best value and thus ensure that no important information was lost during the filtering process.

We used the Picture Processing Toolbox (PPT) function to eliminate tiny items—sometimes called “specks"—from a binary image. The function sets all linked components (objects) in the binary image with less than n pixels to zero. The value of n defines the smallest item size that will be retained in the picture. Objects with a smaller area than n pixels are eliminated from the picture.

To help us understand the overall impact of successive filters or modifications on the data, we plot the cumulative difference plot for each cluster value. Those plots offer insights into the efficiency or effectiveness of the filtering process over time. The x axis of the plot is the cumulative absolute difference in the total number of pixels after applying a filter, and the y axis is the filtering values.

After that, we conducted a study using polynomial curve fitting for each cluster value result to find the best value for the small area filter so as to remove areas without removing the veins and arteries.

The first derivative of a function f(x) is the rate of change of the function with respect to x, and it tells us how the function is changing at any given point. The second derivative of a function is the rate of change of the first derivative with respect to x,

and it tells us how the rate of change of the function is changing at any given point. In other words, the second derivative describes the curvature of the function.

We carried out an experiment to determine the optimal value. After that, the number of pixels, denoted by the variable n, was set to one of several possible values ranging from one to five hundred pixels to be removed from each image.

To find the best value, we selected the lowest standard deviation that represents the most stable result with the fewest variants in the data.

4.3. Brain Extraction

In the phase of brain extraction also involved several steps, all aimed at obtaining the boundary of the brain, also known as the skull. This process is crucial because it helps to figure out how far away the injection site is from the artery or vein that will receive the medicine.

Brain extraction, also referred to as edge detection, is a common task in image processing. It is applied to identify the boundaries or edges of objects in an image. This is important because boundaries often correspond to the object's shape and can be used to separate objects from each other or from the background. There are many ways to locate the edges of an object, including gradient-based, morphological, and machine learning methods.

In our study, we used morphological brain extraction, a process in which the boundaries of objects or regions in an image are identified and marked. This is typically done using morphological operations, which are mathematical functions that analyze the shape and structure of an image.

To determine the location of the brain's boundary, we used the following steps to find the edge of each image:

1. Made the image black and white.
2. Eliminated the noise.
3. Filled in any gaps so that region properties may be used to estimate the amount of space that is included inside each of the boundaries.
4. Found the borders that only look at the outside edges.

5. Used the "no holes" option to speed up the process by telling the borders not to look for the objects inside edges.

4.4. 3D Map Construction

After completed segmenting the images, we fed them into a 3D modeling software to produce a model of the brain in three dimensions. This computerized model, which is called a three-dimensional medical map, is created to locate the most effective route that overseeing medical staffers can take in order to deliver the medication from the site of injection to the desired location. When making the 3D model, each pixel in the model is given a different value. This includes the background, arteries, veins, and the boundary, which is the skull.

To build a 3D model from the images, we applied the following steps:

1. Acquired the slices: These are output images from the veins extraction, which provided a series of 2D slices of the arteries and veins. For their part, the images from the brain extraction phase reflect the skull of the head, while other pixels demonstrated the background of the 3D model.
2. Aligned the slices: The slices need to be aligned according to each segment. The skull will have its own value, which is different from the same value assigned to all.
3. Reconstructed the model: Once the slices were aligned, a 3D model was created.

4.5. Best Route

To select the best route, we used Dijkstra's algorithm, which is a graph search algorithm that can be used to find the shortest path between two nodes in a graph. It can be used to find the shortest path in a 2D, or 3D map, as long as the map can be represented as a graph.

To use Dijkstra's algorithm on a 3D map, we represented the map as a graph by treating each location on the map as a node in the graph and connecting nodes with edges that represent the distance between them.

Once the map was represented as a graph, we applied Dijkstra's algorithm to find the shortest path between the source injection and the destination point. The algorithm works by starting at the source injection node and exploring the graph one node at a time, always choosing the node that is closest to the source node. As it explores the graph, it keeps track of the distance from the source node to each node it has visited and uses this information to determine the next node to visit.

In addition, we defined a function that calculates the distance between two nodes. This function considers the altitude of the nodes as well as the distance between them in order to calculate the shortest path through the 3D map. This function can be used to guide the search through the graph, following the shortest path from the source node to the destination node.

Figure 11 provides an overview of all the procedures that were involved in our research.

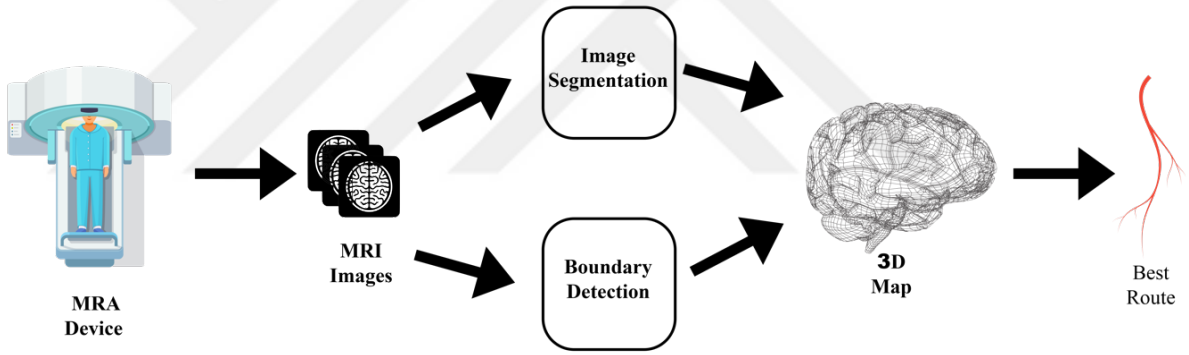

Figure 11 An overview of research procedures.

5. RESULTS

As we described in Chapter 3, we started our pipeline with the segmentation of the scan images, next cleaned the output images from small areas that did not belong to the arteries and veins and then defined the boundaries of the brain in parallel to get the skull area.

Following these steps, we gathered the images in a 3D model that assigned separate values to each artery, the skull, and background.

To get the route from the injection point to the target point, we used a path-finding algorithm to analyze the 3D model and determine the route.

Figure 12 illustrates all the steps we implemented in our study, starting from the collection of the scan images, then segmentation and brain extraction of those images, and finally the construction of 3D map of the brain and locating the shortest path.

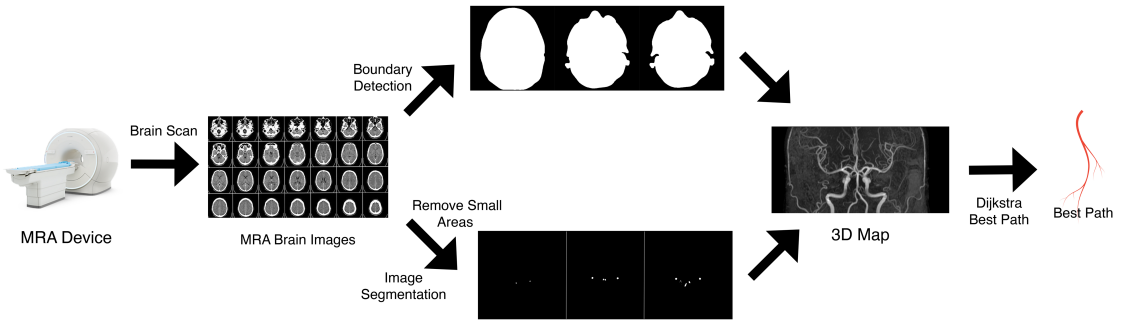

Figure 12 implementation methodology.

Figure 13 shows slices of MRA scans of the brain from the selected dataset. The slices depict various horizontal planes of the brain. They were used to facilitate the segmentation process, aimed at extracting the veins and arteries of the brain.

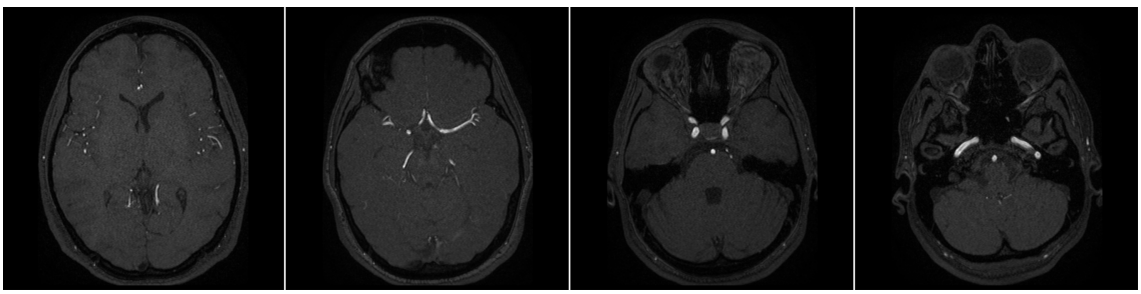

Figure 13 MRA slices of the brain.

Each phase's results will be discussed in detail in the following sections.

5.1. Veins Extraction Results:

In our study, we tested three different algorithms to compare the results and choose the best algorithm for the veins extraction.

We tried different cluster numbers for each algorithm and observed the algorithms' separate performances.

5.1.1. FCM results:

We ran the algorithm multiple times to find the best cluster number for the segmentation, which ranged from 3 to 10 clusters.

Figure 14 shows the brain's slices after the FCM segmentation algorithm is applied with a parameter of 3 - 6 clusters.

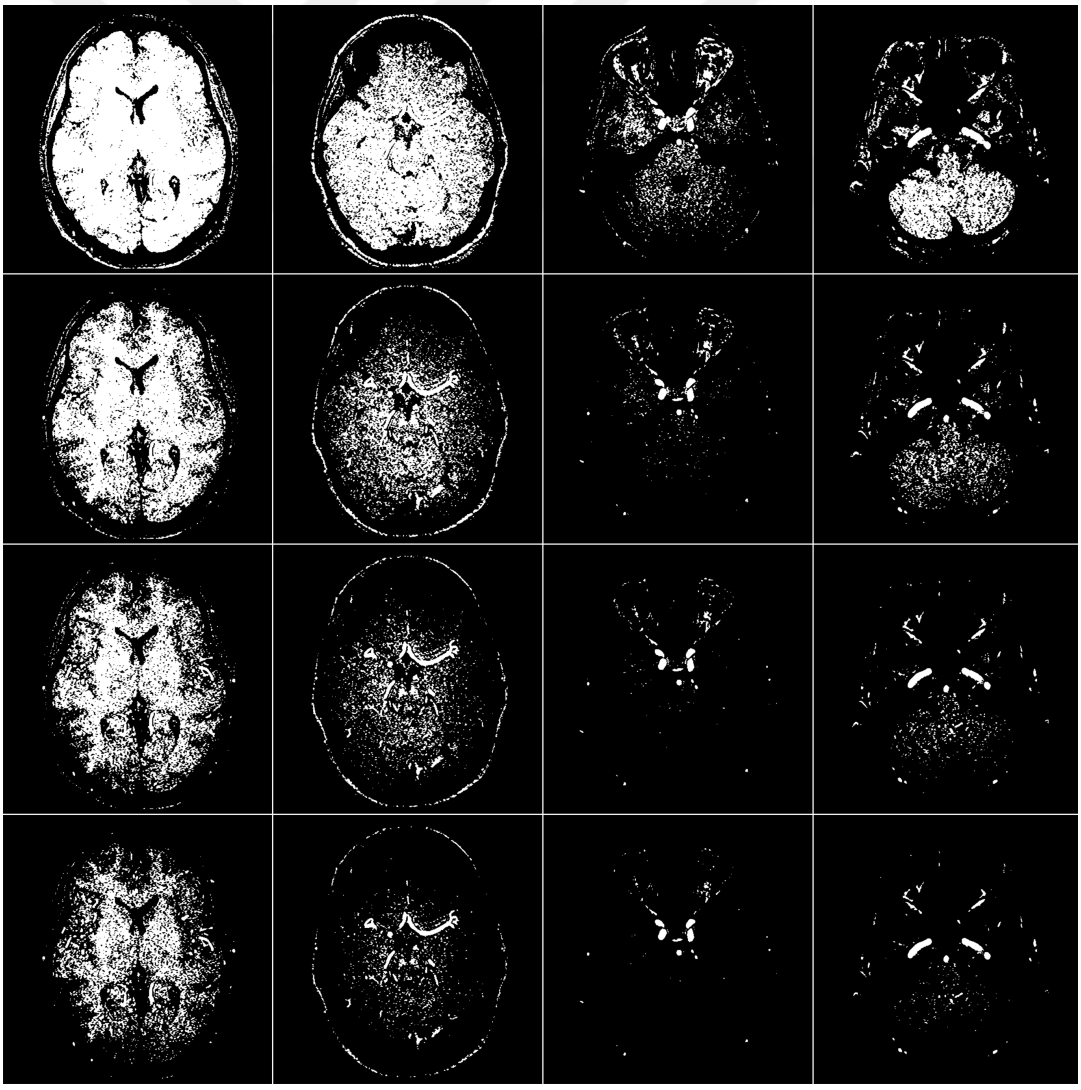

Figure 14 FCM with 3 - 6 clusters.

Figure 15 shows the brain's slices after the FCM segmentation algorithm is applied with a parameter of 7 - 10 clusters.

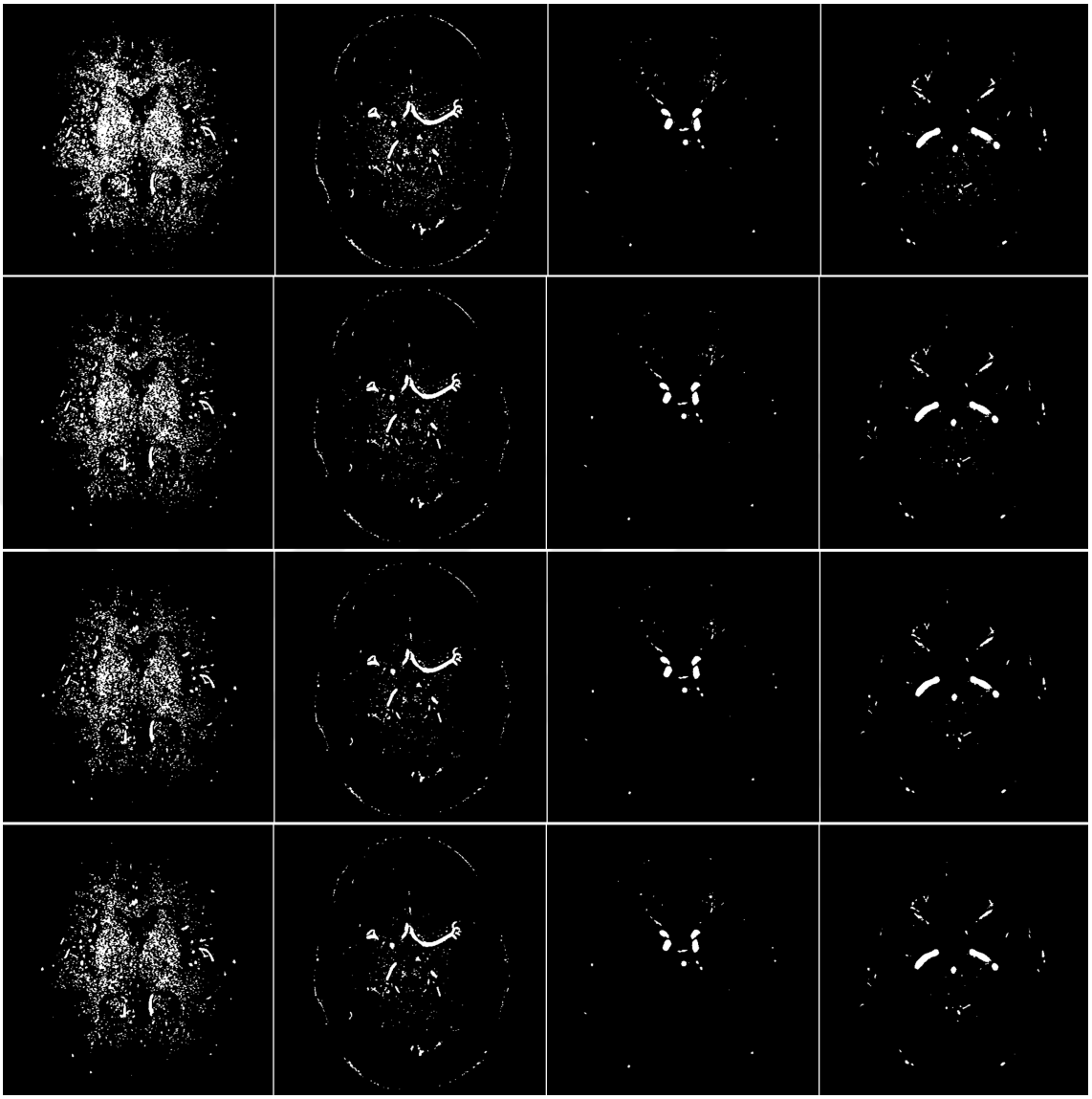

Figure 15 FCM with 7- 10 clusters.

Figure 16 illustrates the relation between the pixel count and the cluster number for the brain scans. The chart shows that after segmenting the images into clusters, the number of pixels decreased while the number of clusters increased. Consequently, a large number of the arteries disappeared from the output images.

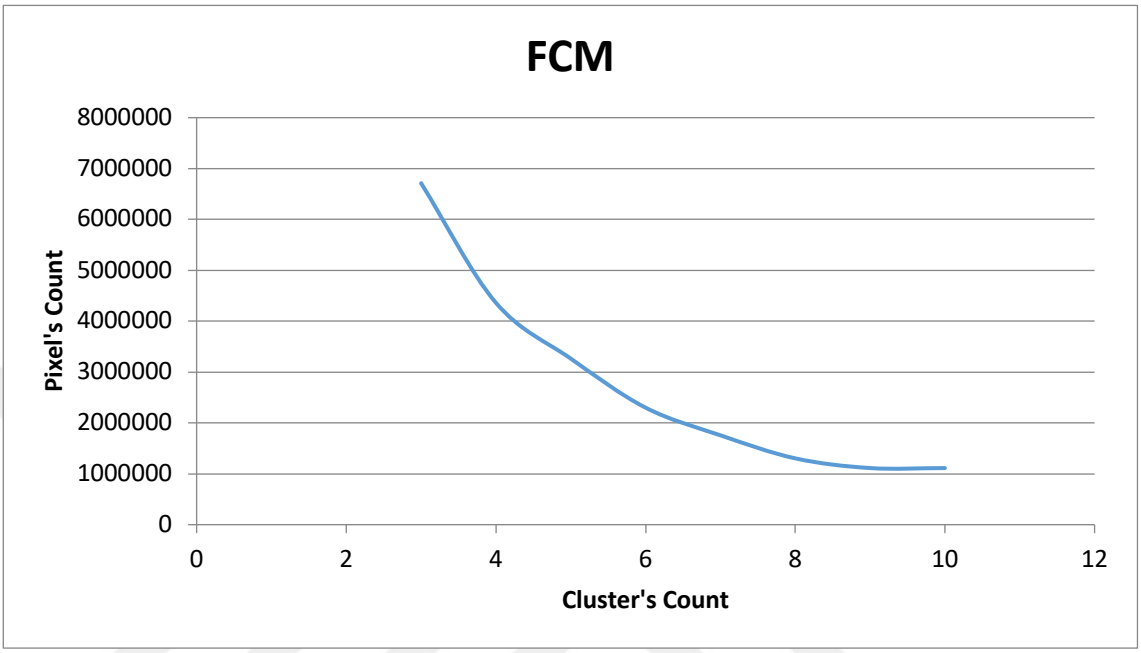

Figure 16 FCM's pixels count by cluster.

After we finalized the FCM based veins extraction, we applied a small area filter to the output images to remove unwanted noise pixels. The values of these removed pixels were ranged from 1 to 500 pixels to determine the best value and thus ensure that no important information was lost during the filtering process.

To help us understand the overall impact of successive filters or modifications on the data, we plot the cumulative difference plot for each cluster value. Those plots offer insights into the efficiency or effectiveness of the filtering process over time. The x axis of the plot is the cumulative absolute difference in the total number of pixels after applying a filter, and the y axis is the filtering values.

Figure 17 shows the cumulative change plot for the output images from the FCM veins extraction with 3 clusters and small area filtering values ranging from 1 to 500 pixels.

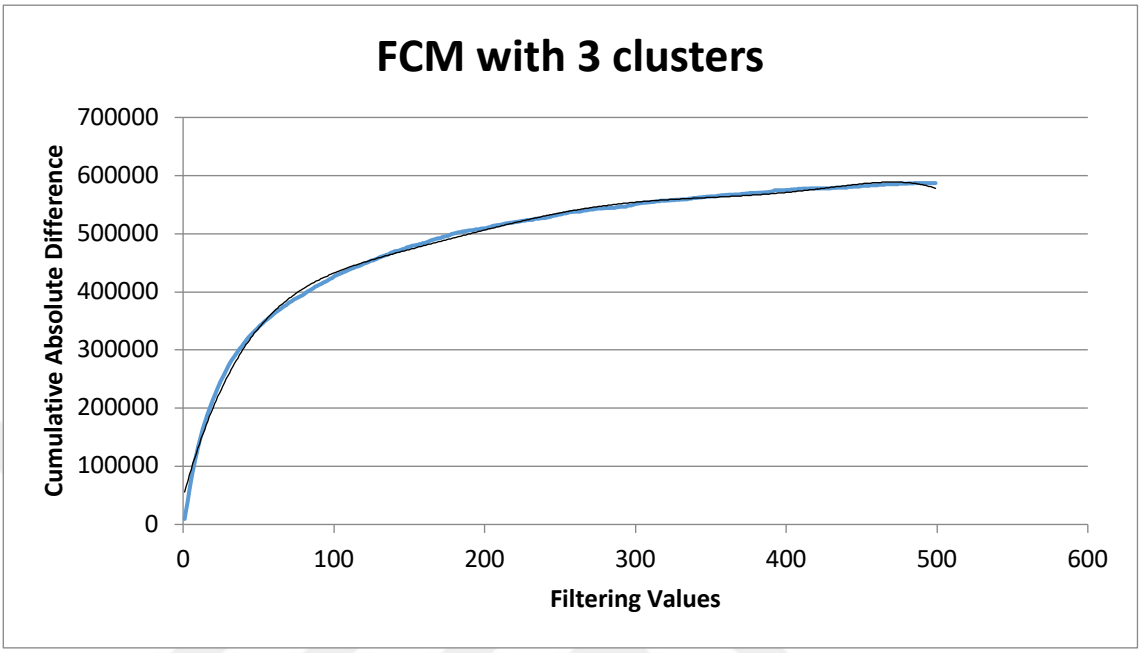

Figure 17 cumulative change plot for FCM with 3 clusters.

Figure 18 shows the cumulative change plot for the output images from the FCM veins extraction with 4 clusters and small area filtering values ranging from 1 to 500 pixels.

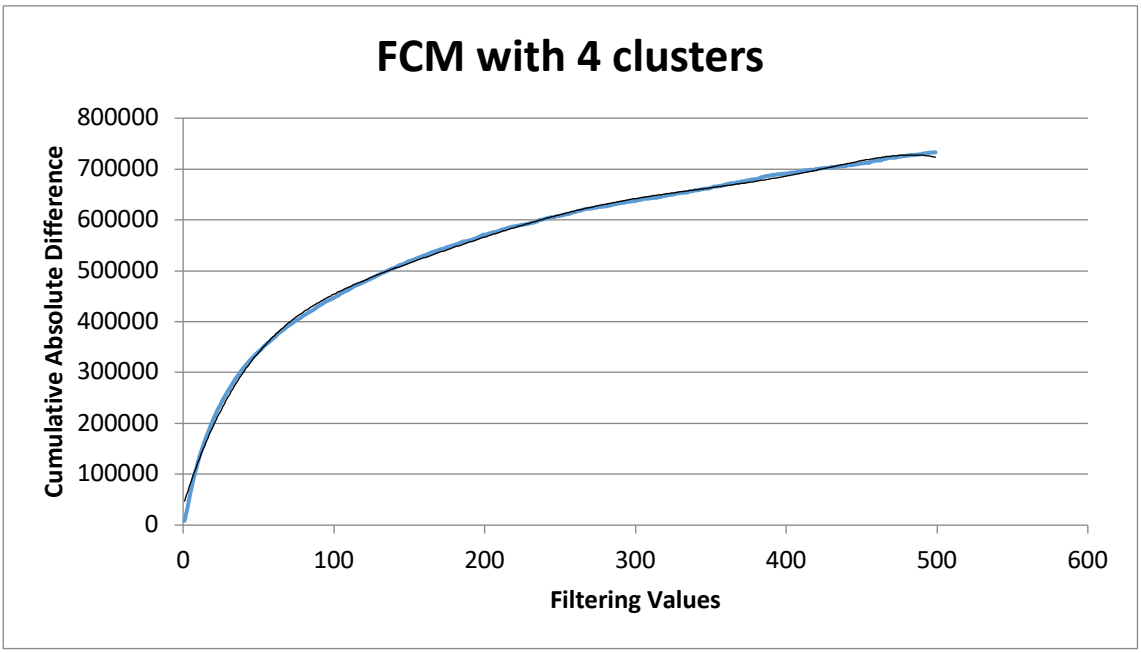

Figure 18 cumulative change plot for FCM with 4 clusters.

Figure 19 shows the cumulative change plot for the output images from the FCM veins extraction with 5 clusters and small area filtering values ranging from 1 to 500 pixels.

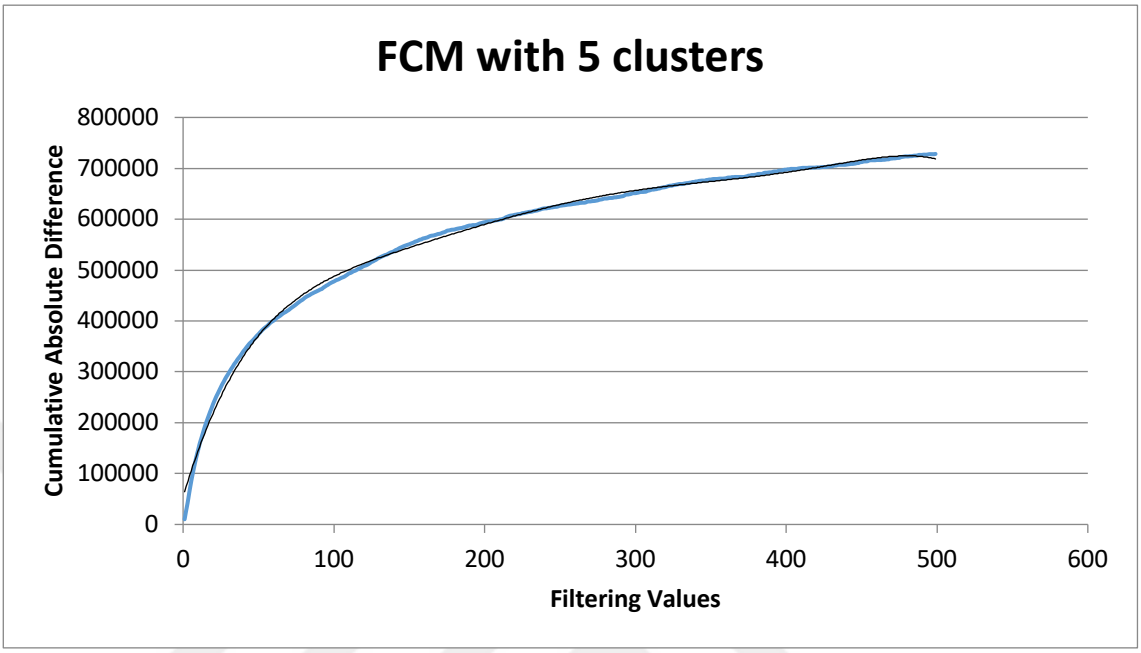

Figure 19 cumulative change plot for FCM with 5 clusters.

Figure 20 shows the cumulative change plot for the output images from the FCM veins extraction with 6 clusters and small area filtering values ranging from 1 to 500 pixels.

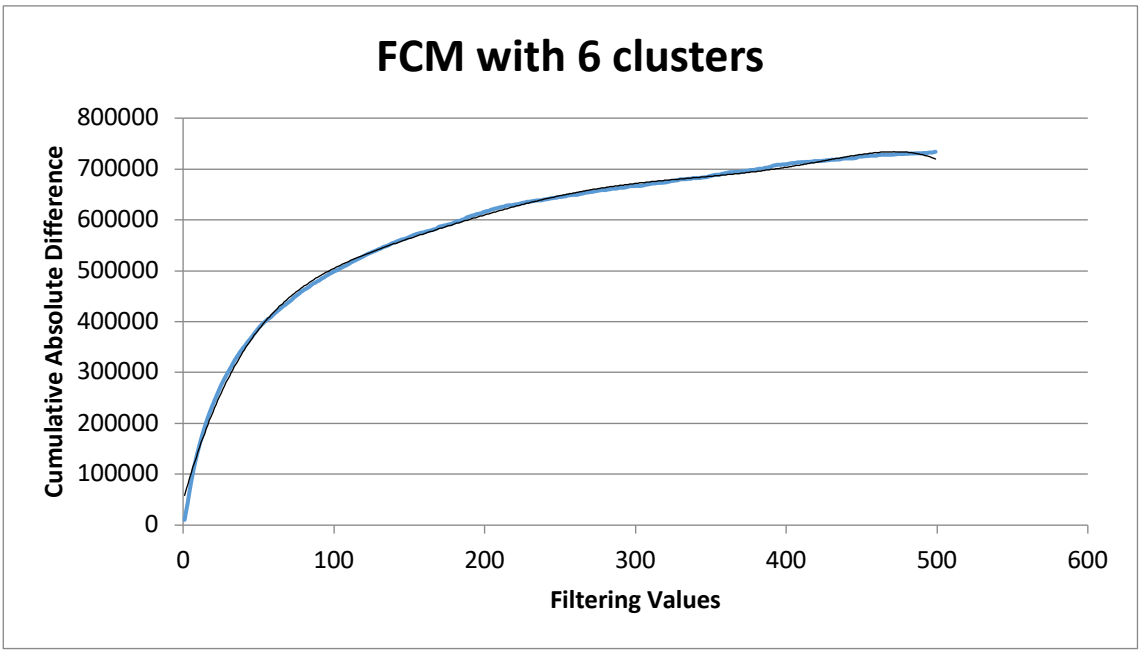

Figure 20 cumulative change plot for FCM with 6 clusters.

Figure 21 shows the cumulative change plot for the output images from the FCM veins extraction with 7 clusters and small area filtering values ranging from 1 to 500 pixels.

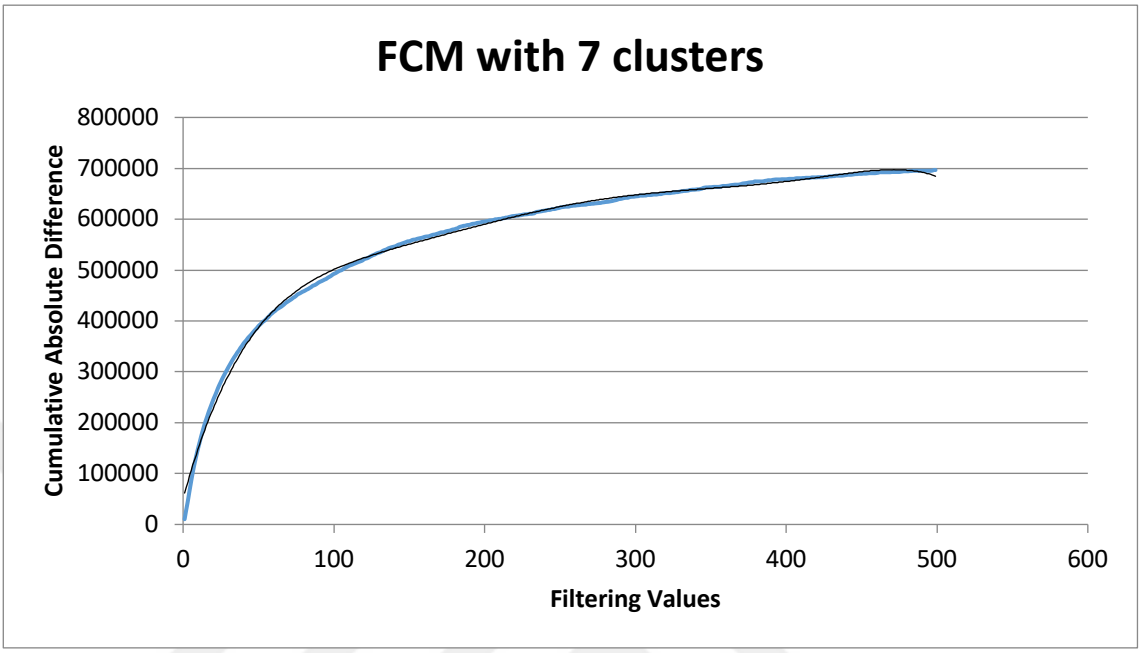

Figure 21 cumulative change plot for FCM with 7 clusters.

Figure 22 shows the cumulative change plot for the output images from the FCM veins extraction with 8 clusters and small area filtering values ranging from 1 to 500 pixels.

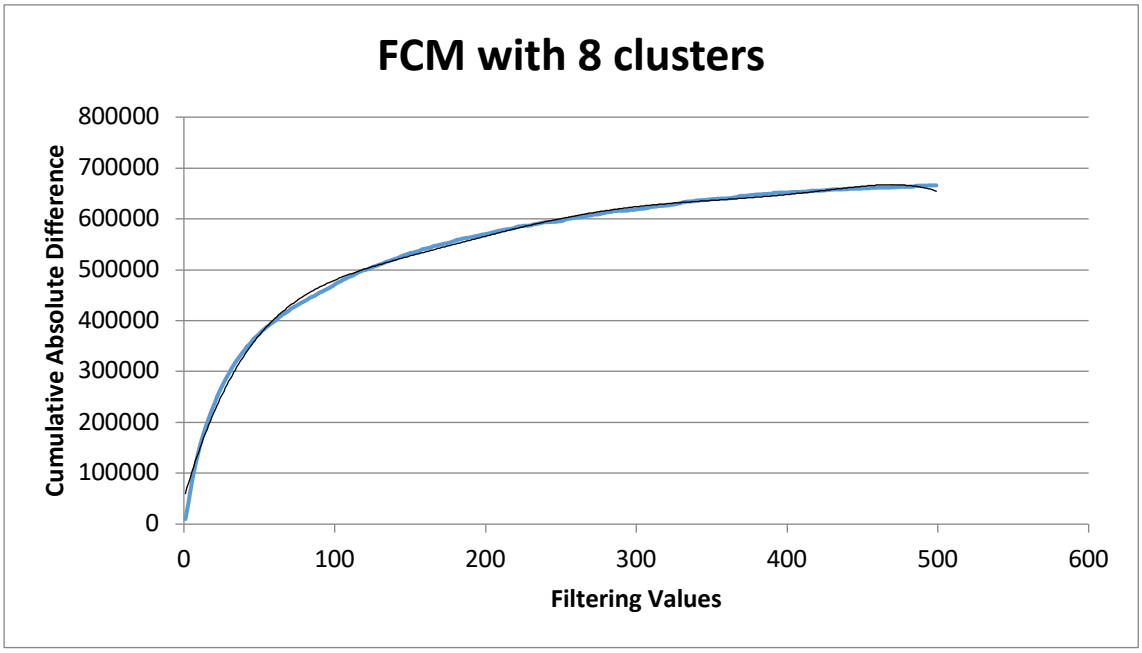

Figure 22 cumulative change plot for FCM with 8 clusters.

Figure 23 shows the cumulative change plot for the output images from the FCM veins extraction with 9 clusters and small area filtering values ranging from 1 to 500 pixels.

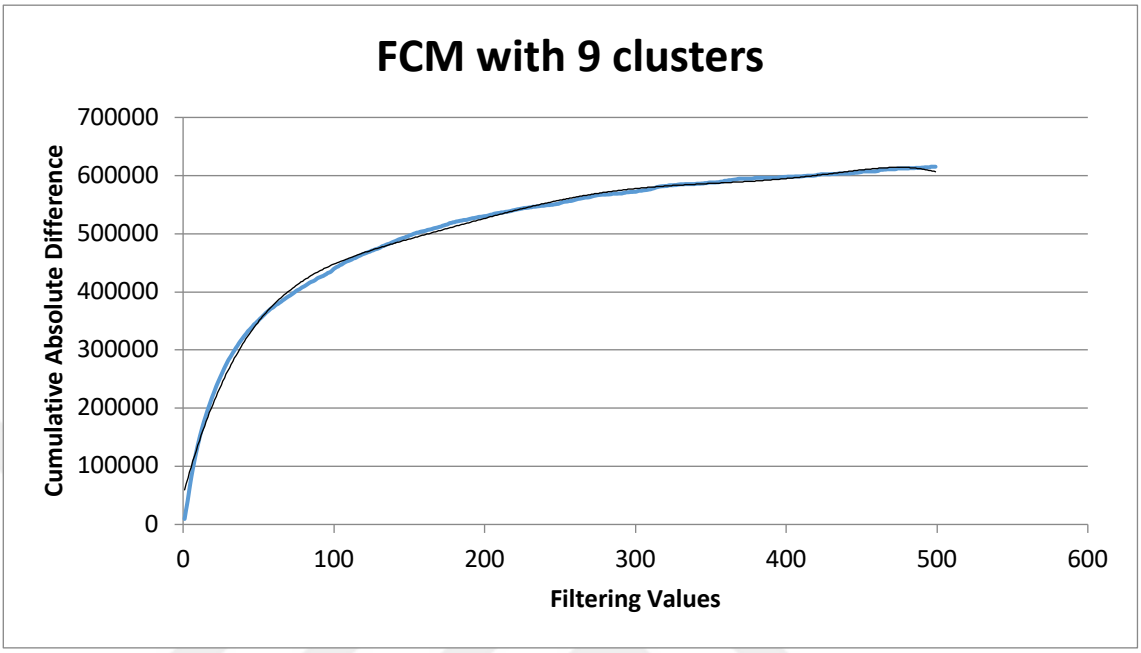

Figure 23 cumulative change plot for FCM with 9 clusters.

Figure 24 shows the cumulative change plot for the output images from the FCM veins extraction with 10 clusters and small area filtering values ranging from 1 to 500 pixels.

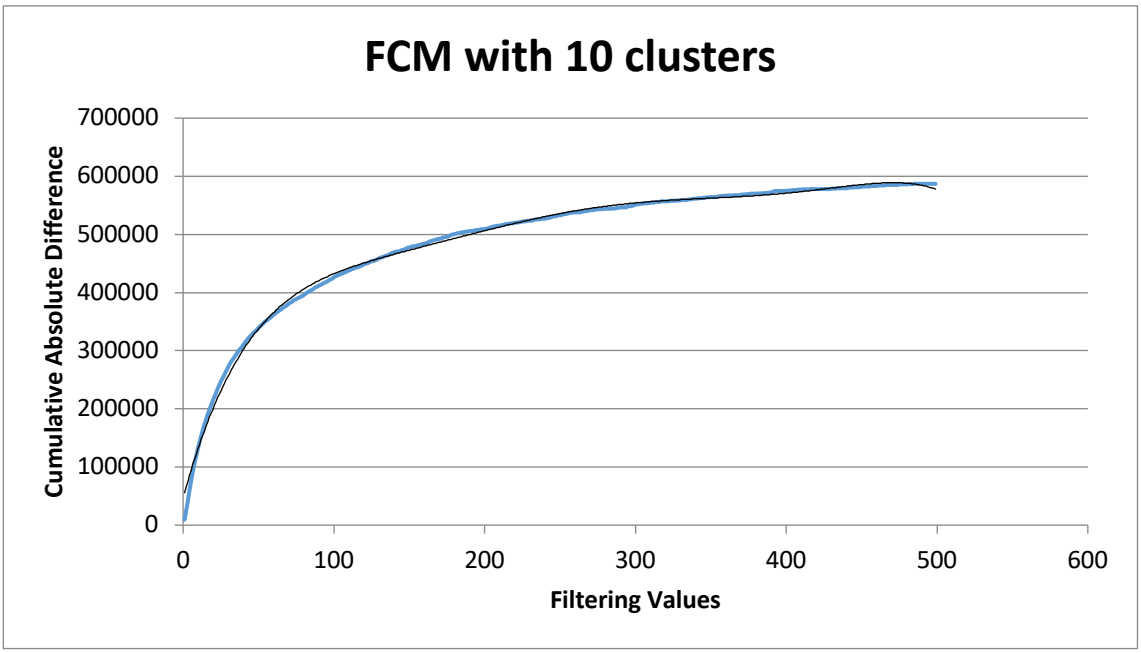

Figure 24 cumulative change plot for FCM with 10 clusters.

We conducted a study using polynomial curve fitting for cumulative change for each cluster value result to find the best value for the small area filter so as to remove areas without removing the veins and arteries. This function gives the coefficients of the polynomial p(x) of degree n that best fit the data in y. The coefficients in p are in descending powers, and p is n+1 elements long.

Figure 25 visualizes the impact of filter size on the remaining area within Cluster 3, modeled by an 8th degree polynomial. On the x-axis, filter size extends from 0 to 500, and the y-axis indicates the remaining area post-filtering. The polynomial (blue line) reveals a rapid rise and plateau in area with increasing filter size, while the first derivative (red dashed line) remains below zero, indicating a decreasing rate of area loss.

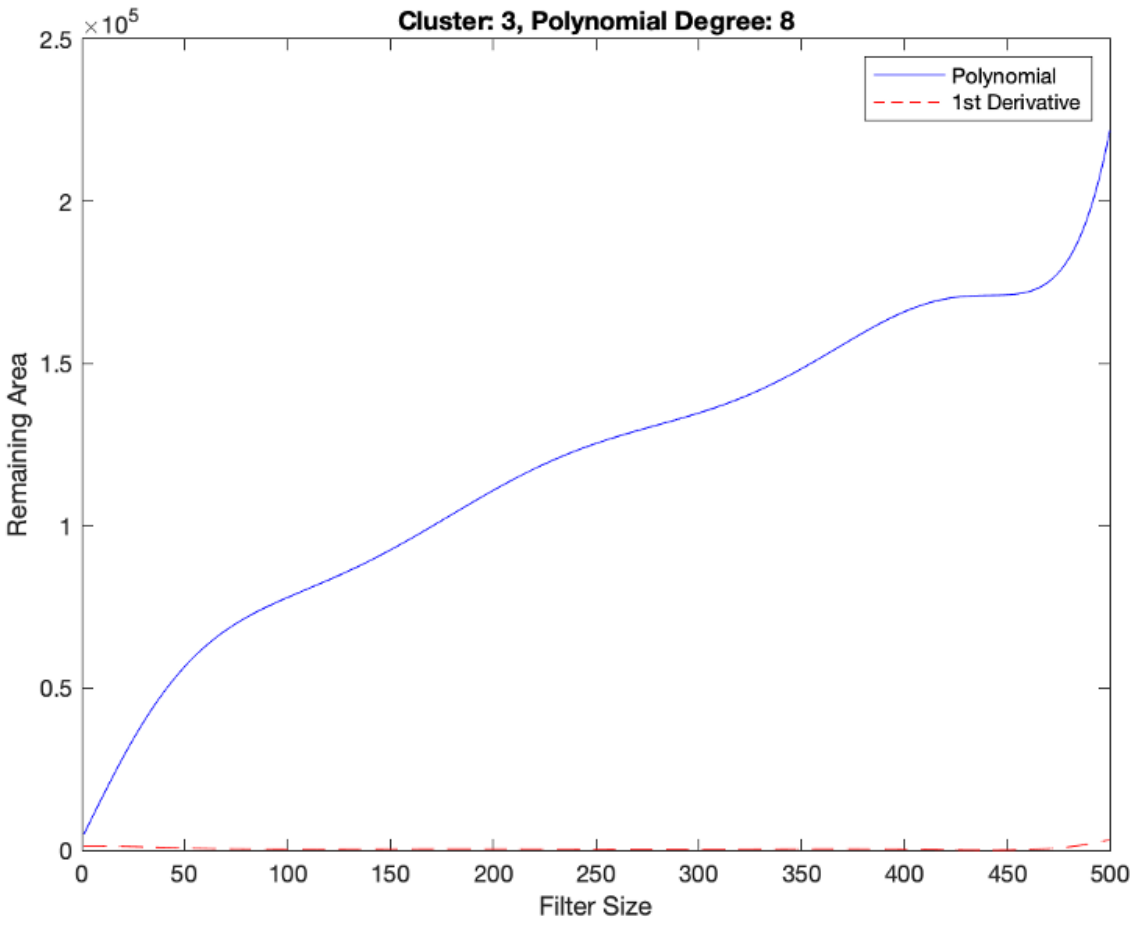

Figure 25 first derivative of polynomial curve of cumulative change of degree 8 and 3 clusters.

Figure 26 presents the second derivative of an 8th degree polynomial for Cluster 3, with filter size on the x-axis ranging from 0 to 500, and the corresponding values of the second derivative on the y-axis. The second derivative, depicted by the green dashed line, measures the rate of change of the rate of change of the remaining area.

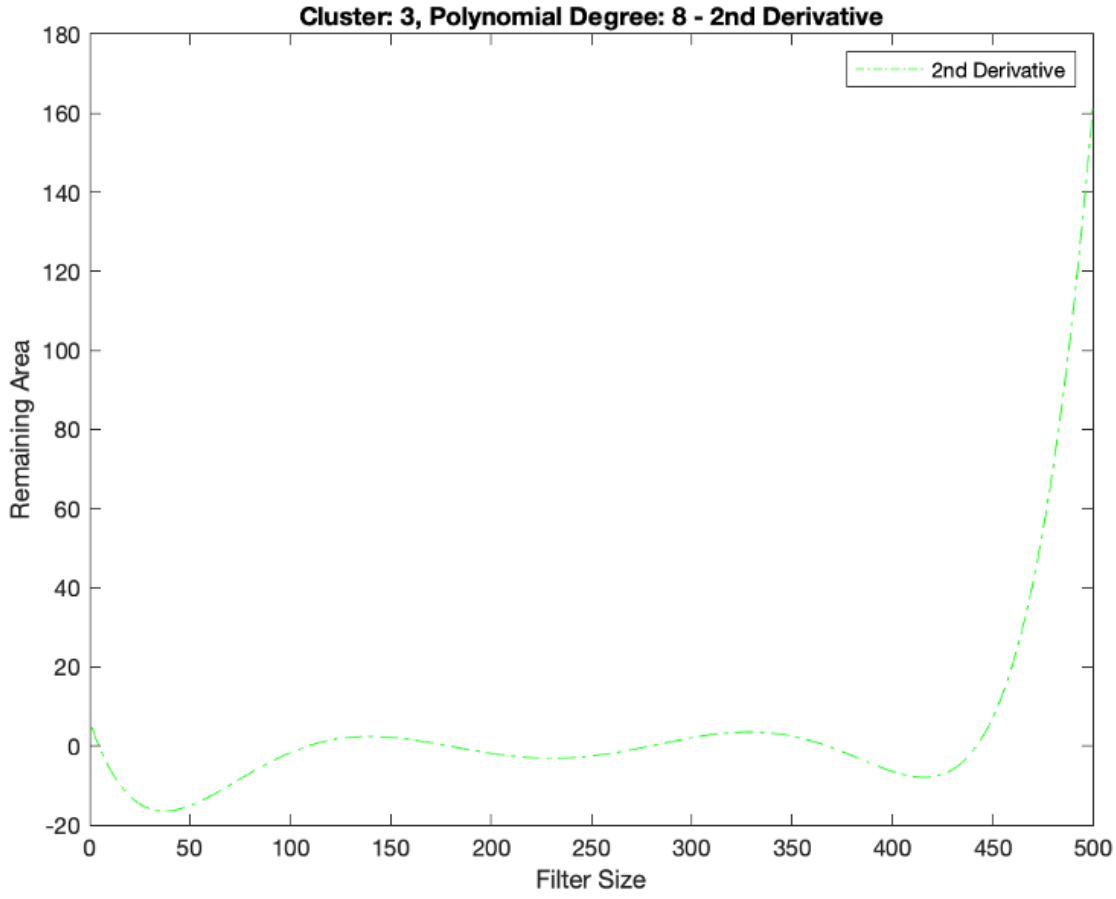

Figure 26 second derivative of polynomial curve of cumulative change of degree 8 and 3 clusters.

After all the polynomial calculations were complete with the first and second derivatives, we put all the values together in a table, which made it easy to compare the results and select the best parameter for filtering the small area by taking the standard deviation of the values and selecting the lowest value.

Table 1 shows all the roots from the second derivative of polynomial curve fitting for all the clusters from 3 to 10.

		Clusters Count							
Polynomial Degree		**3**	**4**	**5**	**6**	**7**	**8**	**9**	**10**
	3	296	286	308	326	313	305	305	296
	4	286	255	285	324	310	291	291	262
	5	308	380	386	386	383	382	382	382
	6	326	282	270	397	392	391	391	390
	7	313	334	327	320	322	332	332	342
	8	305	361	359	357	361	364	364	367
	9	305	389						
	10	296	342	342	346	345	343	343	337
	Average	**304,38**	**328,63**	**325,29**	**350,86**	**346,57**	**344,00**	**344,00**	**339,43**
	Standart Diveation	**12,15**	**49,21**	**40,99**	**30,87**	**33,34**	**37,70**	**37,70**	**46,59**

Table 1 the roots from the second derivative of polynomial curve for FCM.

The values of 3 clusters have the best average and standard deviation values. 304 pixels is selected as the parameter for the small area filter.

Figure 27 shows how the pixel values changed before and after the application of small area filtering to the images.

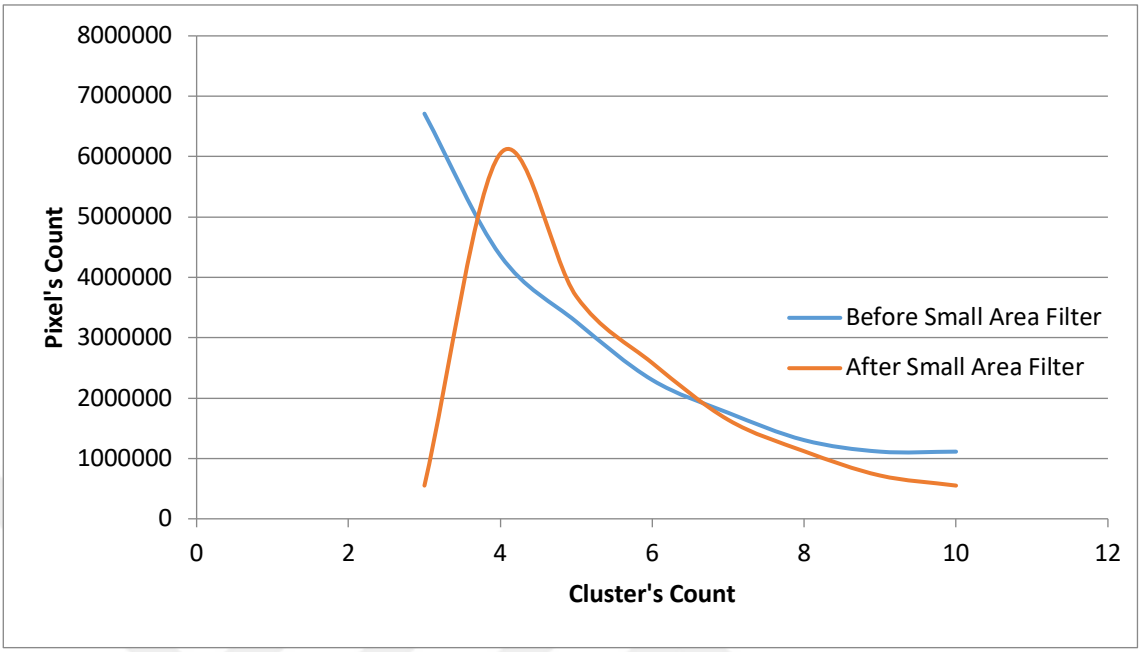

Figure 27 comparison of FCM's pixels' values before and after small area filtering.

The output images from FCM segmentation passed to remove small area filter, with 304 pixel areas to be removed from the images. The veins extraction improved after the small area filter was applied, and the veins and arteries were identified.

Figure 28 shows the brain slices after the segmentation algorithm and small area filter is applied with a parameter of 3 - 6 clusters and 304 pixels.

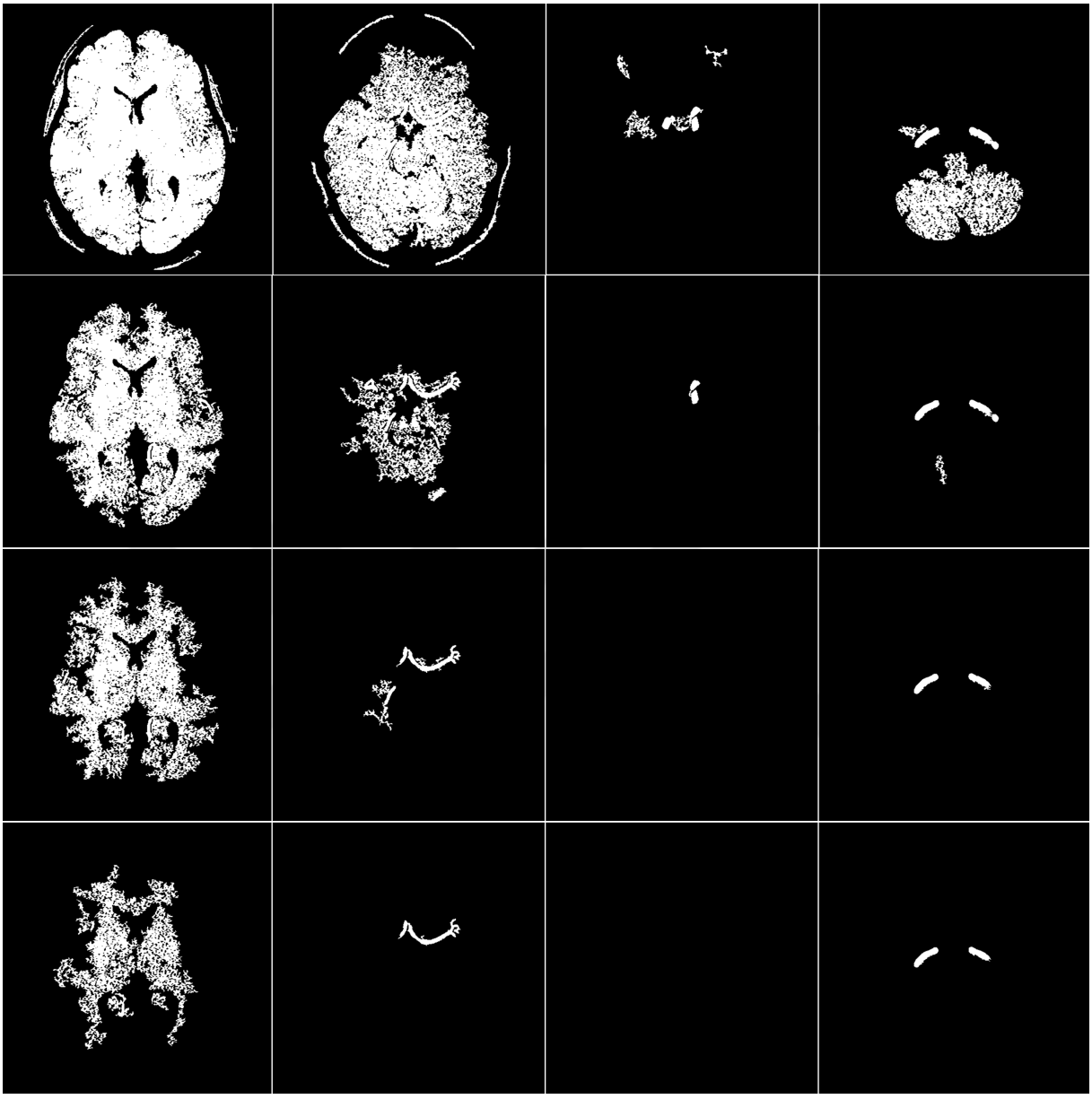

Figure 28 FCM with 3 - 6 clusters and small area filter.

Figure 29 shows the brain slices after the segmentation algorithm and small area filter is applied with a parameter of 7 - 10 clusters and 304 pixels.

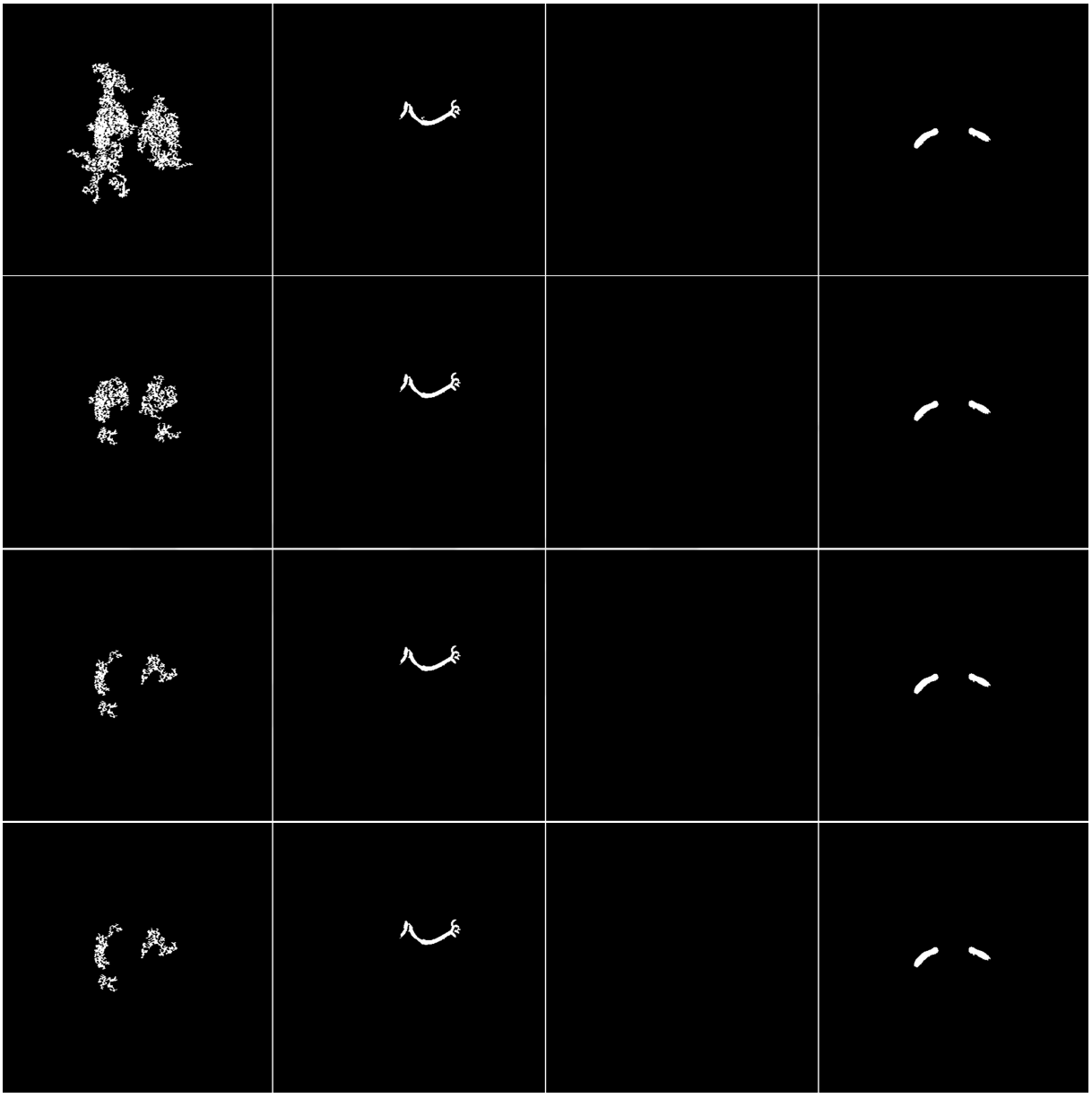

Figure 29 FCM with 7 - 10 clusters and small area filter.

5.1.2. Otus results:

We ran the algorithm multiple times to find the best cluster number for the segmentation, which ranged from 3 to 10 clusters.

Figure 30 shows the brain slices after the Otsu segmentation algorithm is applied with a parameter of 3 - 6 clusters.

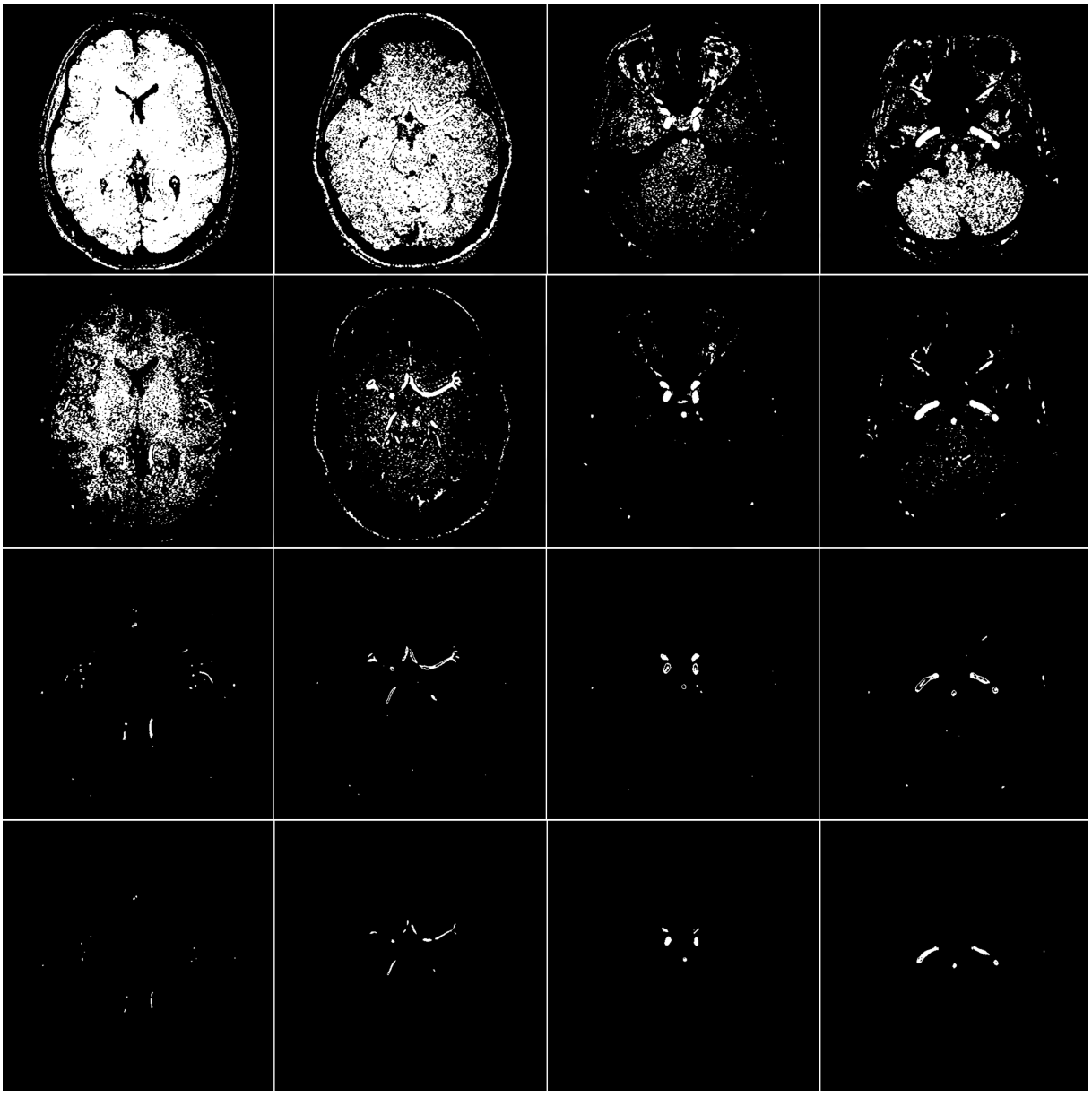

Figure 30 Otsu with 3 - 6 clusters.

Figure 31 shows the brain slices after the Otsu segmentation algorithm is applied with a parameter of 7 - 10 clusters.

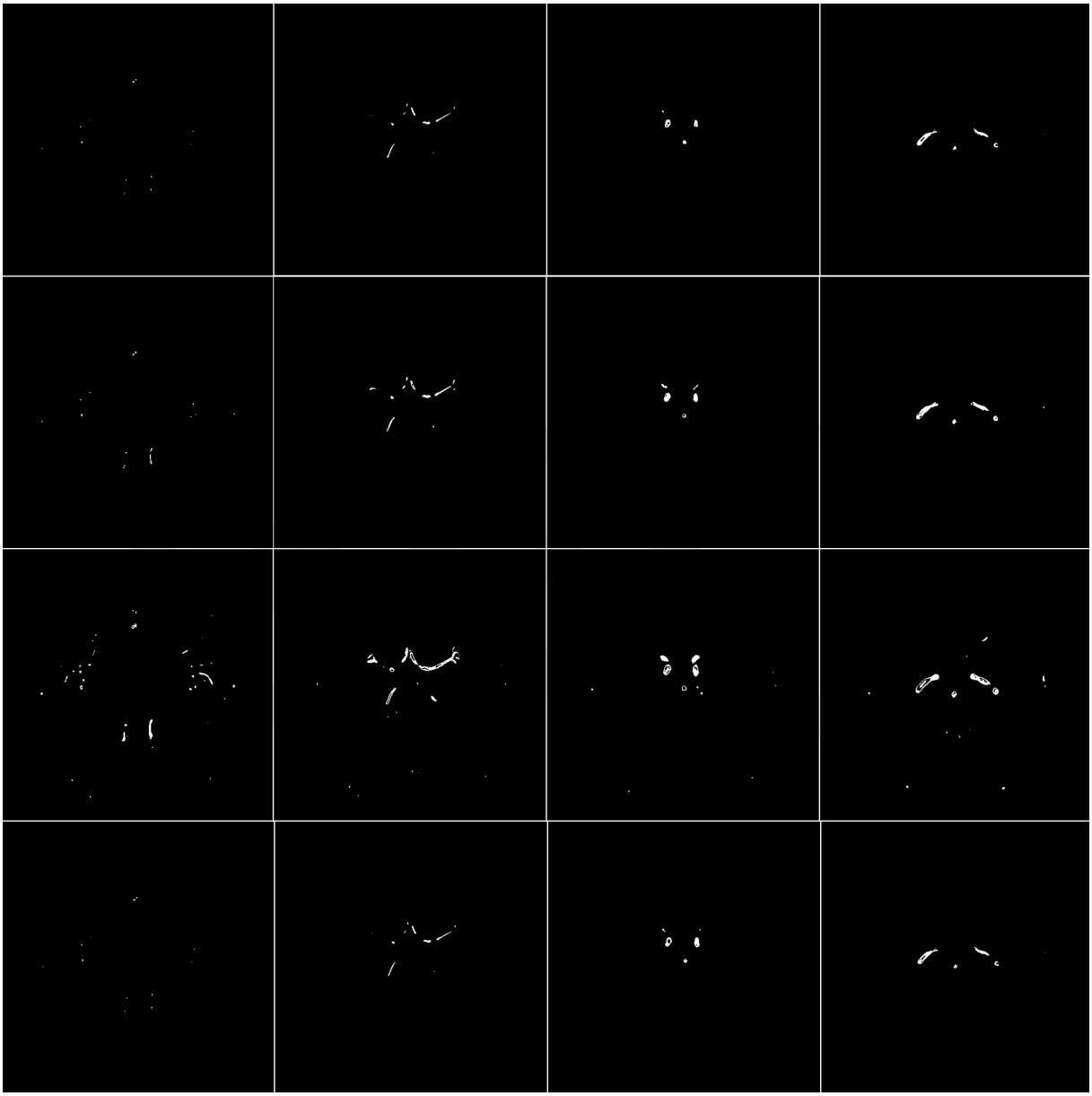

Figure 31 Otsu with 7 - 10 clusters.

Figure 32 illustrates the relation between the pixel count and the cluster number for the brain's scans. The chart shows that after segmenting the images into clusters, the number of pixels decreased while the number of clusters increased. Consequently, a large number of the arteries disappeared from the output images.

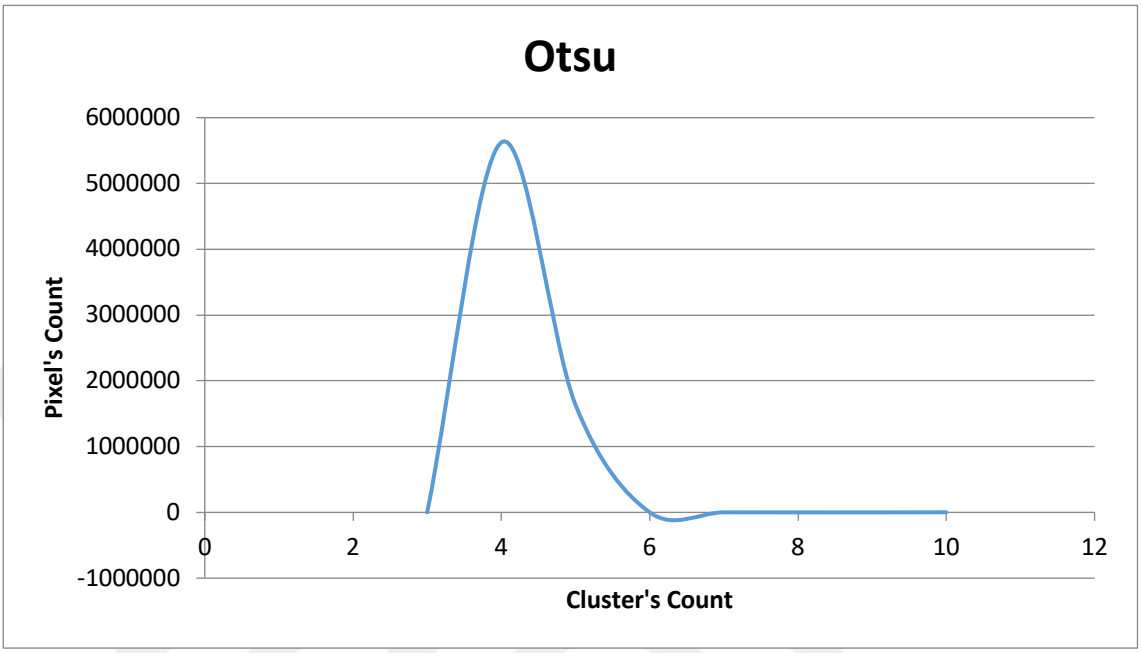

Figure 32 Otsu's pixels count by cluster.

After we finished the Otsu-based veins extraction, we applied a small area filter to the output images to remove unwanted noise pixels from the images. The values of these removed pixels were ranged from 1 to 100 pixels to determine the best value and thus ensure that no important information is lost during the filtering process. The values after 110 pixels were truncated due to the output of 0 pixels.

To help us understand the overall impact of successive filters or modifications on the data, we plot the cumulative difference plot for each cluster value. Those plots offer insights into the efficiency or effectiveness of the filtering process over time. The x axis of the plot is the cumulative absolute difference in the total number of pixels after applying a filter, and the y axis is the filtering values.

Figure 33 shows the cumulative change plot for the output images from the Otsu veins extraction with 3 clusters and small area filtering values ranging from 1 to 100 pixels.

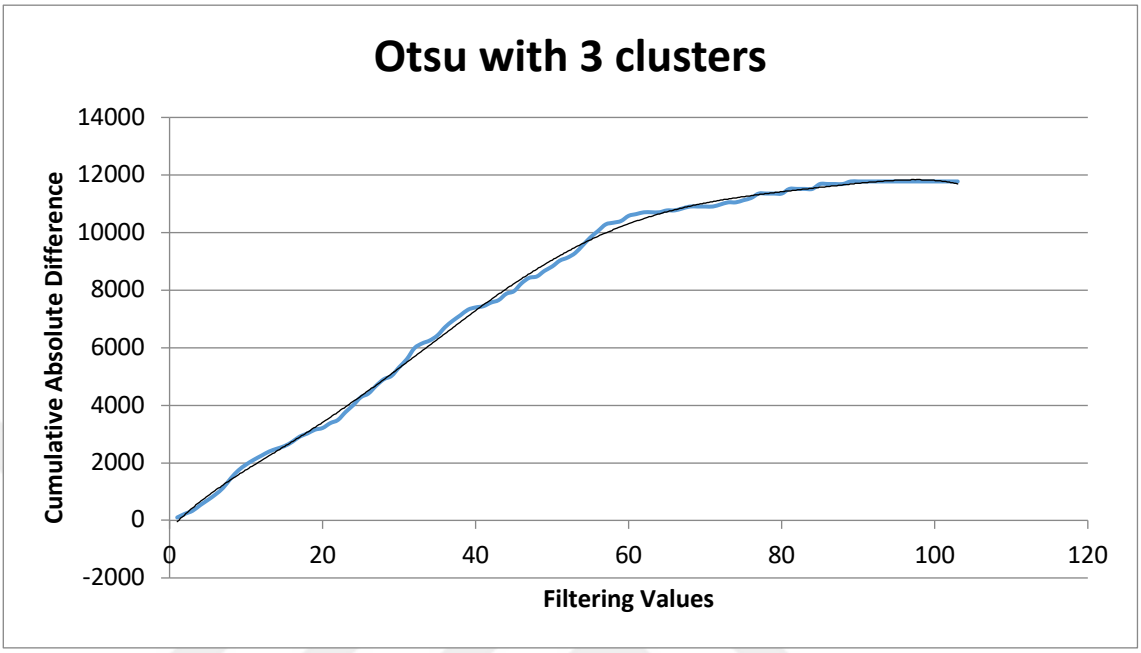

Figure 33 cumulative change plot for Otsu with 3 clusters.

Figure 34 shows the cumulative change plot for the output images from the Otsu veins extraction with 4 clusters and small area filtering values ranging from 1 to 100 pixels.

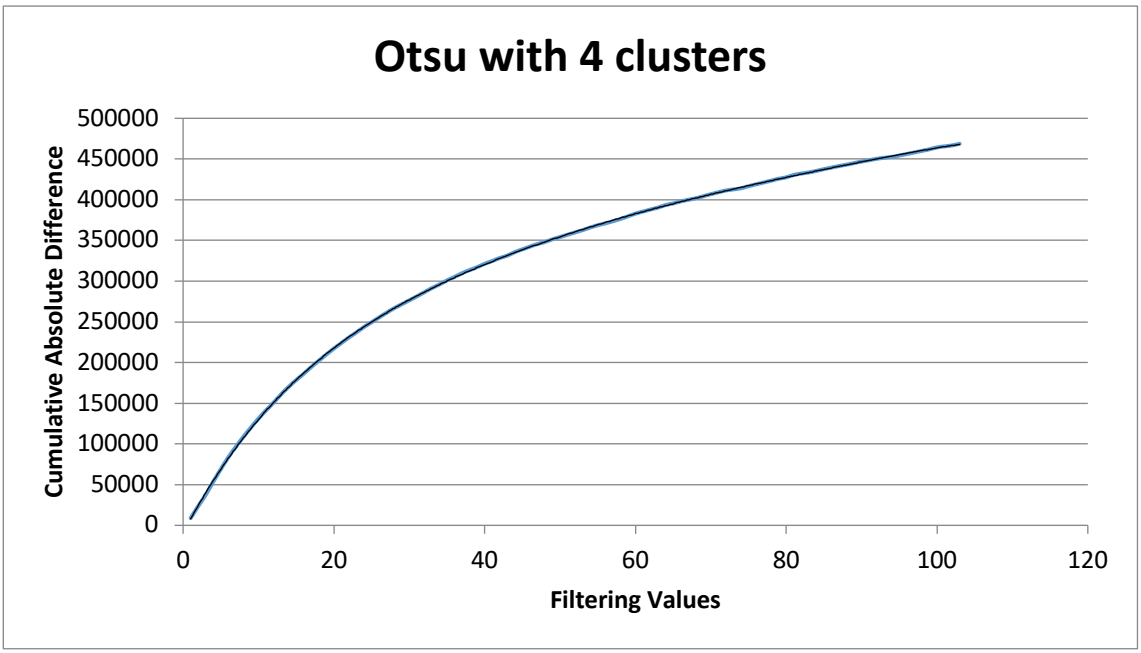

Figure 34 cumulative change plot for Otsu with 4 clusters.

Figure 35 shows the cumulative change plot for the output images from the Otsu veins extraction with 5 clusters and small area filtering values ranging from 1 to 100 pixels.

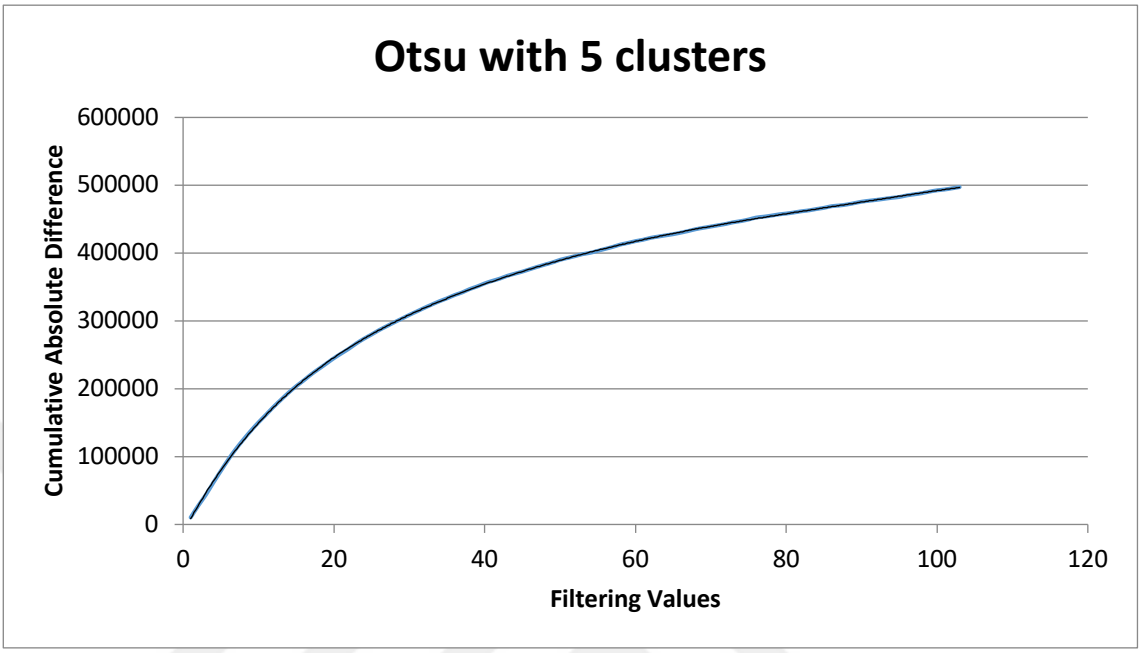

Figure 35 polynomial curve for Otsu with 5 clusters.

Figure 36 shows the cumulative change plot for the output images from the Otsu veins extraction with 6 clusters and small area filtering values ranging from 1 to 100 pixels.

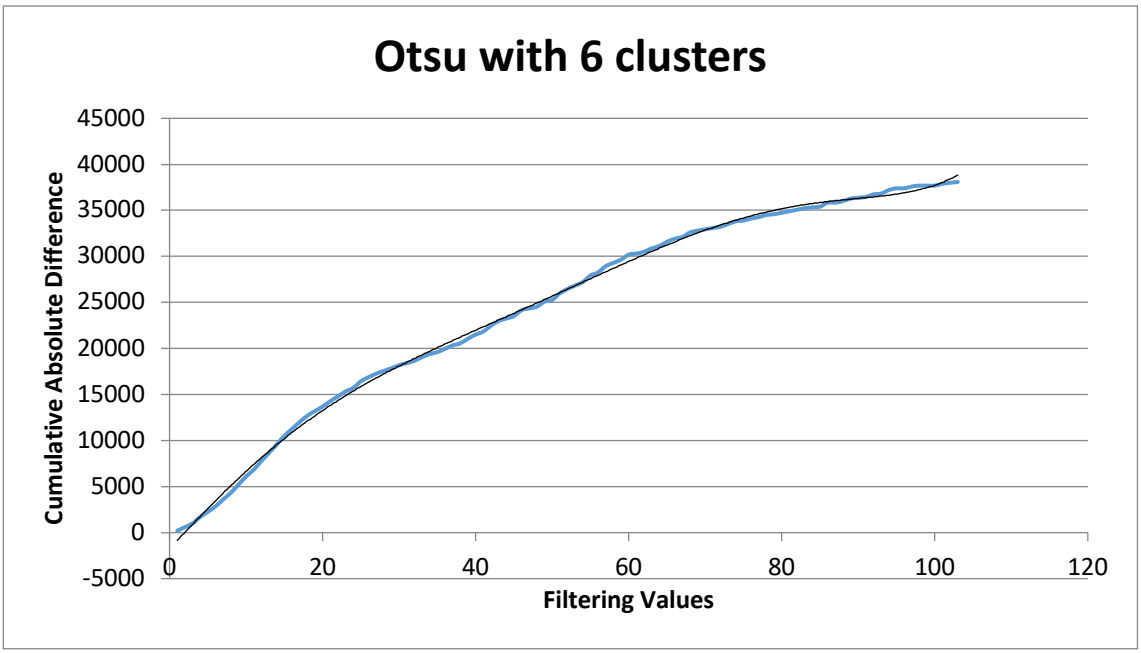

Figure 36 cumulative change plot for Otsu with 6 clusters.

Figure 37 shows the cumulative change plot for the output images from the Otsu veins extraction with 7 clusters and small area filtering values ranging from 1 to 100 pixels.

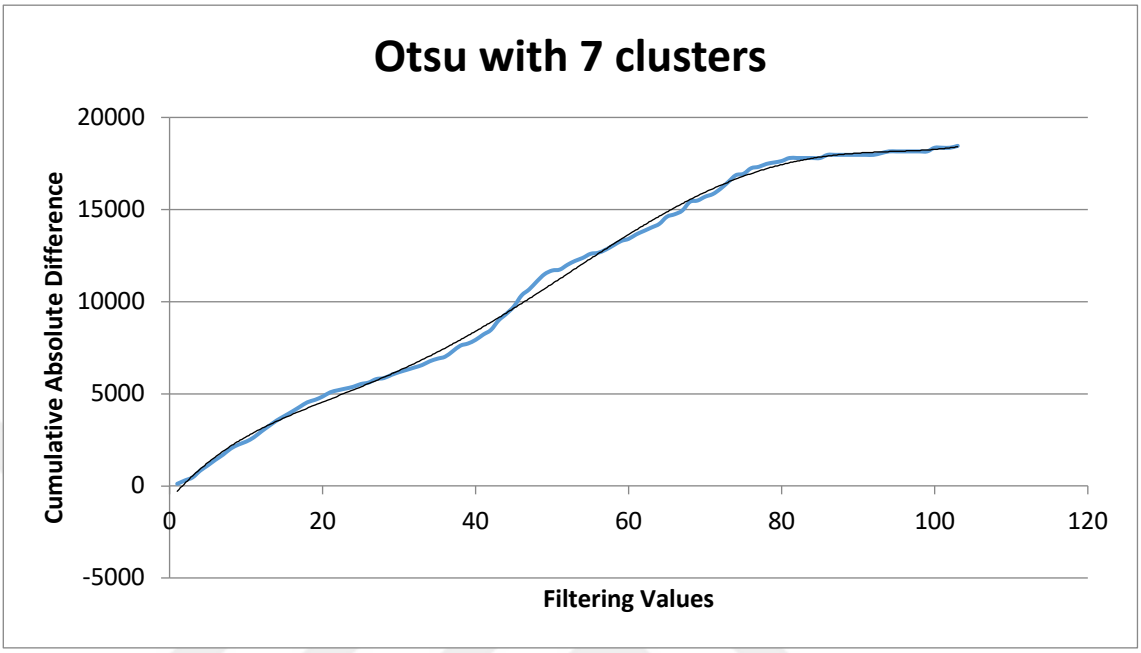

Figure 37 cumulative change plot for Otsu with 7 clusters.

Figure 38 shows the cumulative change plot for the output images from the Otsu veins extraction with 8 clusters and small area filtering values ranging from 1 to 100 pixels.

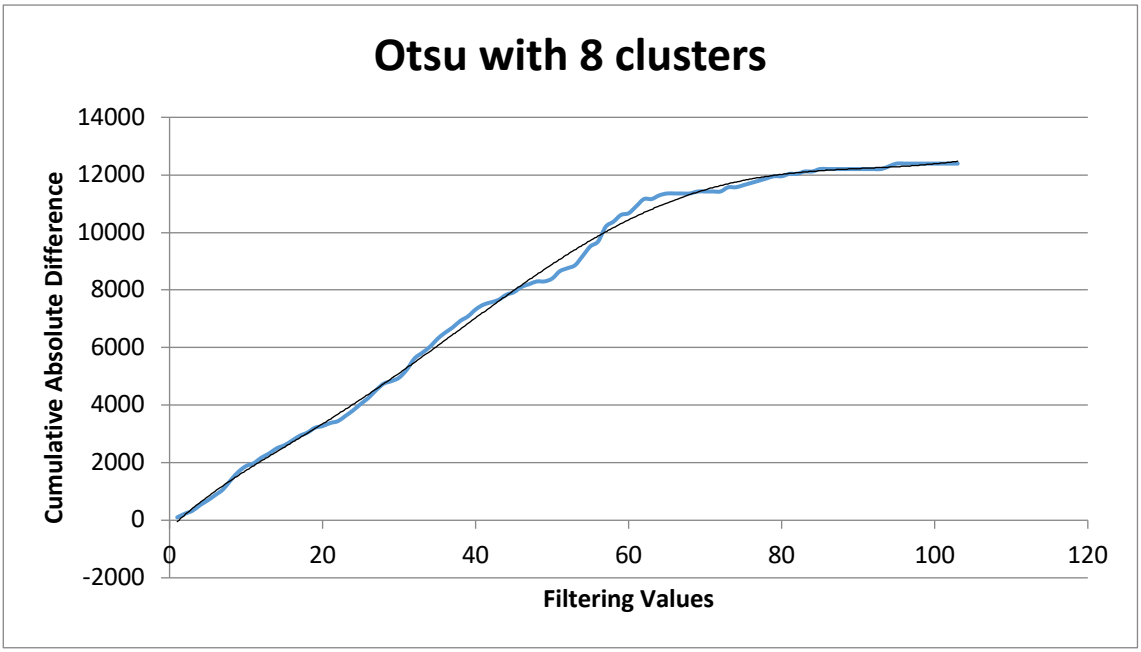

Figure 38 cumulative change plot for Otsu with 8 clusters.

Figure 39 shows the cumulative change plot for the output images from the Otsu veins extraction with 9 clusters and small area filtering values ranging from 1 to 100 pixels.

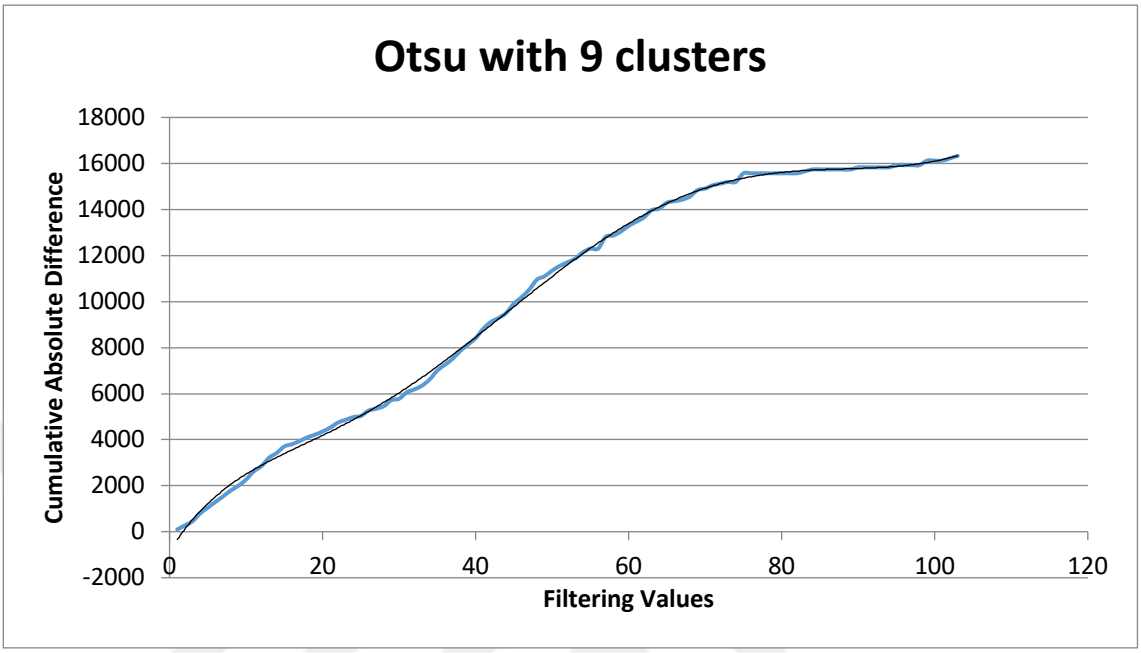

Figure 39 cumulative change plot for Otsu with 9 clusters.

Figure 40 shows the cumulative change plot for the output images from the Otsu veins extraction with 10 clusters and small area filtering values ranging from 1 to 100 pixels.

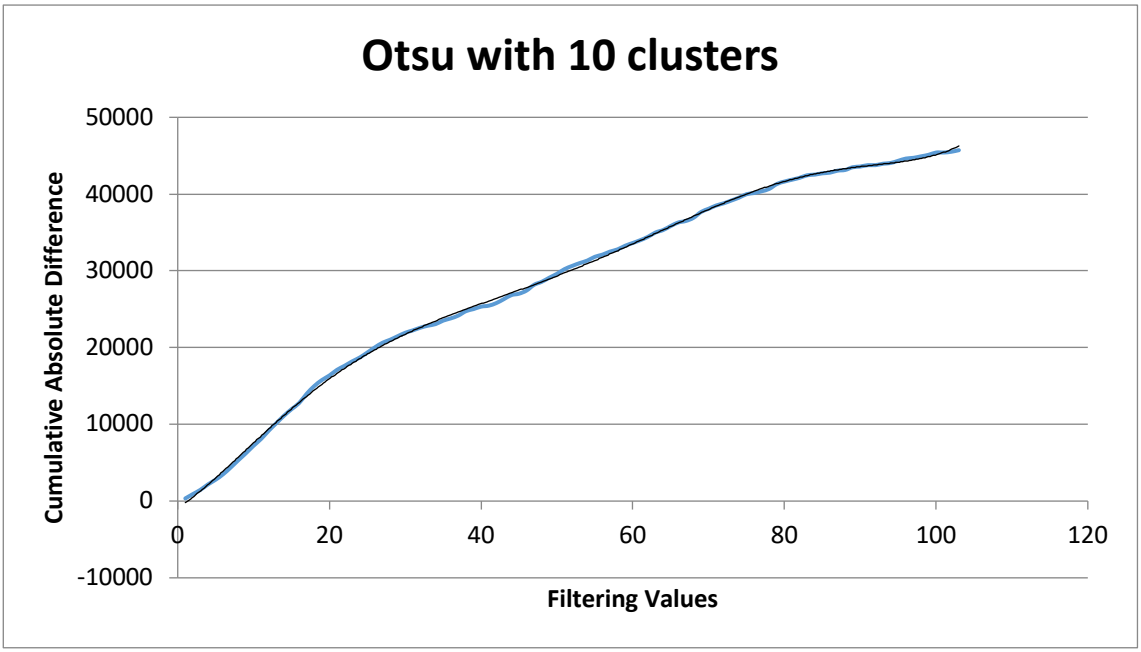

Figure 40 cumulative change plot for Otsu with 10 clusters.

We conducted a study using polynomial curve fitting for the cumulative change for each cluster value result to find the best value for the small area filter to remove areas without eliminating the veins and arteries.

Figure 41 illustrates the relationship between filter size and the remaining area for Cluster 9 using an 8th degree polynomial, depicted by the blue solid line. The x-axis spans filter sizes from 1 to 500, and the y-axis shows the remaining area which sharply increases with filter size and then plateaus. The red dashed line represents the first derivative of the polynomial, indicating the rate of change of the remaining area with respect to the filter size.

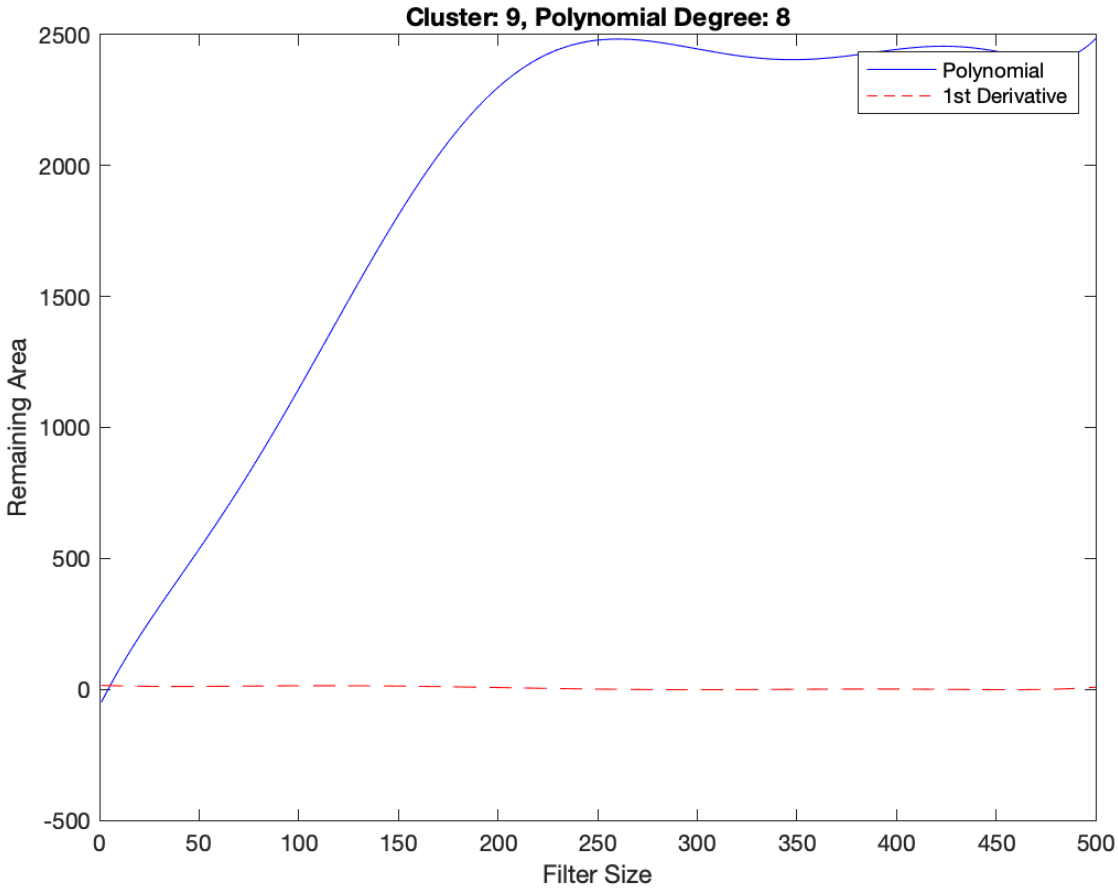

Figure 41 first derivative of polynomial curve of cumulative change of degree 8 and 9 clusters.

Figure 42 shows the second derivative of an 8th-degree polynomial for Cluster 9, with the filter size on the x-axis and the second derivative values on the y-axis. The green dashed line oscillates above and below zero, indicating points where the rate of change of the polynomial's slope varies with filter size. These oscillations suggest the presence of multiple inflection points, where the cavity of the polynomial curve changes. The second derivative approaching zero suggests diminishing acceleration in the change of the remaining area, with a significant increase as the filter size nears 500, hinting at a notable change in cavity or behavior in that region.

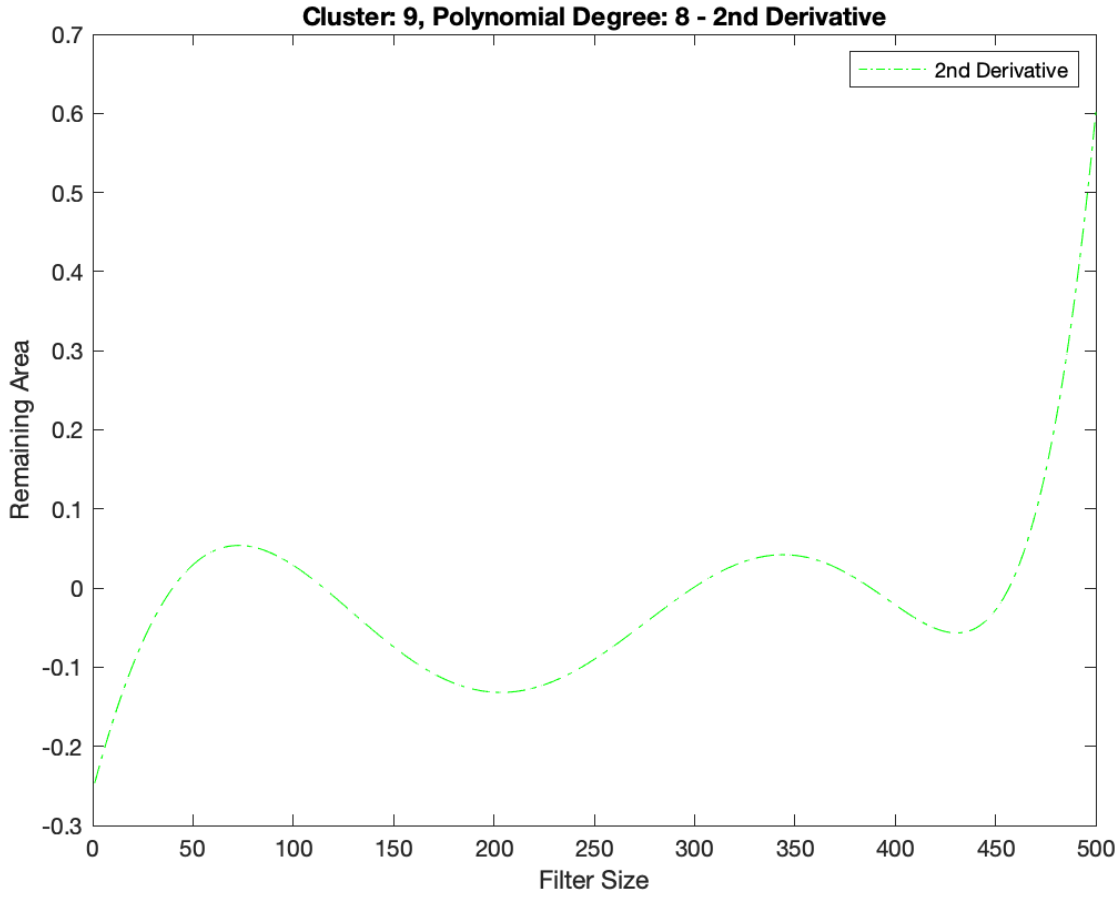

Figure 42 second derivative of polynomial curve of cumulative change of degree 8 and 9 clusters.

After we completed the polynomial calculations with the first and second derivatives, we put all the values together in a table, which made it easy to compare the results and select the best parameter for filtering the small area by taking the standard deviation of the values and selecting the lowest value.

	Clusters Count								
P		3	4	5	6	7	8	9	10

	3	312		322			383	446	362
	4	398	383	292	387	434	361	371	355
	5	397	392	269	384	400	304	330	295
	6	333	395	339	348	409	301	325	387
	7	376		387	348	414	373	388	368
	8	342		387	325		349	387	334
	9	338		348	325	335	342	356	334
	10	372		380	375	342	318	356	
	Average	**358,50**	**390,00**	**340,50**	**356,00**	**389,00**	**341,38**	**369,88**	**347,86**
	Standart Diveation	**31,70**	**6,24**	**44,32**	**26,32**	**40,73**	**31,05**	**38,56**	**29,91**

Table 2 shows all the values from the second derivative of cumulative change plot fitting for all the clusters from 3 to 10.

	Clusters Count								
Polynomial Degree		**3**	**4**	**5**	**6**	**7**	**8**	**9**	**10**
	3	312		322			383	446	362
	4	398	383	292	387	434	361	371	355
	5	397	392	269	384	400	304	330	295
	6	333	395	339	348	409	301	325	387
	7	376		387	348	414	373	388	368
	8	342		387	325		349	387	334
	9	338		348	325	335	342	356	334
	10	372		380	375	342	318	356	
	Average	**358,50**	**390,00**	**340,50**	**356,00**	**389,00**	**341,38**	**369,88**	**347,86**
	Standart Diveation	**31,70**	**6,24**	**44,32**	**26,32**	**40,73**	**31,05**	**38,56**	**29,91**

Table 2 the roots from the second derivative of cumulative change plot for Otsu.

The values of 9 clusters have the best average and standard deviation values which give the stable result that is equal to lowest average and lowest standard deviation, with 339 pixels as the parameter for the small area filter.

Figure 43 shows how the pixel values changed before and after small area filtering was applied to the images.

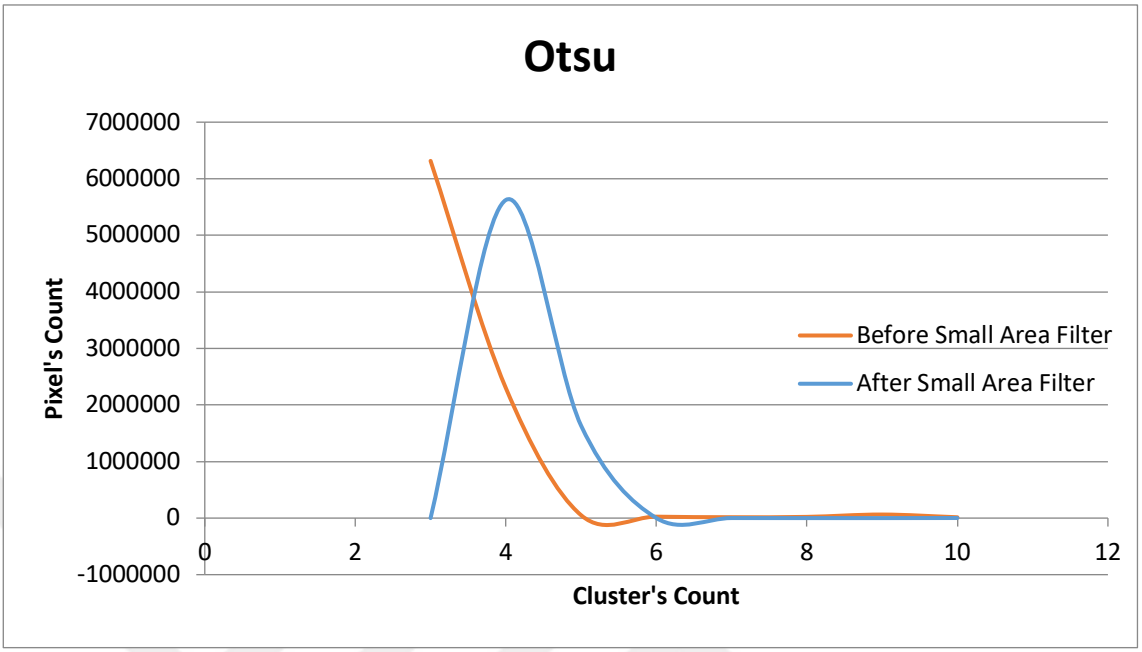

Figure 43 comparison of Otsu's pixels' values before and after small area filtering.

The output images from Otsu segmentation passed to remove small area filter, with 339 pixel areas to be removed from the images. The veins extraction improved after the small area filter was applied, and the veins and arteries were identified.

Figure 44 shows the brain slices after the segmentation algorithm and small area filter is applied with a parameter of 3 - 6 clusters and 339 pixels.

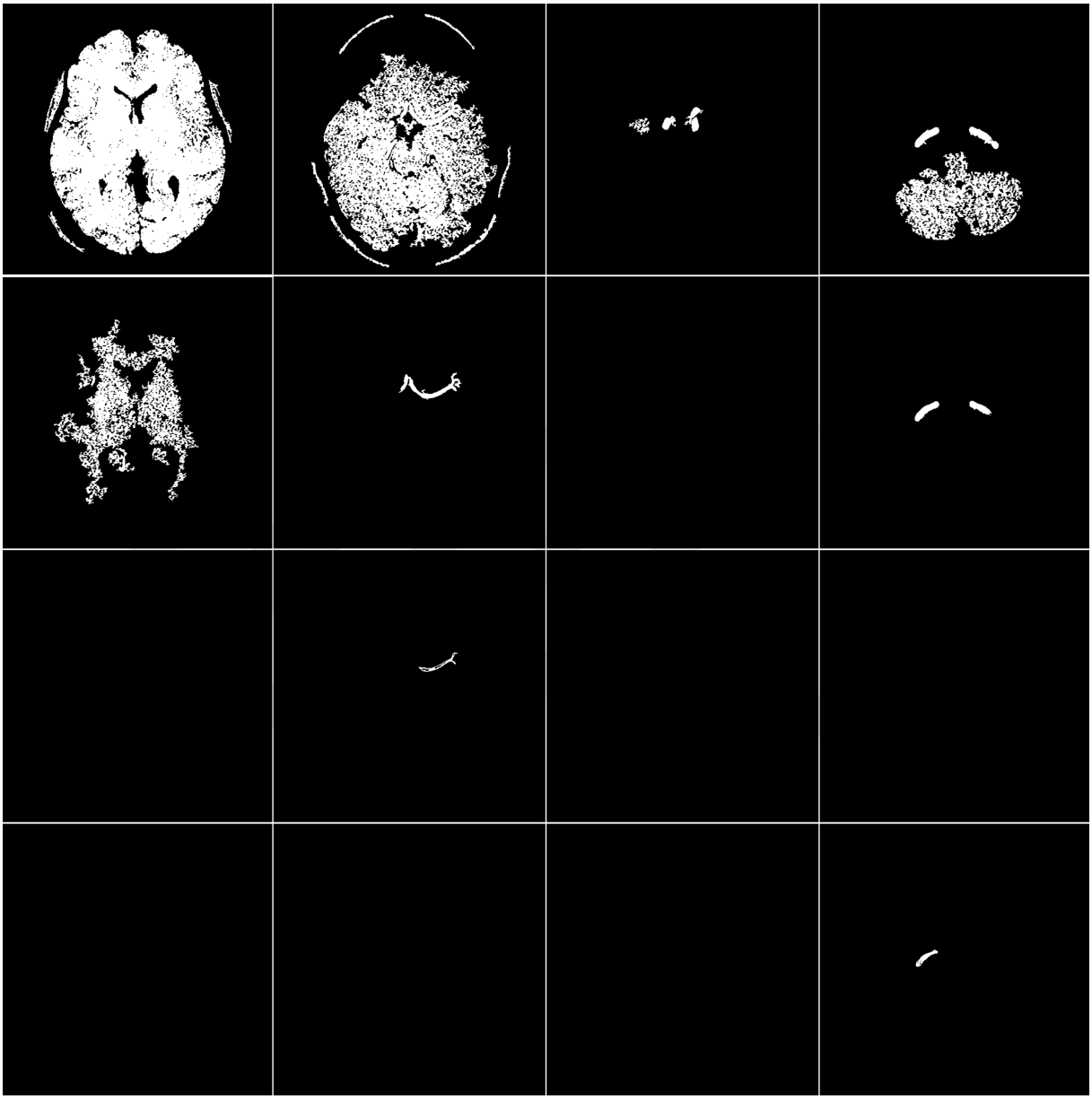

Figure 44 Otsu with 3 - 6 clusters and small area filter.

Figure 45 shows the brain's slices after the segmentation algorithm and small area filter is applied with a parameter of 7 - 10 clusters and 339 pixels.

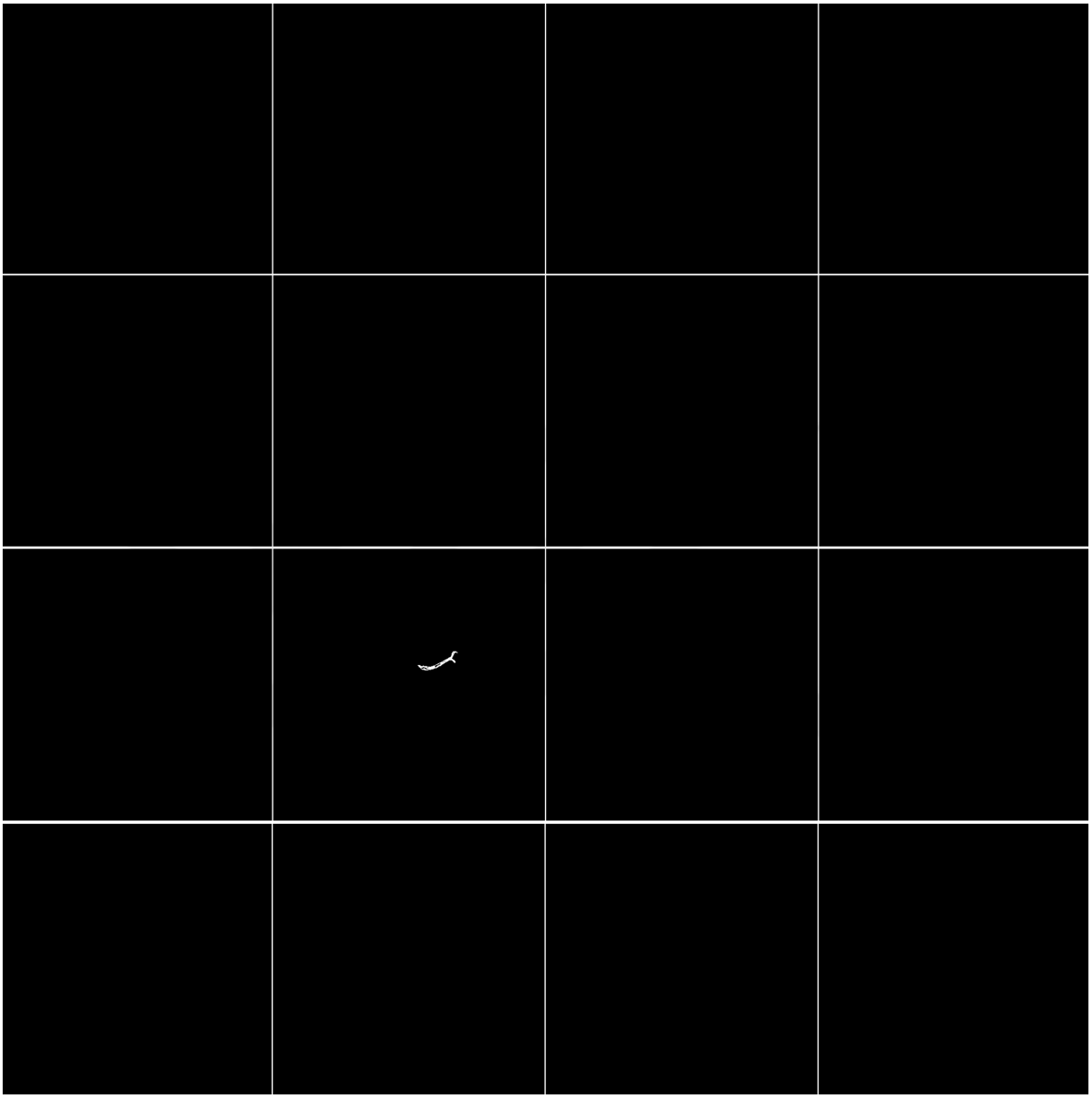

Figure 45 Otsu with 7 – 10 clusters and small area filter.

As we pointed earlier, the arteries vanished once the cluster count reached 6 or higher. Based on this, we concluded that the arteries were only visible in smaller clusters and when these clusters were broken up.

5.1.3. K-means results:

We ran the algorithm multiple times to find the best cluster number for the segmentation, which ranged from 3 to 10 clusters.

Figure 46 shows the brain slices after the K-means segmentation algorithm is applied with a parameter of 3 - 6 clusters.

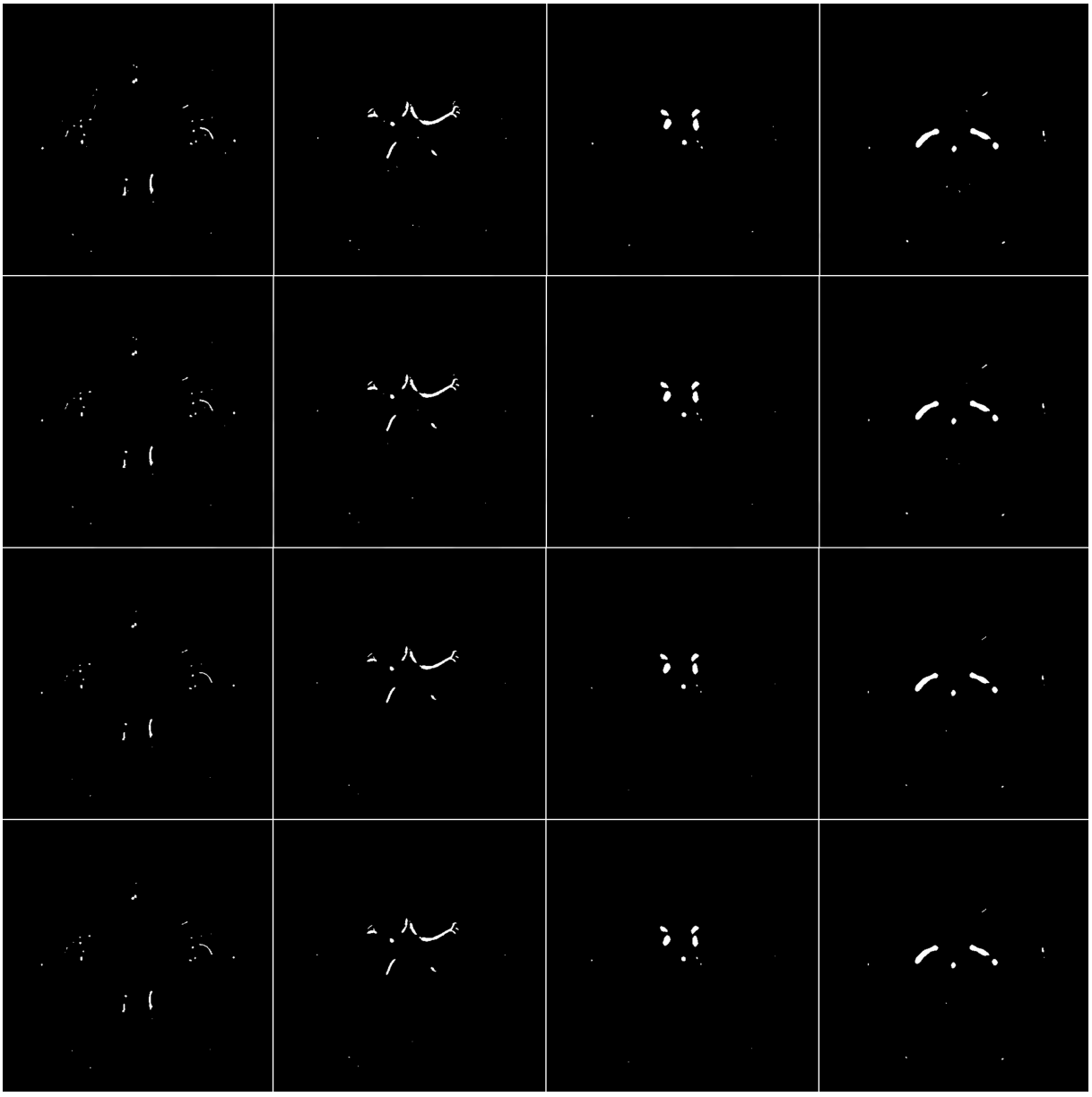

Figure 46 K-means with 3 – 6 clusters.

Figure 47 shows the brain slices after the K-means segmentation algorithm is applied with a parameter of 7 - 10 clusters.

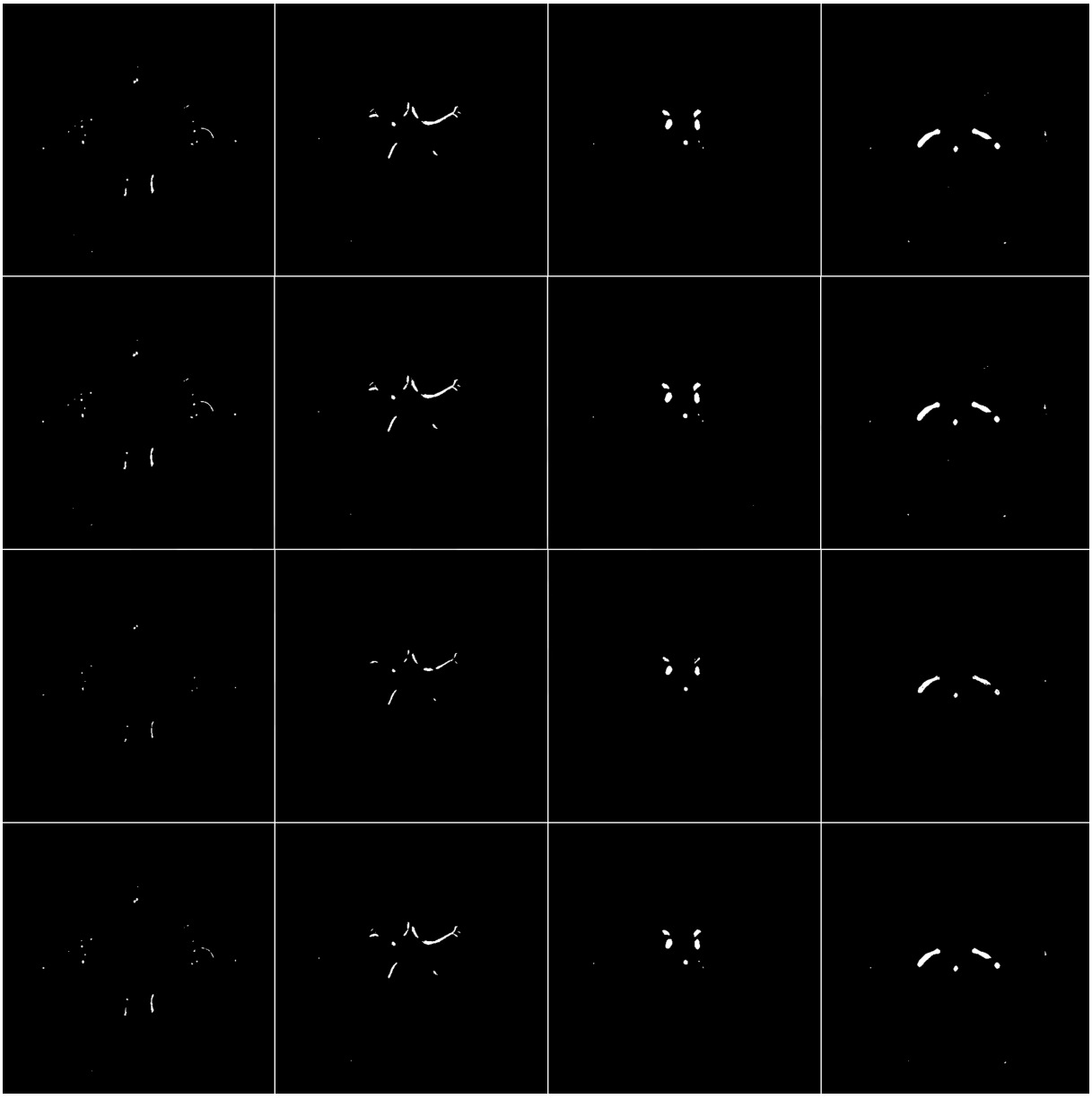

Figure 47 K-means with 7 - 10 clusters.

Figure 48 illustrates the relation between the pixel count and the cluster number for the brain scans. The chart shows that after segmenting the images into clusters, the number of pixels decreased while the number of clusters increased. Consequently, a large number of the arteries disappeared from the output images.

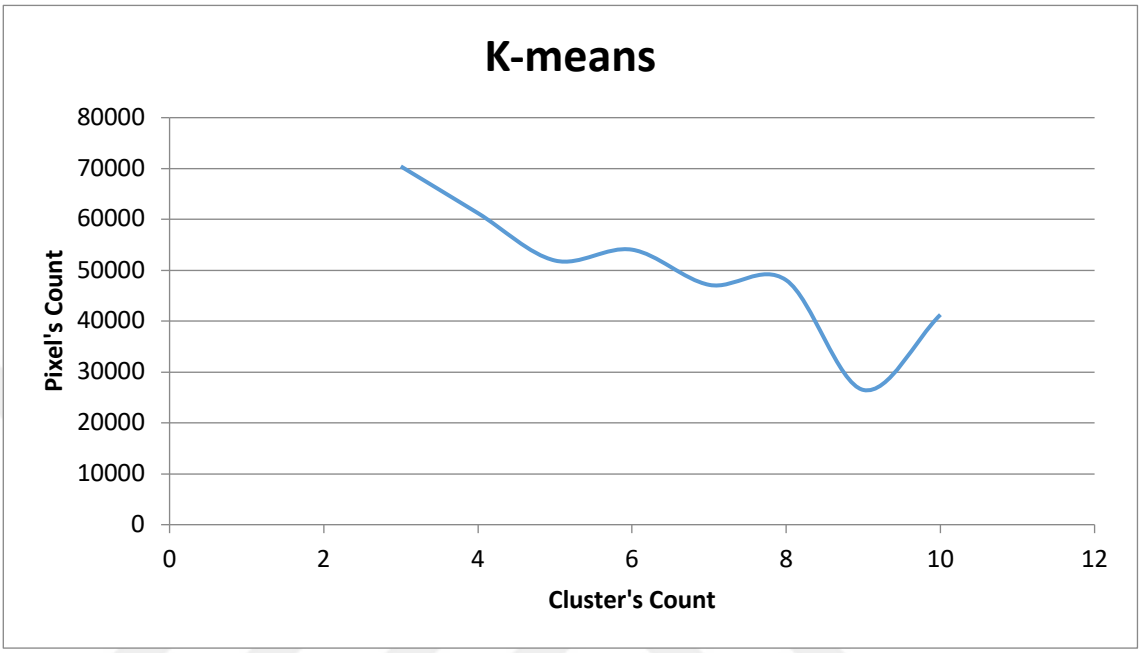

Figure 48 K-means pixels count by cluster.

After we finished the K-means-based veins extraction, we applied a small area filter to the output images to remove unwanted noise pixels from the images. The values of these removed pixels were ranged from 1 to 500 pixels to determine the best value and thus ensure that no important information is lost during the filtering process.

To help us understand the overall impact of successive filters or modifications on the data, we plot the cumulative difference plot for each cluster value. Those plots offer insights into the efficiency or effectiveness of the filtering process over time. The x axis of the plot is the cumulative absolute difference in the total number of pixels after applying a filter, and the y axis is the filtering values.

Figure 49 shows the cumulative change plot for the output images from the K-means veins extraction with 3 clusters and small area filtering values ranging from 1 to 500 pixels.

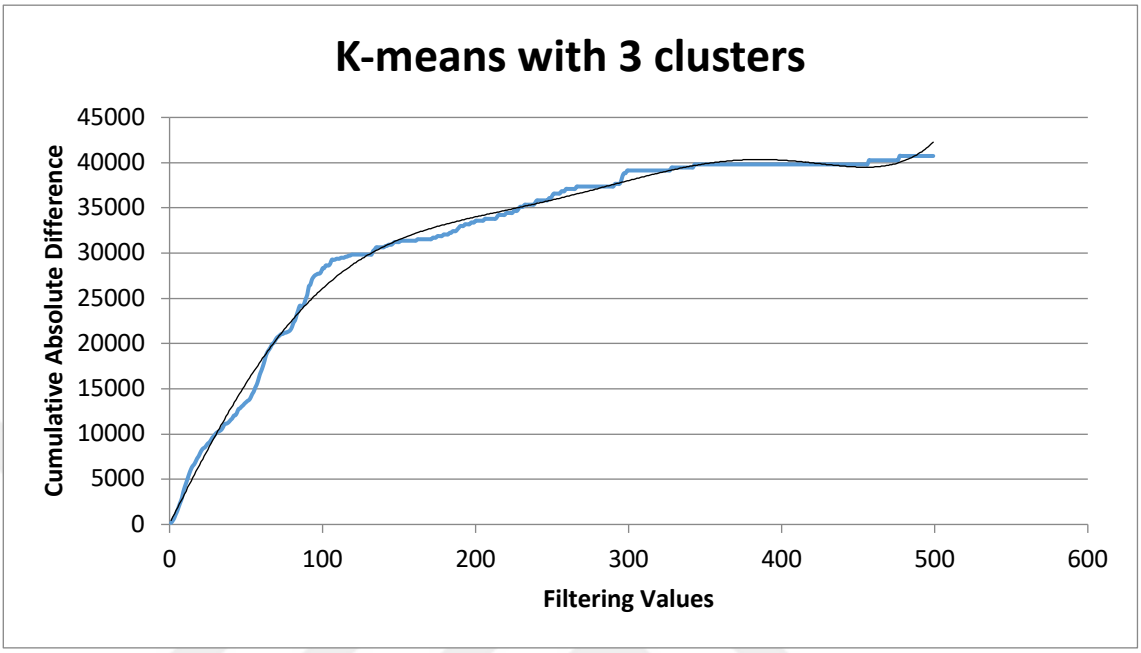

Figure 49 cumulative change plot for K-means with 3 clusters.

Figure 50 shows the cumulative change plot for the output images from the K-means veins extraction with 4 clusters and small area filtering values ranging from 1 to 500 pixels.

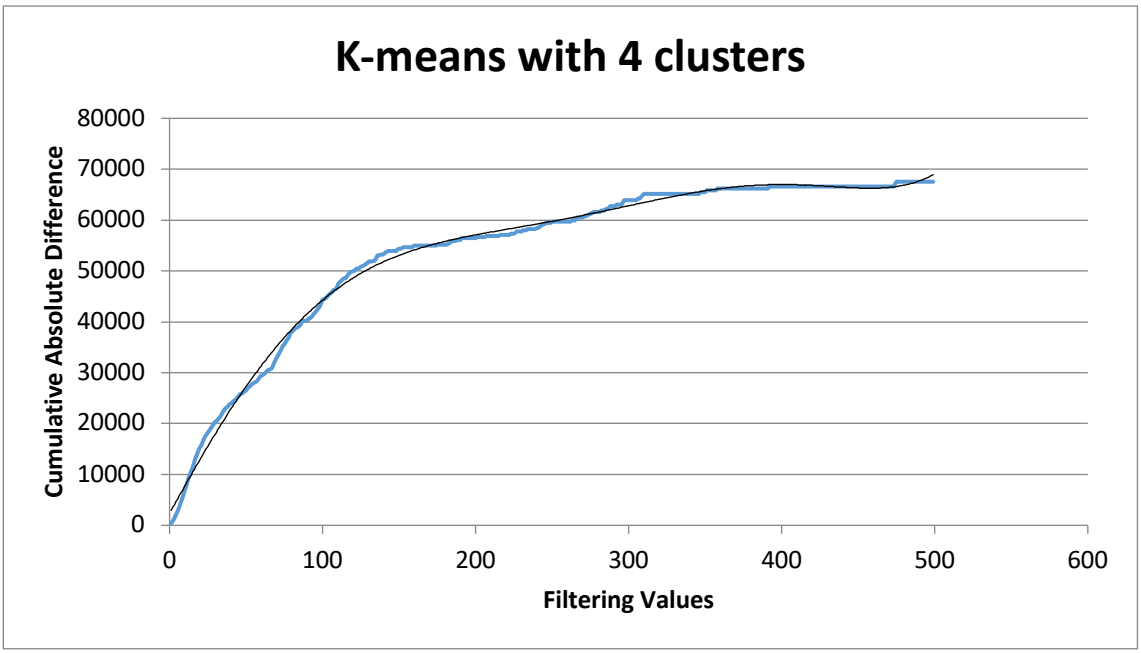

Figure 50 cumulative change plot for K-means with 4 clusters.

Figure 51 shows the cumulative change plot for the output images from the K-means veins extraction with 5 clusters and small area filtering values ranging from 1 to 500 pixels.

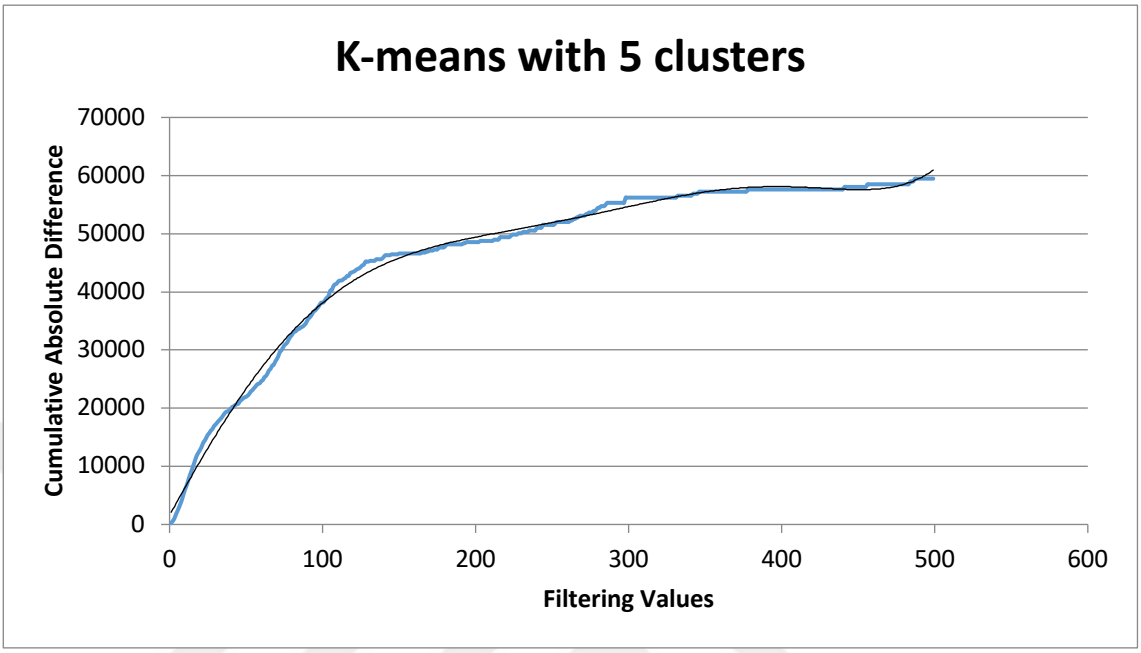

Figure 51 cumulative change plot for K-means with 5 clusters.

Figure 52 shows the cumulative change plot for the output images from the K-means veins extraction with 6 clusters and small area filtering values ranging from 1 to 500 pixels.

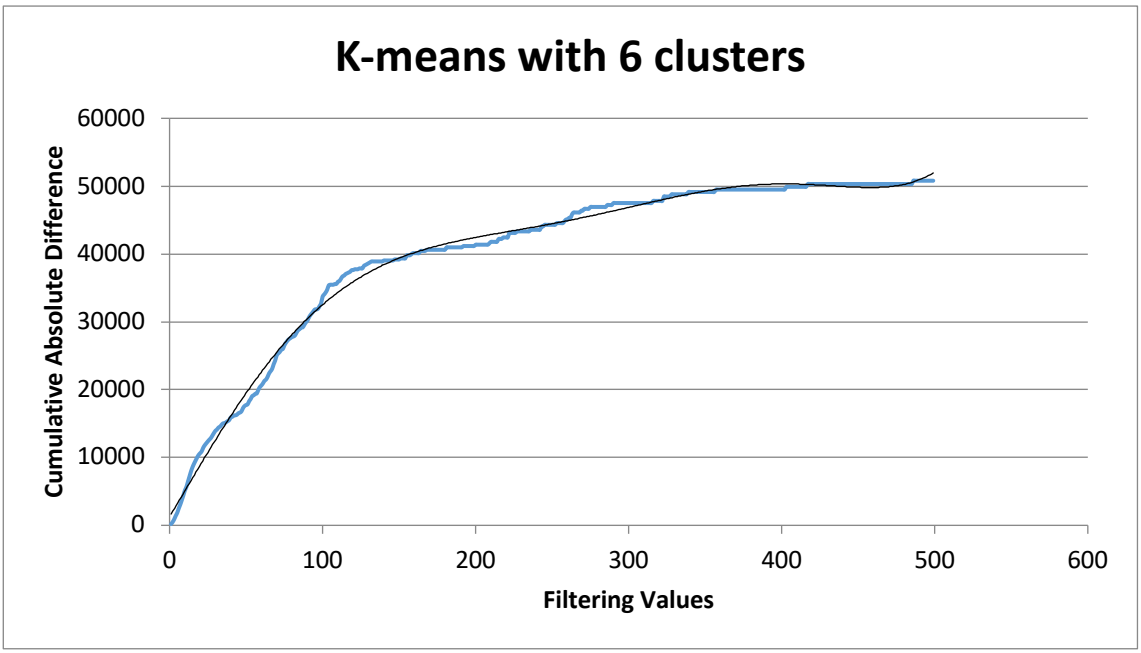

Figure 52 cumulative change plot for K-means with 6 clusters.

Figure 53 shows the cumulative change plot for the output images from the K-means veins extraction with 7 clusters and small area filtering values ranging from 1 to 500 pixels.

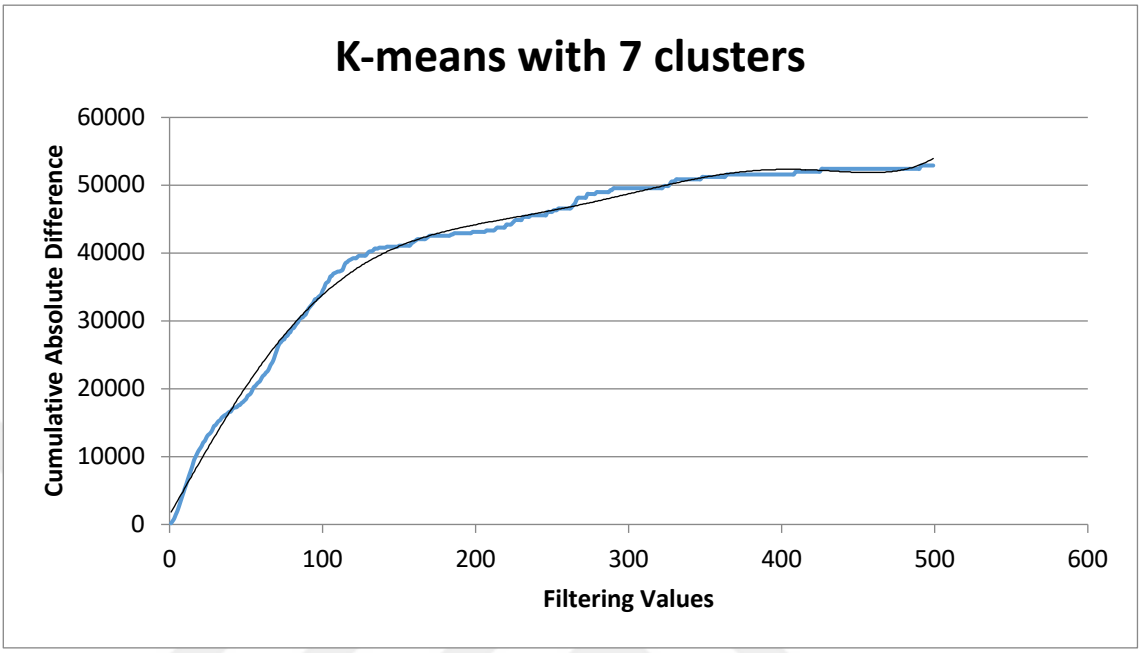

Figure 53 cumulative change plot for K-means with 7 clusters.

Figure 54 shows the cumulative change plot for the output images from the K-means veins extraction with 8 clusters and small area filtering values ranging from 1 to 500 pixels.

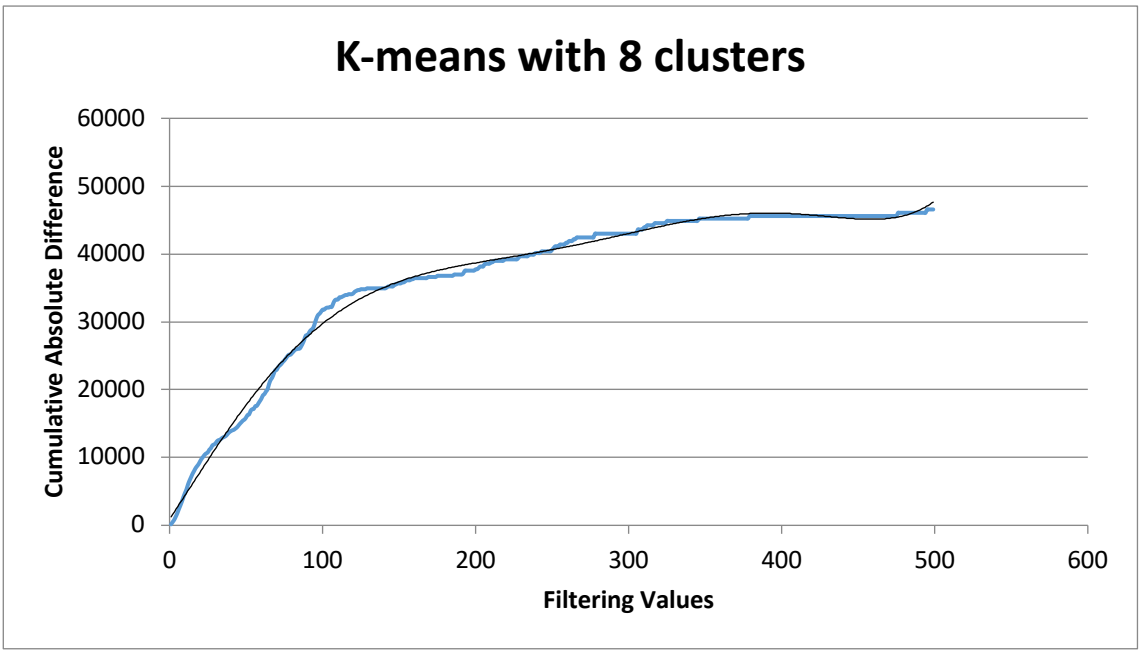

Figure 54 cumulative change plot for K-means with 8 clusters.

Figure 55 shows the cumulative change plot for the output images from the K-means veins extraction with 9 clusters and small area filtering values ranging from 1 to 500 pixels.

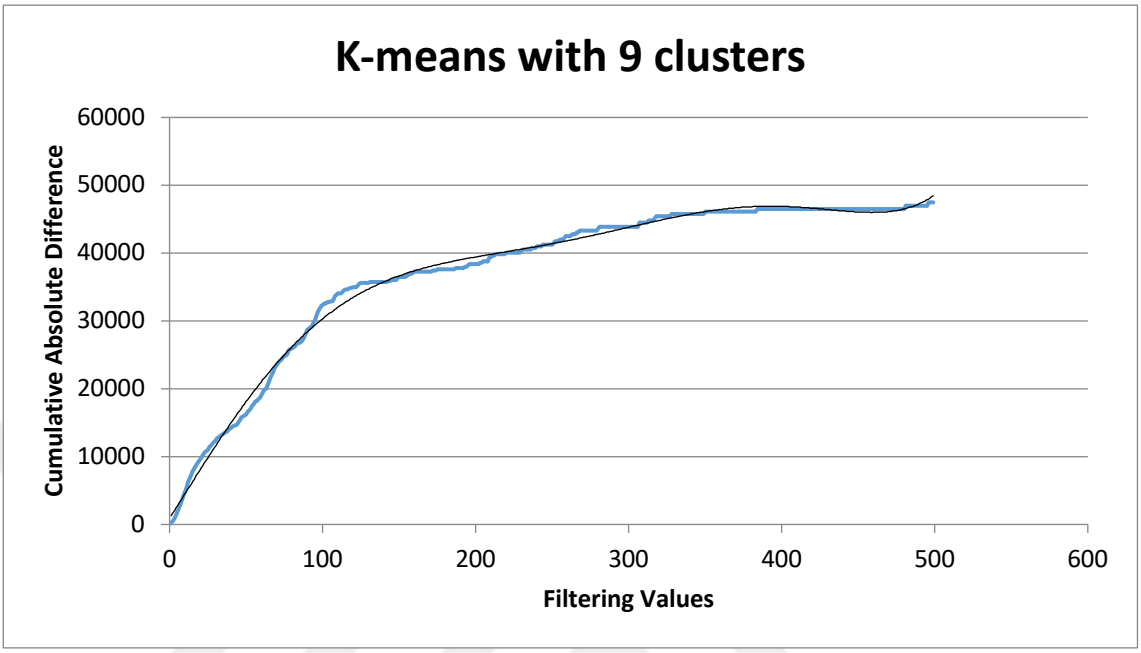

Figure 55 cumulative change plot for K-means with 9 clusters.

Figure 56 shows the cumulative change plot for the output images from the K-means veins extraction with 10 clusters and small area filtering values ranging from 1 to 500 pixels.

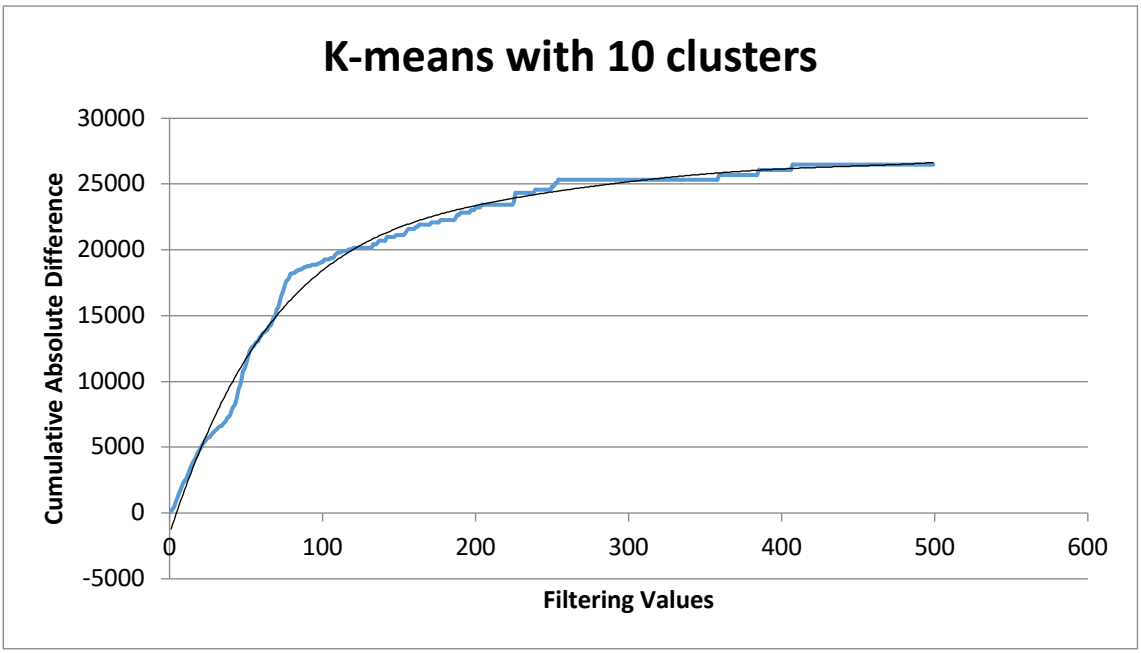

Figure 56 cumulative change plot for K-means with 10 clusters.

Figure 57 illustrates a 4th-degree polynomial function for Cluster 4, mapping the remaining area against filter size, which is scaled from 1 to 500. The blue solid line, representing the polynomial, shows a consistent increase in the remaining area as the filter size increases, indicative of a direct relationship between filter size and area. The red dashed line indicates the first derivative of the polynomial and remains above zero throughout the plot, signifying a continuous increase in the remaining area without any local maxima or minima.

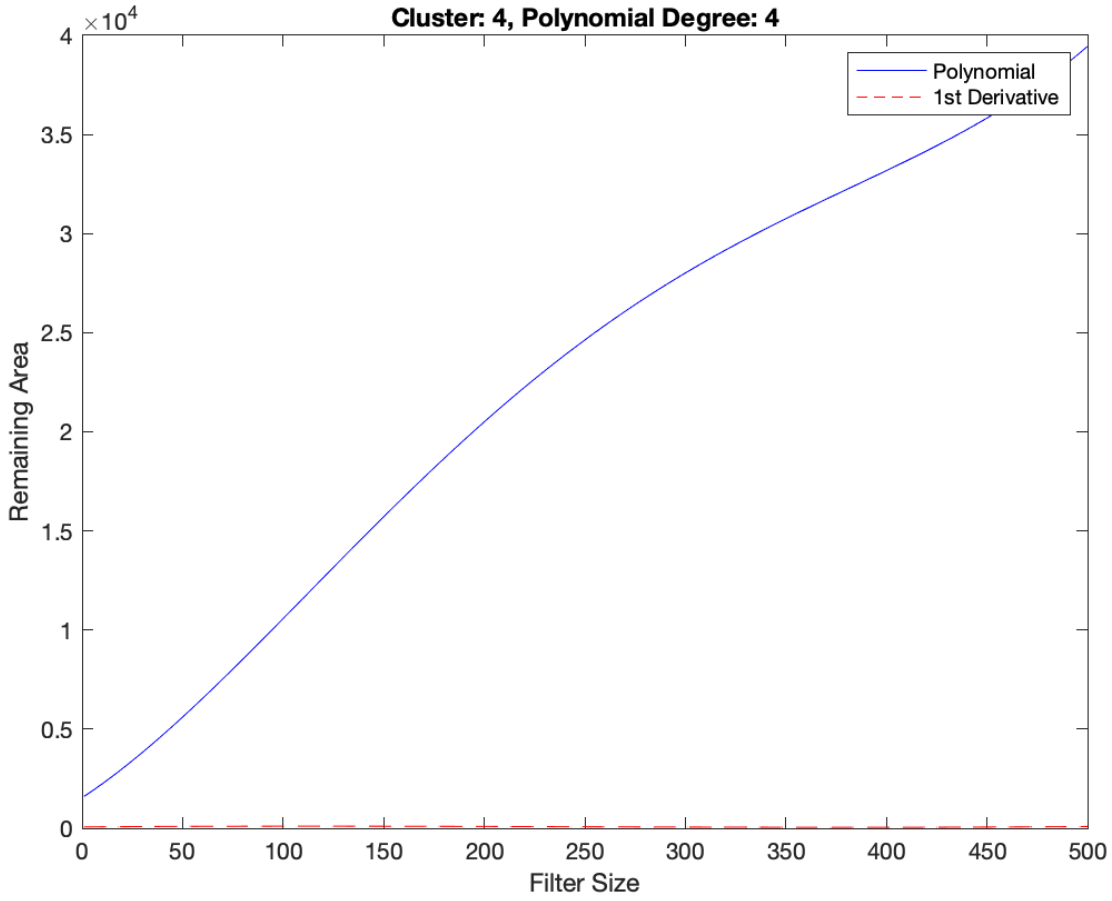

Figure 57 first derivative of polynomial curve of cumulative change of degree 4 and 4 clusters.

Figure 58 shows the second derivative of a 4th-degree polynomial for Cluster 4, with filter size on the x-axis and the second derivative on the y-axis. The green dashed line displays a concave upward curve, starting with positive values, decreasing through zero, and then increasing back into the positive range as the filter size goes from 1 to 500. The zero-crossing point indicates an inflection point where the rate of acceleration of the remaining area changes from positive to negative and then back to positive. This suggests that initially, the rate of change of the remaining area increases, then it decreases around the inflection point, and begins to increase again as the filter size continues to grow.

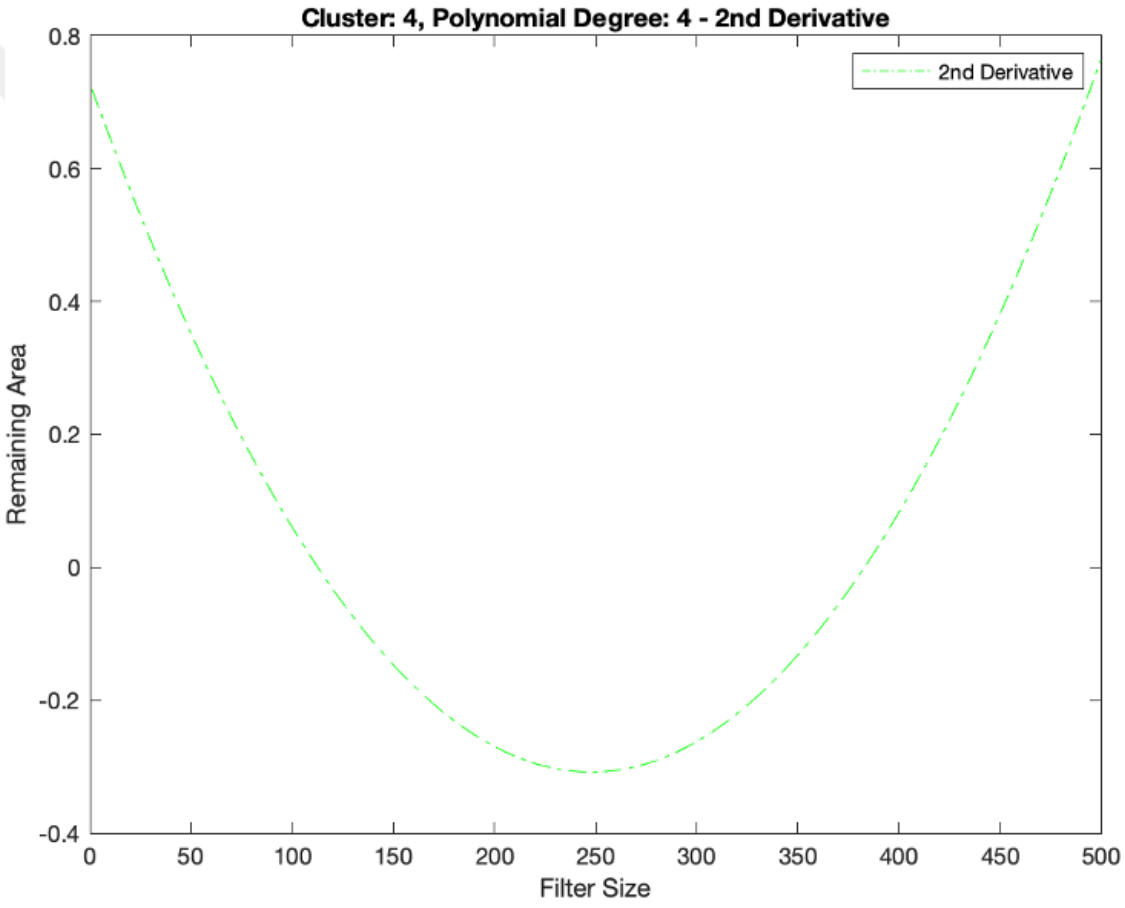

Figure 58 second derivative of polynomial curve of cumulative change of degree 4 and 4 clusters.

After we carried out polynomial calculations with the first and second derivatives, we put all the values together in a table, which made it easy to compare the results and select the best parameter for filtering the small area by taking the standard deviation of the values and selecting the lowest value.

Table 3 shows all the values from the second derivative of cumulative change plot fitting for all the clusters from 3 to 10.

		Clusters Count							
Polynomial Degree		**3**	**4**	**5**	**6**	**7**	**8**	**9**	**10**
	3					99		490	
	4	396	383	363	411	397		373	
	5	396	392	383	414	399		316	
	6	364	395	374	358	348	311	305	435
	7					383		326	424
	8	341		374	381	385	358	394	425
	9			377		383	348	391	
	10	321					357	380	390
	Average	**374,25**	**390,00**	**374,20**	**391,00**	**342,00**	**343,50**	**371,88**	**418,50**
	Standart Diveation	**26,81**	**6,24**	**7,26**	**26,57**	**108,45**	**22,13**	**59,25**	**19,64**

Table 3 the values from the second derivative of cumulative change plot for K-means.

The values of 5 clusters have the best average and standard deviation values, with 374 pixels as the parameter for the small area filter.

Figure 59 shows how the pixel values changed before and after small area filtering was applied to the images.

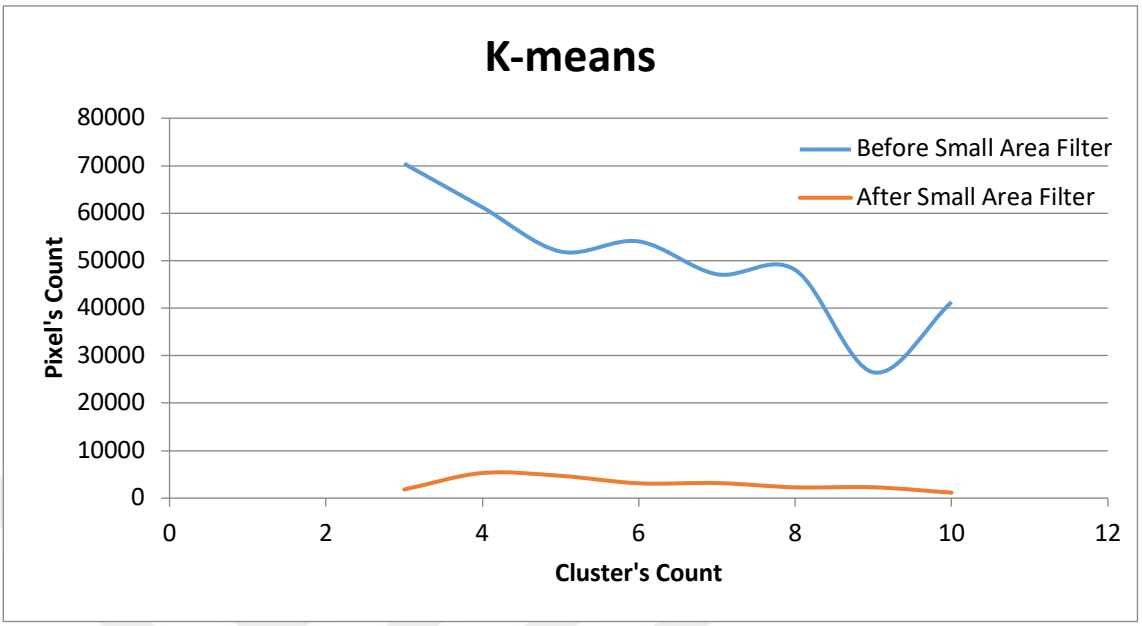

Figure 59 comparison of K-means pixels' values before and after small area filtering.

The output images from K-means segmentation have been given to remove small area filter, with 374 pixel areas to be removed from the images. The veins extraction improved after the small area filter was applied, and the veins and arteries were identified.

Figure 60 shows the brain slices after the segmentation algorithm and small area filter is applied with a parameter of 3 - 6 clusters and 374 pixels.

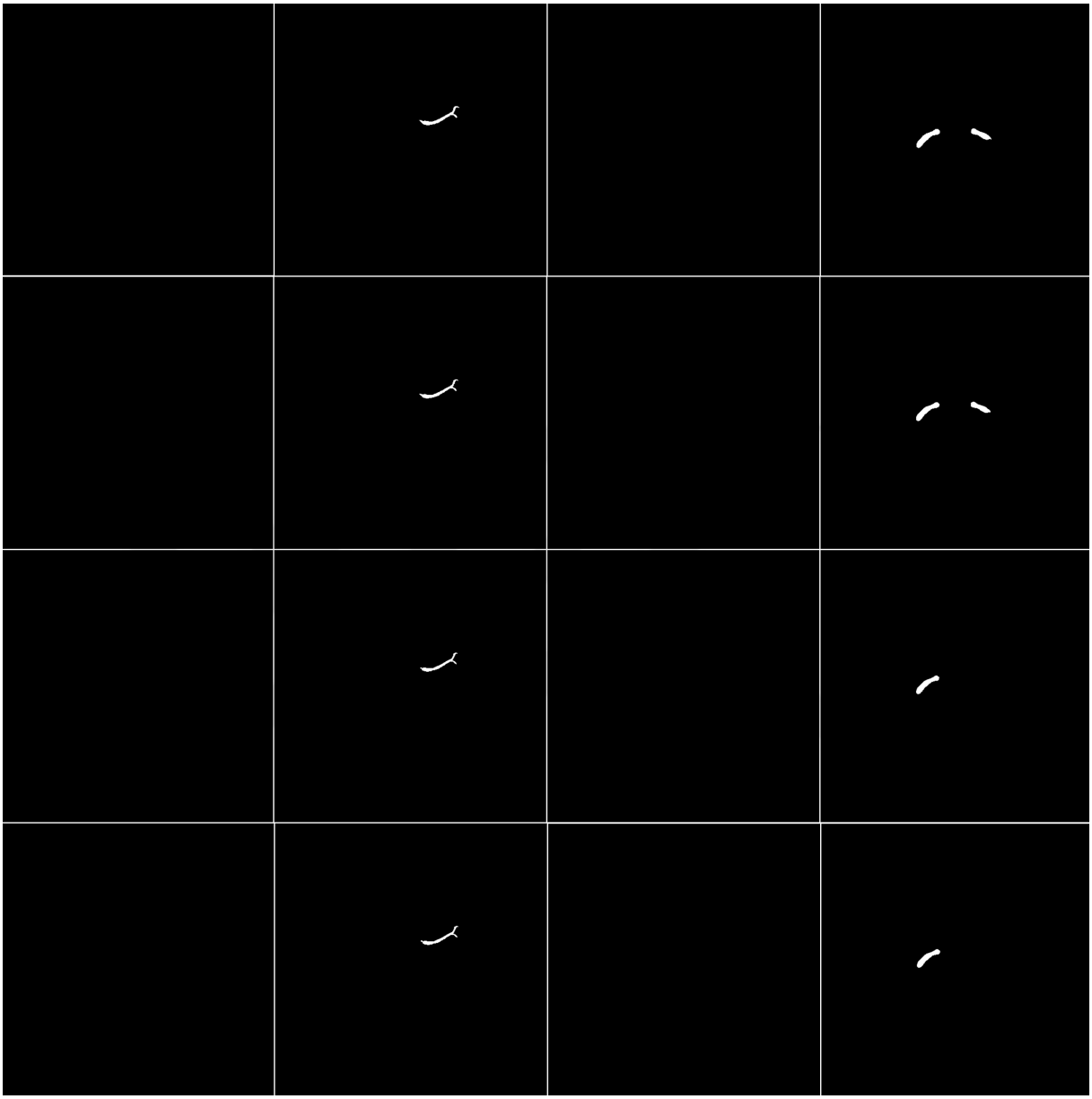

Figure 60 K-means with 3 - 6 clusters and small area filter.

Figure 61 shows the brain slices after the segmentation algorithm and small area filter is applied with a parameter of 7 - 10 clusters and 374 pixels.

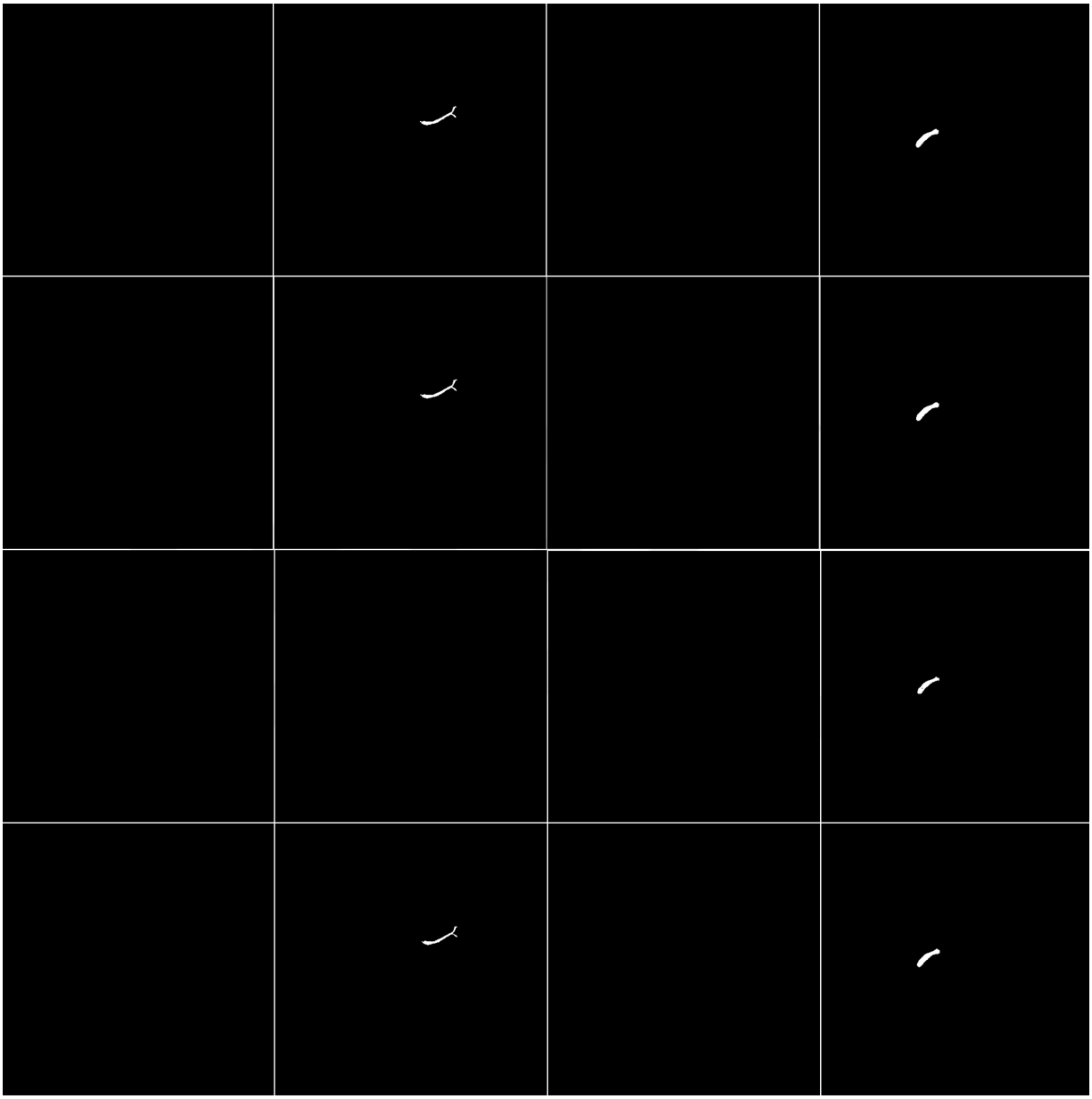

Figure 61 K-means with 7 - 10 clusters and small area filter.

After we conducted all the segmentation and small area filtering processes, we brought all the results from the quantitative analysis together and subjected them to a qualitative analysis.

We found out that Otsu and k-means reduce the total area of the veins, whereas the FCM leaves a bigger area. Additionally, we noticed that the increase in the counts of segmentation cluster leads to a decrease in the area of the veins.

We compared the results and searched for the best cross-area section of all veins and all values based on the cost function. As a result, we found out that the K-means algorithm with a parameter of five clusters performed the best in terms of accuracy, which can be attributed to the fact that it is able to more precisely identify and distinguish veins in different areas. The FCM and Otsu algorithms, on the other hand, were hardly functional in this area, with Otsu even failing to identify some of the veins properly.

The polynomial representing the cumulative difference of pixel values was derived for filter sizes ranging from 1 to 500 pixels. Subsequently, the first derivative of this polynomial was computed to find out the rate of change. Due to the inability to identify critical points through the first derivative, the second derivative was calculated to determine the rate of the rate of change, which aids in identifying inflation points where changes are minimal. This differentiation process was applied to polynomials of degrees ranging from third to tenth, aiming to pinpoint inflation points indicative of minimal change.

Upon increasing the filter size, a noticeable expansion in the gap was observed, prompting an investigation into the roots of the polynomial to identify points at which changes plateaued. The rationale behind focusing on the second derivative was to effectively discern the peak of the cavity, especially as the increment in filter size gradually eliminated smaller areas.

In refining our analysis, values falling outside predefined boundaries (between 1 and 500), along with imaginary and negative values that were deemed irrelevant to our context, were excluded.

The analysis culminated in identifying the roots of the second derivative that corresponded to the lowest average, signifying the peak of the cavity. This specific metric, coupled with the lowest standard deviation, was evaluated across polynomial degrees from three to ten and for cluster counts ranging from three to ten. This comprehensive approach ensured the identification of points where changes in pixel values, following the application of varying filter sizes, reached a saturation point, thereby providing insights into the optimal filter size for image processing tasks.

5.2. Brain Extraction Results:

For the brain extraction phase, we used morphological brain extraction. This is typically done using morphological operations, which are mathematical functions that analyze the shape and structure of an image. By performing these operations on the input image, features such as edges, contours, and corners are detected.

These images can then be used to accurately measure the injection depth and ensure that the correct amount of medication is administered.

Figure 62 shows an example of the output slices from the brain extraction phase, which outline the borders of the skull. These slices are then used to create a 3D image of the skull, which can then be studied in more detail.

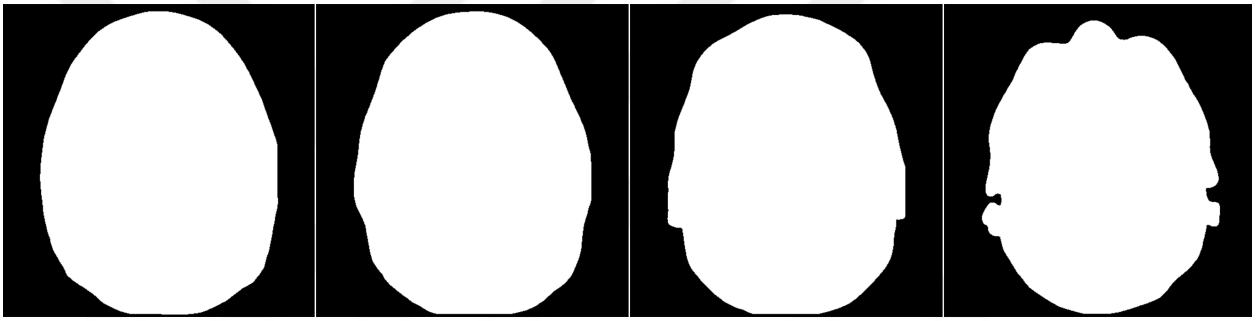

Figure 62 Output slices of brain extraction.

5.3. 3D Map Results:

We fed the slices from the segmentation and brain extraction to the software that constructs a 3D map of the brain. The software reads each image set and assigns a unique value to every pixel. The values of the veins and arteries are different from the values of the skull and the background. It then puts the pixels together to create a 3D model of the brain, which provides the opportunity for a detailed observation of the structures of the brain.

Notably, the 3D brain map can be used to figure out the shortest route from an injection point to the target point. This helps medical staffers to decide the best way to give treatments like drug injections.

Figure 63 depicts various projections of brain scan images. The slices depicted contain the skull in gray and the arteries in white.

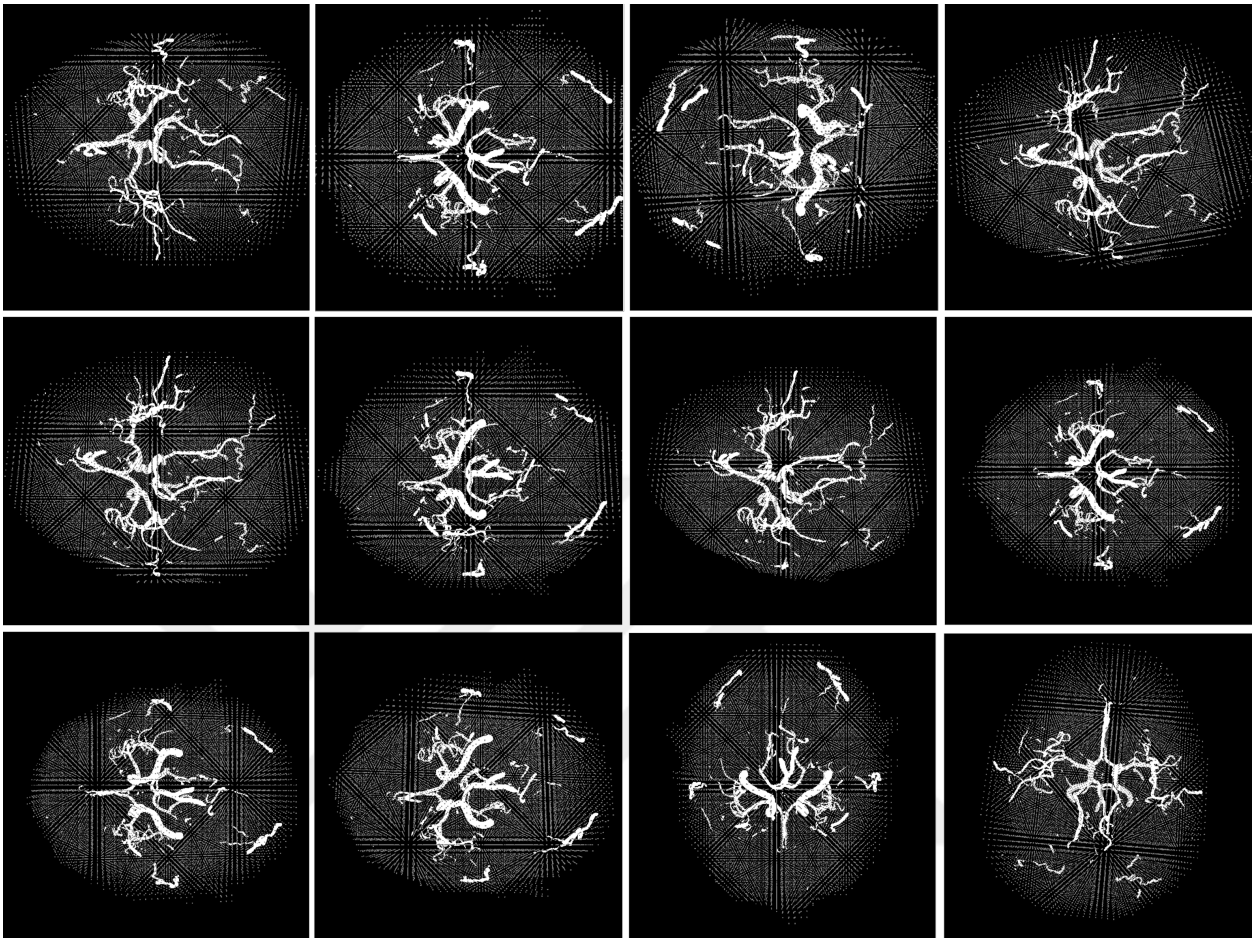

Figure 63 Brain's skull and arteries 3D map.

Figure 64 depicts various projections of brain arteries in white.

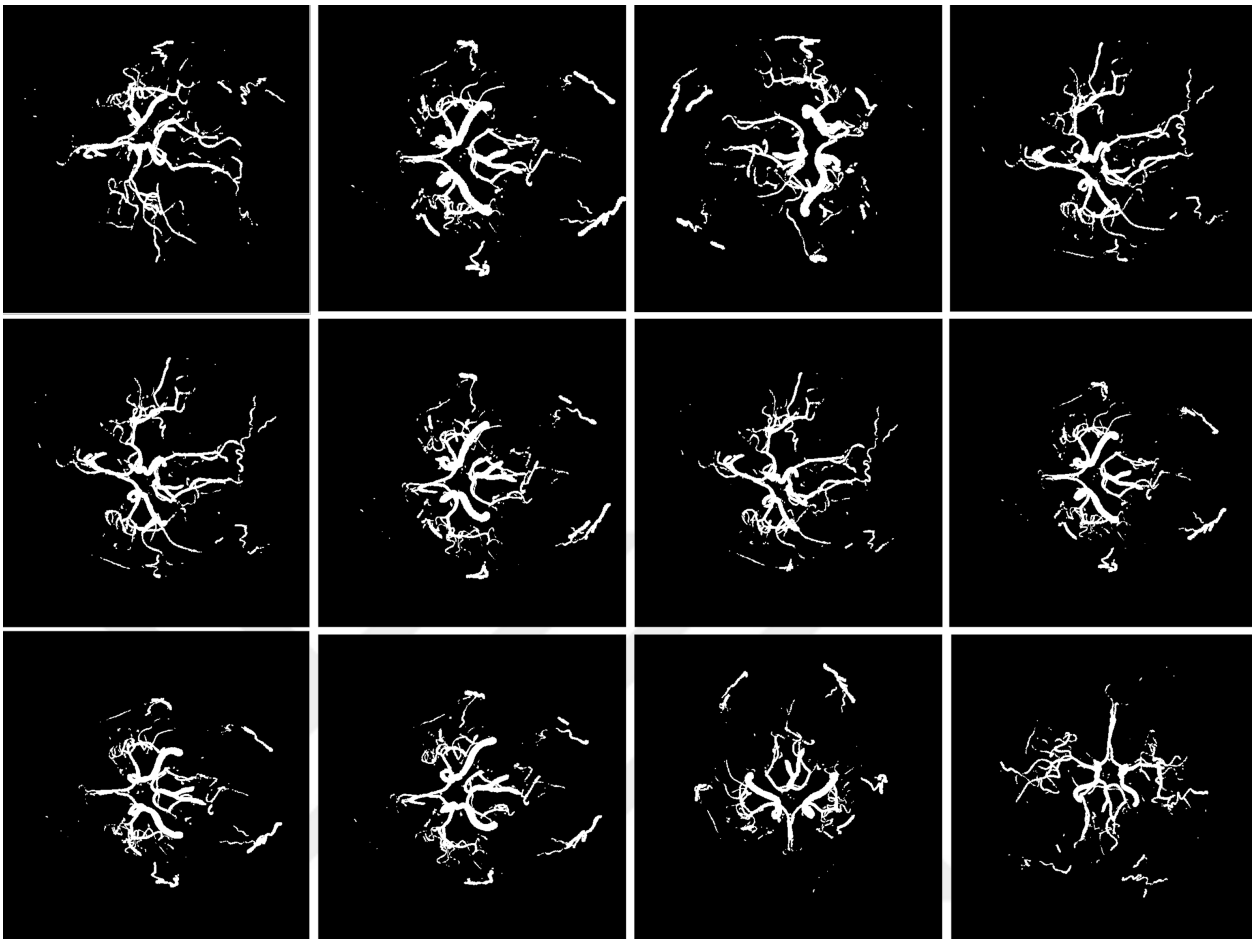

Figure 64 Brain's arteries 3D map.

5.4. Shortest Path Results:

From the 3D map, we sent the values to the Dijkstra algorithm to find the shortest path starting from a given injection point to the target point. The Dijkstra algorithm then looks at each step of the route, the distance between two points, and the values for obstacles like veins that cannot be reached, to determine the shortest path to the target point. Once the shortest route is calculated, it can be visualized on the 3D map, which offers ease of navigation and assists medical professionals to decide exactly where to give the drug injection. Additionally, this enhances the speed and precision of drug injections.

Figure 65 shows different projections of a 3D map of the brain. The slices show the skull in gray, the arteries in white, and the best path for drug delivery in red.

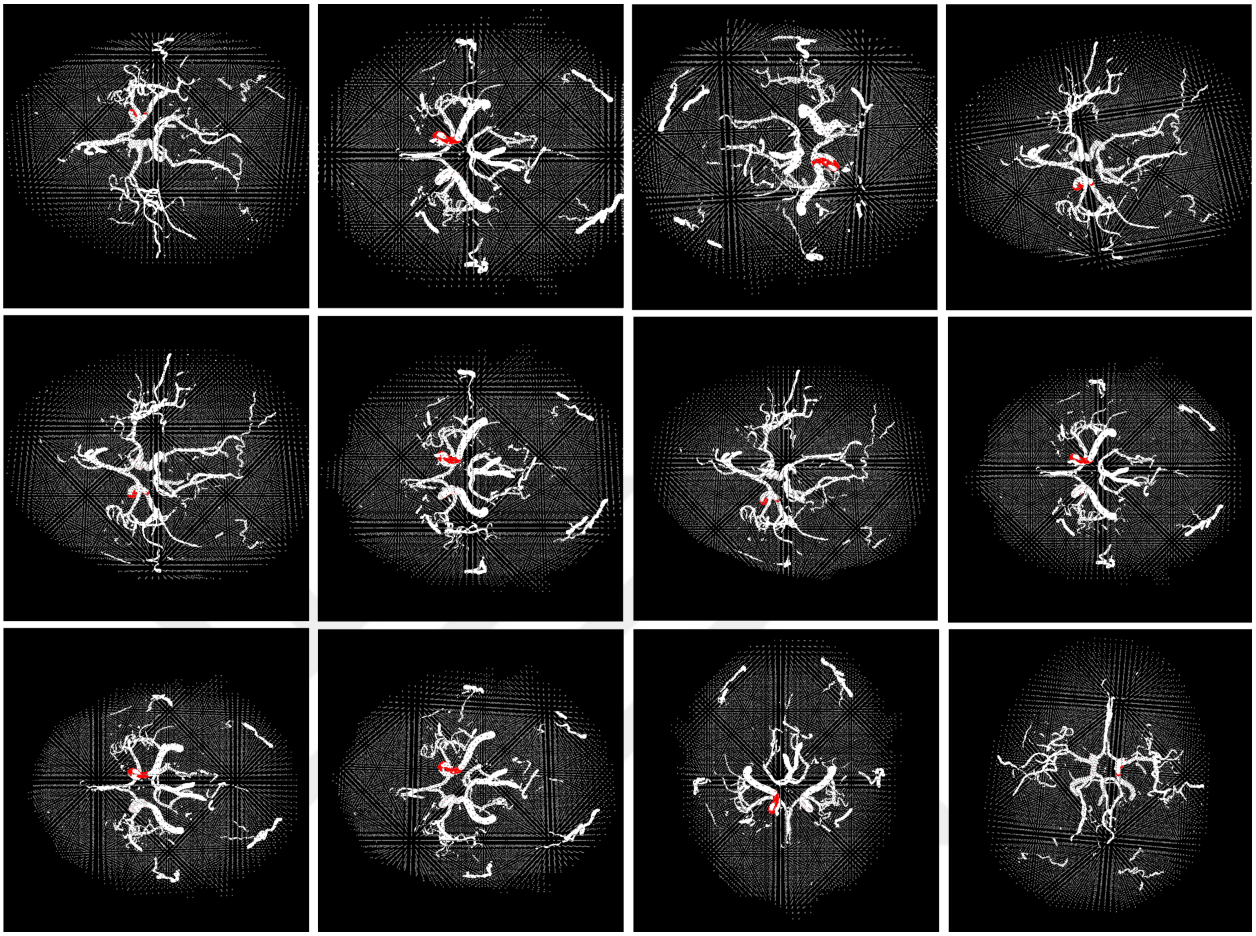

Figure 65 3D map of brain's skull, arteries, and drug delivery best path.

Figure 66 shows different projections of a 3D map of the brain. The slices show the arteries in white and the best path for drug delivery in red.

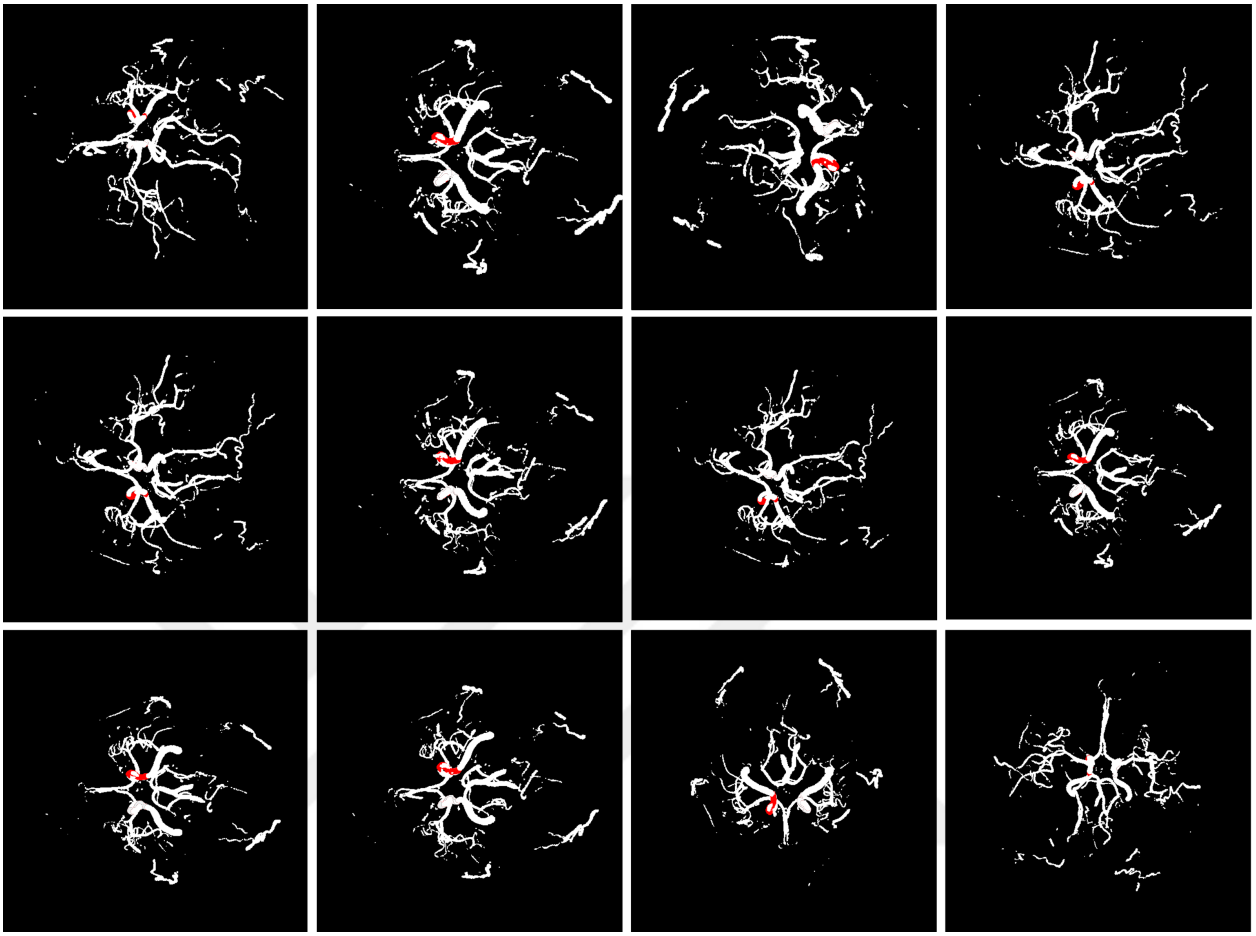

Figure 66 3D map of brain's arteries, and drug delivery best path.

6. CONCLUSION AND FUTURE WORKS

In this thesis, we compared targeted drug delivery systems (DDSs), particularly those that hinge on veins extraction methods. DDSs try to increase the amount of drugs in some parts of the body, make sure the drug does not hurt tissue that does not need to be treated, and figure out where to inject a drug.

To contextualize the thesis' aims and efforts, we visited existing work on DDSs, including several studies on cancer treatment DDSs, which used ultrasound, milk exosomes, therapeutic nanoparticles (NPs), electricity, and external magnetic fields.

Diverging from existing methods, our study was carried out with the help of a medical image dataset from a collection of MRA brain scans. This dataset included 112 scans of a man whose left arm gets weak after work out.

We tested different methods for segmenting images into arteries and veins from the given scans. This procedure separates the picture into multiple segments that represent different components of the brain. For example, Otsu's method used discriminant analysis to try to find a threshold value from a histogram of gray levels that gave the most space between pixels. However, K-means clustering divides a set of data points into distinct clusters based on the mean distance between them and each other. For its part, the fuzzy c-means (FCM) technique for clustering adds geographical information to the membership function. It creates areas that are more even, reduces false blobs, gets rid of noisy spots, and is less sensitive to noise.

After the veins extraction, we implemented the brain extraction phase of the brain, also known as the skull. This phase is important because it determines how far the injection site is from the artery or vein that will receive medicine. In our study, we delineated the brain's edge by using morphological brain extraction.

Images from the veins extraction provided us with a series of 2D slices of the arteries and veins. We used these slices to create a 3D map from those scans to represent the shape of the brain, including the skull, the veins, and the arteritis in it.

By using the 3D map, we managed to use the Dijkstra's algorithm. This algorithm can find and determine the shortest path by analyzing the 3D model, which is a task the algorithm can fulfil as long as the map is represented as a graph. The algorithm was

used to trace the shortest path between two points of interest—one being the injection site and the other being the target artery or vein.

Building on our study, future efforts into the domain might concentrate on diversifying the patient group and extending the dataset to include more types of medical imaging.

Additionally, researchers interested in the subject matter can also place external magnets around an organ to generate a magnetic field that directs the drug to its intended location. This is an operative measure, especially in organs with complicated and hard-to-reach regions, such as the brain and liver. Using magnetic fields, the medicine can be delivered directly to the area of the organ that requires treatment. This minimizes the likelihood of adverse effects and improves the effectiveness of the medication.

Furthermore, we advise researchers to address the size of the arteries and veins in the targeted region, as it is one of the key factors affecting the efficacy of this medication delivery method. The bigger the arteries and veins, the easier it will be for the drug to pass through them and reach its intended location. On the other hand, if the blood vessels are very small, the magnetic field might not be strong enough to send the drug where it needs to go.

Another factor researchers might as well focus on is the direction of blood flow at the target location. If the blood flow is going in the opposite direction of the magnetic field, the drug may not reach the intended location. However, if the blood flow is traveling in the same direction as the magnetic field, there is a greater chance that the drug will reach the intended spot.

Aside from these factors, the success of the treatment will also depend on the size and shape of the organ and the type of drug used, which researchers have to address as critical factors in the heart of the therapeutic treatment.

RESOURCES

[1] Svalastog, A. L., Donev, D., Kristoffersen, N. J., & Gajović, S. (2017). Concepts and definitions of health and health-related values in the knowledge landscapes of the digital society. Croatian Medical Journal, 58(6), 431-435. https://doi.org/10.3325/cmj.2017.58.431

[2] Tiljak, M. K. (2017). The 90th anniversary of Andrija Štampar School of Public Health. Croatian Medical Journal, 58(5), 330-331. https://doi.org/10.3325/cmj.2017.58.330

[3] Seidlein, AH., Salloch, S. Illness and disease: an empirical-ethical viewpoint. BMC Med Ethics 20, 5 (2019). https://doi.org/10.1186/s12910-018-0341-y

[4] Escorpizo, R., Kostanjsek, N., Kennedy, C. et al. Harmonizing WHO's International Classification of Diseases (ICD) and International Classification of Functioning, Disability and Health (ICF): importance and methods to link disease and functioning. BMC Public Health 13, 742 (2013). https://doi.org/10.1186/1471-2458-13-742

[5] Jakob, R. (2008). Disease Classification. International Encyclopedia of Public Health, 215-221. https://doi.org/10.1016/B978-012373960-5.00181-7

[6] A Standard Classified Nomenclature of Disease. Nature 133, 551 (1934). https://doi.org/10.1038/133551b0

[7] Mehta, Y.R. (2014). Physiological Diseases. In: Wheat Diseases and Their Management. Springer, Cham. https://doi.org/10.1007/978-3-319-06465-9_8

[8] Petersen, I. (2021). Classification and Treatment of Diseases in the Age of Genome Medicine Based on Pathway Pathology. International Journal of Molecular Sciences, 22(17). https://doi.org/10.3390/ijms22179418

[9] Krämer, A., Akmatov, M., & Kretzschmar, M. (2009). Principles of Infectious Disease Epidemiology. Modern Infectious Disease Epidemiology: Concepts, Methods, Mathematical Models, and Public Health, 85–99. https://doi.org/10.1007/978-0-387-93835-6_5

[10] van Seventer, J. M., & Hochberg, N. S. (2017). Principles of Infectious Diseases: Transmission, Diagnosis, Prevention, and Control. International Encyclopedia of Public Health, 22–39. https://doi.org/10.1016/B978-0-12-803678-5.00516-6

[11] Dorland, W. A. N. 1. (2000). Dorland's illustrated medical dictionary. 29th ed. Philadelphia, Saunders.

[12] Jackson, M., Marks, L., May, G. H. W., & Wilson, J. B. (2018). The genetic basis of disease. Essays in biochemistry, 62(5), 643–723. https://doi.org/10.1042/EBC20170053

[13] Norfolk GA. 2. Physiological Illnesses and Their Potential for Influencing Testimony. Medicine, Science and the Law. 1999;39(2):105-112. doi:10.1177/002580249903900204

[14] Hepler, C. D., & Strand, L. M. (1990). Opportunities and responsibilities in pharmaceutical care. American journal of hospital pharmacy, 47(3), 533–543.

[15] Law Insider. (n.d.). Medication therapy. https://www.lawinsider.com/. Retrieved August 25, 2022, from https://www.lawinsider.com/dictionary/medication-therapy

[16] Cousins, S., Blencowe, N. S., & Blazeby, J. M. (2019). What is an invasive procedure? A definition to inform study design, evidence synthesis and research tracking. BMJ open, 9(7), e028576. https://doi.org/10.1136/bmjopen-2018-028576

[17] Bojrab, M. J., Bojrab, M. J., Waldron, D. R., Toombs, J. P., Bailey, J. E., & Freeman, L. J. (2014). Minimally Invasive Surgery. In Current techniques in small animal surgery (pp. 71–72). essay, Teton NewMedia.

[18] Wilkinson, H.A. (1992). Noninvasive Therapy. In: The Failed Back Syndrome. Springer, New York, NY. https://doi-org.proxy.uskudar.edu.tr/10.1007/978-1-4612-4394-6_5

[19] Vllasaliu, D. (2021). Non-Invasive Drug Delivery Systems. Pharmaceutics, 13(5), 611. https://doi.org/10.3390/pharmaceutics13050611

[20] Merriam-Webster. (n.d.). Drug. In Merriam-Webster.com dictionary. Retrieved November 24, 2022, from https://www.merriam-webster.com/dictionary/drug

[21] InformedHealth.org [Internet]. Cologne, Germany: Institute for Quality and Efficiency in Health Care (IQWiG); 2006-. Using medication: Oral medications. 2011 Apr 13 [Updated 2017 Aug 10]. Available from: https://www.ncbi.nlm.nih.gov/books/NBK361020/

[22] Ker, K., Tansley, G., Beecher, D., Perner, A., Shakur, H., Harris, T., & Roberts, I. (2015). Comparison of routes for achieving parenteral access with a focus on the management of patients with Ebola virus disease. The Cochrane database of systematic reviews, 2015(2), CD011386. https://doi.org/10.1002/14651858.CD011386.pub2

[23] File: Needle-insertion-angles-1.png. (2022, April 2). Wikimedia Commons, the free media repository. Retrieved 20:47, December 18, 2022, from https://commons.wikimedia.org/w/index.php?title=File:Needle-insertion-angles-1.png&oldid=646080536.

[24] Hua S. (2019). Advances in Nanoparticulate Drug Delivery Approaches for Sublingual and Buccal Administration. Frontiers in pharmacology, 10, 1328. https://doi.org/10.3389/fphar.2019.01328

[25] Jannin, V., Lemagnen, G., Gueroult, P., Larrouture, D., & Tuleu, C. (2014). Rectal route in the 21st Century to treat children. Advanced Drug Delivery Reviews, 73, 34-49. https://doi.org/10.1016/j.addr.2014.05.012

[26] Gaudana, R., Ananthula, H. K., Parenky, A., & Mitra, A. K. (2010). Ocular Drug Delivery. The AAPS Journal, 12(3), 348-360. https://doi.org/10.1208/s12248-010-9183-3

[27] Ball, D. R., & McGuire, B. E. (2013). Airway Pharmacology. Benumof and Hagberg's Airway Management (Third Edition), 159-183.e9. https://doi.org/10.1016/B978-1-4377-2764-7.00006-3

[28] Alkilani, A. Z., McCrudden, T. C., & Donnelly, R. F. (2015). Transdermal Drug Delivery: Innovative Pharmaceutical Developments Based on Disruption of the Barrier Properties of the stratum corneum. Pharmaceutics, 7(4), 438-470. https://doi.org/10.3390/pharmaceutics7040438

[29] Katz, D. F., Yuan, A., & Gao, Y. (2015). Vaginal Drug Distribution Modeling. Advanced drug delivery reviews, 92, 2. https://doi.org/10.1016/j.addr.2015.04.017

[30] Sengupta, S., & Balla, V. K. (2018). A review on the use of magnetic fields and ultrasound for non-invasive cancer treatment. Journal of advanced research, 14, 97–111. https://doi.org/10.1016/j.jare.2018.06.003

[31] Stax, O., & Taylor, C. (2020, July 20). Circulatory Pathways. OpenStax CNX. Retrieved December 19, 2022, from https://cnx.org/contents/GqYHW4Z4@7/Circulatory-Pathways

[32] Yan, W., Lang, T., Zhu, R., Zhu, X., Li, Y., Wu, T., Yin, Q., & Li, Y. (2022). Anti-hypoxia nanosized drug delivery systems improving cancer therapy. Nano Today, 42, 101376. https://doi.org/10.1016/j.nantod.2022.101376

[33] Joshi, B., & Joshi, A. (2019). Ultrasound-based drug delivery systems. Bioelectronics and Medical Devices, 241-260. https://doi.org/10.1016/B978-0-08-102420-1.00014-5

[34] Sengupta, S., & Balla, V. K. (2018). A review on the use of magnetic fields and ultrasound for non-invasive cancer treatment. Journal of advanced research, 14, 97–111. https://doi.org/10.1016/j.jare.2018.06.003

[35] Torre, L.A., Bray, F., Siegel, R.L., Ferlay, J., Lortet-Tieulent, J. and Jemal, A. (2015), Global cancer statistics, 2012. CA: A Cancer Journal for Clinicians, 65: 87-108. https://doi.org/10.3322/caac.21262

[36] Gelet, A., Chapelon, J. Y., Bouvier, R., Pangaud, C., & Lasne, Y. (1999). Local control of prostate cancer by transrectal high intensity focused ultrasound therapy: preliminary results. The Journal of urology, 161(1), 156–162.

[37] Zhang, Q., Xiao, Q., Yin, H., Xia, C., Pu, Y., He, Z., Hu, Q., Wang, J., & Wang, Y. (2020). Milk-exosome based pH/light sensitive drug system to enhance anticancer activity against oral squamous cell carcinoma. RSC advances, 10(47), 28314–28323. https://doi.org/10.1039/d0ra05630h

[38] Wang, Xiaoyou & li, Chong & Wang, Yiguang & Chen, Huabing & Zhang, Xinxin & Luo, Cong & Zhou, Wenhu & Li, Lili & Teng, Lesheng & Yu, Haijun & Wang, Jiancheng. (2022). Smart drug delivery systems for precise cancer therapy. Acta Pharmaceutica Sinica B. 10.1016/j.apsb.2022.08.013.

[39] Kalaydina RV, Bajwa K, Qorri B, Decarlo A, Szewczuk MR. Recent advances in "smart" delivery systems for extended drug release in cancer therapy. Int J Nanomedicine. 2018 Aug 20;13:4727-4745. doi: 10.2147/IJN.S168053. PMID: 30154657; PMCID: PMC6108334.

[40] Liu, Zhirong & Li, Linlin. (2021). Self-Powered Drug-Delivery Systems Based on Triboelectric Nanogenerator. Advanced Energy and Sustainability Research. 2. 2100013. 10.1002/aesr.202100013.

[41] A. Nacev et al., "Towards Control of Magnetic Fluids in Patients: Directing Therapeutic Nanoparticles to Disease Locations," in IEEE Control Systems Magazine, vol. 32, no. 3, pp. 32-74, June 2012, doi: 10.1109/MCS.2012.2189052.

[42] Shapiro, B., Kulkarni, S., Nacev, A., Muro, S., Stepanov, P.Y. and Weinberg, I.N. (2015), Open challenges in magnetic drug targeting. WIREs Nanomed Nanobiotechnol, 7: 446-457. https://doi.org/10.1002/wnan.1311

[43] Liu, Q., Ye, X., Wu, H., & Zhang, X. (2022). A multiphysics model of magnetic hydrogel under a moving magnet for targeted drug delivery. International Journal of Mechanical Sciences, 215, 106963. https://doi.org/10.1016/j.ijmecsci.2021.106963

[44] Abbes, M., Belharet, K., Souissi, M., Mekki, H., & Poisson, G. (2022). Design of a Robotized Magnetic Platform for Targeted Drug Delivery in the Cochlea. IRBM. https://doi.org/10.1016/j.irbm.2022.06.003

[45] Chuang, Keh-Shih & Tzeng, Hong-Long & Chen, Sharon & Wu, Jay & Chen, Tzong-Jer. (2006). Fuzzy c-means clustering with spatial information for image segmentation. Computerized Medical Imaging and Graphics, 30, 9-15. Computerized medical imaging and graphics: the official journal of the Computerized Medical Imaging Society. 30. 9-15. 10.1016/j.compmedimag.2005.10.001.

[46] Wikipedia contributors. "Fuzzy clustering." Wikipedia, The Free Encyclopedia. Wikipedia, The Free Encyclopedia, 29 Jan. 2022. Web. 13 Apr. 2022.

[47] Moon, T.K. (1996). The expectation-maximization algorithm. Signal Processing Magazine, IEEE. 13. 47 - 60. 10.1109/79.543975.

[48] Otsu, Nobuyuki. (1979). A Threshold Selection Method from Gray-Level Histograms. Systems, Man and Cybernetics, IEEE Transactions on. 9. 62-66.

[49] MacQueen, J. B. (1967). Some Methods for Classification and Analysis of MultiVariate Observations. In L. M. L. Cam & J. Neyman (eds.), Proc. of the fifth Berkeley Symposium on Mathematical Statistics and Probability (p./pp. 281-297),: University of California Press.

[50] Wikipedia contributors. "Fuzzy clustering." Wikipedia, The Free Encyclopedia. Wikipedia, The Free Encyclopedia, 29 Jan. 2022. Web. 13 Apr. 2022.

[51] Wikipedia contributors. "Expectation–maximization algorithm." Wikipedia, The Free Encyclopedia. Wikipedia, The Free Encyclopedia, 10 Apr. 2022. Web. 13 Apr. 2022.

[52] Otsu's method. (2022, November 6). In Wikipedia. https://en.wikipedia.org/wiki/Otsu%27s_method

[53] Dijkstra, E. W. (1959). "A note on two problems in connexion with graphs" (PDF). Numerische Mathematik. 1: 269 - 271. doi:10.1007/BF01386390. S2CID 123284777.

[54] P. E. Hart, N. J. Nilsson and B. Raphael, "A Formal Basis for the Heuristic Determination of Minimum Cost Paths," in IEEE Transactions on Systems Science and Cybernetics, vol. 4, no. 2, pp. 100-107, July 1968, doi: 10.1109/TSSC.1968.300136.

[55] Bickle I, Normal brain MRI including MRA. Case study, Radiopaedia.org (Accessed on 15 Dec 2022) https://doi.org/10.53347/rID-48748